

Rockefeller University

Digital Commons @ RU

Student Theses and Dissertations

2021

Non-Canonical Axonal Insulin Receptor signaling Drives Aversive Olfactory Learning

Du Cheng

Follow this and additional works at: https://digitalcommons.rockefeller.edu/student_theses_and_dissertations



Part of the [Life Sciences Commons](#)



NON-CANONICAL AXONAL INSULIN RECEPTOR SIGNALING
DRIVES AVERSIVE OLFACTORY LEARNING

A Thesis Presented to the Faculty of
The Rockefeller University
in Partial Fulfillment of the Requirements for
the degree of Doctor of Philosophy

by

Du Cheng

Lxpg"4243

NON-CANONICAL AXONAL INSULIN RECEPTOR SIGNALING DRIVES AVERSIVE OLFACTORY LEARNING

Du Cheng, PhD

The Rockefeller University 2021

Animals rely on their flexible nervous systems to learn to navigate the changing environment around them. One important function of the nervous system is to form associative memories. A simple model of associative learning is provided by nematode *C. elegans*, which can form memories of different types of odor stimuli through its simple yet sophisticated nervous system. *C. elegans* uses its sensory neurons to detect and navigate towards the odors of its food source - edible bacteria. Thus, it is crucial for worms to form memories between odors and availability of food. The volatile chemical butanone is a common product of bacterial metabolism, and therefore a bacterial odor that is attractive to worms. However, exposing *C. elegans* to butanone vapor while depriving them of food can suppress this attraction. *C. elegans* senses butanone with its AWC^{ON} neuron, and the information is further integrated before its delivery onto a network of interneurons, where it is processed for control of navigation. In my thesis, I systematically characterize aversive learning induced by pairing butanone odor with food deprivation. I employ a wide variety of experiments to understand *C. elegans*' changes in molecular pathways, neuronal dynamics, and behavior output mechanics during aversive learning.

In Chapter 1, I introduce how studying the neuronal and genetic mechanism of learning in *C. elegans* can contribute to the understanding of our brains and diseases of the brain. I briefly

describe how insulin and insulin-like growth factor pathways regulate learning in humans and other mammals. In Chapter 2, I explore and refine the stimulation conditions that decrease or enhance *C. elegans*'s attraction to butanone. I separate the effect of odor exposure alone (desensitization) and odor-starvation paired conditioning (aversive learning) using a comprehensive behavior testing approach. I conduct a candidate gene screen for aversive learning defects, and identify the *C. elegans* homolog of the Insulin Receptor Substrate (IRS) (*ist-1*) as a gene required for aversive odor learning. I also demonstrate odor- and cell-specific functions of *ist-1*. In Chapter 3, I characterize insulin signaling in the aversive learning process. I describe the cell-specific activity of an axonally-localized isoform of the insulin receptor DAF-2 in aversive learning. I perform epistasis studies of *ist-1* with other members of the insulin signaling pathway to ask how they regulate aversive learning together. In Chapter 4, I characterize neuronal mechanisms involved in odor detection and learning through AWC^{ON} cell body calcium imaging and pHluorin imaging of synaptic glutamate release, and ask how *ist-1* modifies these mechanisms during learning. I show that these molecular and neuronal mechanisms result in behavior changes during biased random walk chemotaxis.

What makes me me? How is it different from you? We as human beings possess a vast amount of knowledge, skills, experiences, emotions, and memories. These attributes seem to collectively define who each of us is as an individual, different from others. As early as Hippocrates, these ideas have been circling, who thought that our emotions and intelligence are produced by the brain and brain alone. However, each of us is so complex and so unique, it makes it hard to believe that we are just collections of organs, and the organs are a collection of cells, and the cells are collections of molecules. Are we just combinations of molecular dust down to the basic level? To some, when a brain is compared to a computer and electronic components, it is incomprehensible how a human brain, roughly equivalent to 2-3 lbs of flesh, can store as much as 2.5 million gigabytes equivalence of data in a confined space (Reber, 2010). There must be something more to it, above the physical level, to make us intelligent, make us what we are, above other materials and beings. Call it a soul, perhaps.

Questions like this have been driving me to pursue the field of science and medicine, to understand ourselves, to cure diseases, and to build the future. I dedicate this thesis to all my fellow scientists who push humanity forward with their hard work.

ACKNOWLEDGMENTS

I was incredibly fortunate to have had the opportunity to pursue my graduate studies in the Bargmann Lab. Cori has been a fantastic mentor to me during these years. Her enthusiasm for science and passion for pursuing the unknown only grows as we learn more. She's a living encyclopedia, an idea factory, and a compassionate human being. She does not settle for just being a good scientist; she also takes on challenges like running the Chan Zuckerberg Initiative, which was inspirational to my career choices. As busy as she is, working two full-time jobs on the two coasts, she always has time for us, not only as a mentor but also as a life coach, a friend, and to help us grow professionally and individually.

I want to thank my thesis committee, Vanessa Ruta, Connor Liston, and Sohail Tavazoie. I have greatly appreciated your support, expertise, and insight before and throughout my Ph.D. I would also like to thank Gary Ruvkun for graciously agreeing to serve as my external committee member.

I want to thank the members of the Bargmann Lab; you have been there every step of the way to help and support me. You made the laboratory a fun, vibrant place and made it feel like a second home. I want to thank Christine Cho, who welcomed me to the lab and gave me all the early training to start in the lab, and Sara Abrahamsson, Navin Pokala and Joshua Greene who taught me a variety of techniques. I would also like to thank my bay-mates and good friends, Elias Sheer and Alejandro Lopez. You taught me many things by hand and shared many memories with me in the lab and on trips. I want to thank May Dobosiewicz, and Aylesse Sordillo, who taught me sophisticated microscopy and Phil Kidd, who's always there to troubleshoot for me. I would also like to thank Margaret, who taught me how to make complicated designs in molecular biology. I am also grateful for good friends like James Lee, Javier Marquina, and Likui Feng, with who I enjoyed working together and had great times hanging out outside of the lab. They also helped me prepare for experiments when I was out of town. I'd also like to thank the support staff in the lab: Hernan Jaramillo, Priscilla Kong, and Manoush Ardzivian. They keep the lab running efficiently and are also so much fun to be around.

I want to thank all my mentors that helped me get to where I am now—starting from Humboldt State University when I just came to the US. Dr. Jianmin Zhong led me into the gateway of scientific research. It begun with how to hold a pipette, he taught me how to conduct

rigorous lab work over three years. His wife took us to their house for dinner all the time, a kindness I appreciated as a hungry student. Dr. Rollin Richmond, president of HSU, a graduate from Rockefeller University, met with me regularly and encouraged me to develop my business. Dr. Amy Sprowles and Dr. Jacob Varkey, two adventurous professors, further trained me on cell biology. They sent me to Stanford University through a state-funded program that they sponsored, where Dr. Jill Helms set me up with amazing research projects, sat me in her office all the time, teaching me how to make figures and write papers. She even stepped forward as my collateral person when I needed a sponsor for my green card application, as if I was her child. I would also like to thank good friends Paula Schanes, Andrew Smith, and Humberto Contreras, who were always there to help me throughout my science career. I would never forget all the kindness and help I received on the pathway of becoming an American citizen.

I want to thank the MD-PhD Program, especially Dr. Olaf Andersen, who took a chance on me, allowed me to interview here when 30 other institutions that I applied to did not. I would also like to thank the Paul and Daisy Soros Fellowship that financially sponsored me during my Ph.D. and provided me a network of new immigrant fellows who share the same background and ambition as me. I am grateful to have good friends Daniel Cabrera, Alexandra Kramer, Evan O'Dea, Serena Andrus, Andrew Cho, Steven Cajamarca, Fumitaka Sugiguchi, Francesca Valentin, Susan Duan, Jake and Emily Reed, Rachel Babij, Sudha Guttikonda, Emma Schatoff, and Sohn Kim, Jared Moon, Khatiya Chelidze and Tyler Eastland to grow with me during these years.

I want to thank my parents, who taught me everything and shaped me who I am, who believed in me and borrowed money to send me overseas. Although I didn't understand it when I was young and had been a rebellious trouble maker, I benefited from the education and opportunities they provided me every day.

The greatest thing I have gained in life is my partner Heather, my son Quinn and my other two little friends Ben and Arthur. Heather is an extraordinary data scientist who works on health policy research. She is talented and innovative. She truly cares about her making policy changes, which is already starting to help people's life. She is my source of inspiration and passion. She has been genuinely supportive, taking care of the whole family when I am away in New York pursuing my career. She's taught me the meaning of family, and she's made the past few years some of the happiest of my life.

TABLE OF CONTENTS

LIST OF FIGURES	vii
LIST OF TABLES	ix
CHAPTER 1. Introduction.....	1
1.1 Neuroscience and diseases of the brain	2
1.2 <i>C. elegans</i> as a model to study neuronal mechanisms.....	4
1.3 Molecular and neuronal mechanism of learning in <i>C. elegans</i>	9
1.4 Insulin pathway and learning in worm and mammals	12
CHAPTER 2. Behavior screening and the <i>ist-1</i> function in aversive learning	18
2.1 Conditions of chemotaxis.....	21
2.2 Conditions of different types of olfactory learning	25
2.3 Identifying mutants with aversive learning defects.....	29
2.4 Genetic characterization of <i>ist-1</i>	36
2.5 <i>ist-1</i> mutants and other odors sensed by AWC neurons	43
CHAPTER 3. Insulin signaling and aversive learning	46
3.1 Insulin pathway overview	47
3.2 Cell specific insulin receptor function in aversive learning.....	51
3.3 Axonal localization of DAF-2c in AWC ^{ON}	59
3.4 <i>ist-1</i> interacts with other insulin pathway genes in aversive learning.. ..	64
CHAPTER 4. Neuronal mechanism of aversive learning.....	71
4.1 Neuronal activity of AWC ^{ON}	74
4.2 Synaptic change in aversive learning	77
4.3 Behavioral change in aversive learning	83
4.4 Future directions.....	90
EXPERIMENTAL PROCEDURES	93
REFERENCES	106

LIST OF FIGURES

Figure 1.1 Simplified neural circuit diagram and graphic illustration for <i>C. elegans</i> chemotaxis behavior	7
Figure 2.1 Schematic of experimental procedure used to study aversive learning behavior.....	23
Figure 2.2 Schematic and chemotaxis index of fed vs food deprived worms.....	24
Figure 2.3 Amount of butanone required for different types of behavioral plasticity in wild-type and in learning deficient <i>ist-1</i> mutant animals.....	27
Figure 2.4 Candidate gene screen for mutants with defects in aversive learning.	30
Figure 2.5 Chemotaxis index of <i>npr-1</i> mutants and <i>npr-1</i> mutants with oxygen sensing defects.....	35
Figure 2.6 Genetic structure, mutant alleles and expression pattern of <i>ist-1</i> gene	37
Figure 2.7 Genomic and cell-specific rescue of <i>ist-1</i>	40
Figure 2.8 <i>ist-1</i> mutants have normal aversive learning to several other odors.....	42
Figure 3.1 Simplified diagram of <i>C. elegans</i> insulin pathway relevant to chemosensation and aversive learning.....	48
Figure 3.2 <i>daf-2</i> isoforms, and strategy for <i>daf-2</i> cell-specific knock-out.....	52
Figure 3.3 The function of insulin receptor isoform DAF-2c in aversive leaning	53
Figure 3.4 <i>daf-2</i> cell specific knockout.....	56
Figure 3.5 <i>daf-2</i> cell specific rescue	58
Figure 3.6 Subcellular localization of DAF-2 insulin receptor isoforms.....	60
Figure 3.7 Quantification of subcellular localization of DAF-2 insulin receptor isoforms.....	61

Figure 3.8 Subcellular localization of IST-1	63
Figure 3.9 Epistatic study of insulin pathway members in aversive learning.....	66
Figure 4.1 Calcium imaging of AWC ^{ON} neuron showing desensitization in both wild-type and <i>ist-1</i> mutant animals.....	75
Figure 4.2 Role of glutamate release in butanone chemotaxis.....	78
Figure 4.3 pHluorin imaging reveals that changes in synaptic output during aversive learning are dependent on <i>ist-1</i>	81
Figure 4.4 Selective interneuron silencing can disrupt chemotaxis but does not differentially affect aversive learning.....	85
Figure 4.5 <i>ist-1</i> mutants maintain the ability to chemotaxis after aversive learning by maintaining the biased-random walk.....	87
Figure 4.6 Summary diagram of cellular/molecular mechanisms for aversive learning through the insulin pathway	88

LIST OF TABLES

Table 5.1 Strains generated for this study	105
--	-----

CHAPTER 1.

Introduction

1.1 Neuroscience and diseases of the brain

Historically, molecular studies of the brain have often been focused on the functions of individual neurons or specific types of neurons. The strength of this approach is embedded in its limitations. On one hand, cellular and molecular levels allow us to gain true understanding of mechanisms. On the other hand, we sometimes lose insight into how many of these complicated processes there are and how they work together, in one or many cells. As we discover more and more about how cellular functions and molecular pathways work, we see that each neuron is not just a resister, a capacitor, or an inductor that delivers one function, or form one memory. Each neuron is more of a mini-computer that has many different points of entry and exit at different synapses, with switch, resistor, capacitor, inductor, and amplifier-like functions that collectively function as a variety of logic gates (Kandel, Schwartz, & Jessell, 2012; McCulloch & Pitts, 1990).

To understand how exactly our brain works has been the crown jewel of science. Apart from our long-term goal as a human race to be able to comprehend our own minds, there are also pressing problems to be solved. Mental health problems have been worsening in recent years, and most are only partially understood and treated (Reinert, Nguyen, & Fritze, 2021). The complexity and lack of understanding of these diseases themselves remain a major barrier to treatment development. Our brain is an intricate system where fine structures operate in close temporal and spatial proximity. Common psychiatric interventions such as chemical agents that boost a single neurotransmitter over the entire brain, or physical methods to stimulate or suppress an entire area like transcranial magnetic stimulation or electro-convulsive therapy, lack fine resolution. They are analogous to pouring oil all over a machine to attempt to lubricate one part. Apart from not being effective a lot of times, these therapies often have unintended side effects.

Yet, these are the best we have in the arsenal to combat diseases that one-in-five people experiencing over their lifetime (McCance-Katz, 2020).

In the animals with more intelligence, the number of cells, cell types, and structure of the brain increase many-fold in complexity. Moreover, brain structures increase in thickness and fold upon themselves to form gyrations. This increases the difficulty of access to the brain during active behaviors, especially to study neuronal genetics in deep brain structures. Although amazing progress has been made in modern neuroscience techniques, direct analyses of neurons remains extremely challenging. For example, for monitoring activity in organisms like mice, two-photon microscopy requires highly specialized surgery and is low throughput (Ulivi, et al., 2019). In humans, we mostly can only study activity with functional magnetic resonance (fMRI) that has low temporal and spatial resolution compared to indicated neurons and their activity, preventing genetic based studies in the neurons (Theysohn, et al., 2009).

1.2 *C. elegans* as a model to study neuronal mechanisms

To overcome these technical hurdles and gain insight into how each neuron operates on the level of a single cell, synapses, or even a molecule, we turned to a fantastic model organism *Caenorhabditis elegans*, a nematode worm, to study learning. *C. elegans* has a simple yet complicated neural system that consists of 302 neurons. Its sensory neurons are capable of sensing environmental stimuli such as odors, temperature, salt concentration, oxygen and light and can drive the animal to navigate towards or away from them. They are even capable of forming memories of these stimuli based on their coupling to nutritional status or the presence of pathogen (Ward S., 1973; Bargmann, Hartwig, & Horvitz, 1993; L'Etoile, et al., 2002; Zhang, Lu, & Bargmann, 2005; Jin, Pokala, & Bargmann, 2016). Yet adult *C. elegans* are only about 1 mm in length and consist of only 959 somatic cells, which means nearly one-third of the somatic cells (302, to be exact) are devoted to its nervous system. Furthermore, *C. elegans* is the only organism whose entire neural system has been mapped out down to individual synaptic connections between all 302 neurons through serial electron micrograph reconstruction (White, Southgate, Thomson, & Brenner, 1986). *C. elegans* was also the first multicellular organism where its entire genome was sequenced. This allow us to take advantage of the huge repertoire of genetic knowledge and tools to study how neurons work. Neurons of behavioral importance can be largely divided into sensory neurons, integrating interneurons, and motor neurons. In this thesis, I examine learning-related changes in sensory neurons that result in differences in behavior output.

C. elegans sensory neurons detect a variety of odors that are produced by its bacterial food. Each of the 11 types of chemosensory neurons in the amphid sensory organ expresses a subset of the 1000-2000 G protein coupled chemoreceptors (GPCRs) in the worm genome (Bargmann C. I., 2006; Troemel, Chou, Dwyer, Colbert, & Bargmann, 1995). Volatile odors detected by AWA and

AWC neurons, such as diacetyl and butanone, elicit chemotaxis, while volatile odors detected by AWB, such as 2-nonanone, lead to avoidance (Bargmann, Hartwig, & Horvitz, 1993; Troemel, Kimmel, & Bargmann, 1997). Most neuron pairs are symmetric in structure and function, but the AWC neurons are asymmetric: one of the two AWC neurons (AWC^{ON}) expresses *str-2* and the other, AWC^{OFF} , does not. AWC^{ON} detects butanone and AWC^{OFF} detects 2,3-pentanedione, and both detect benzaldehyde and isoamyl alcohol (Wes & Bargmann, 2001).

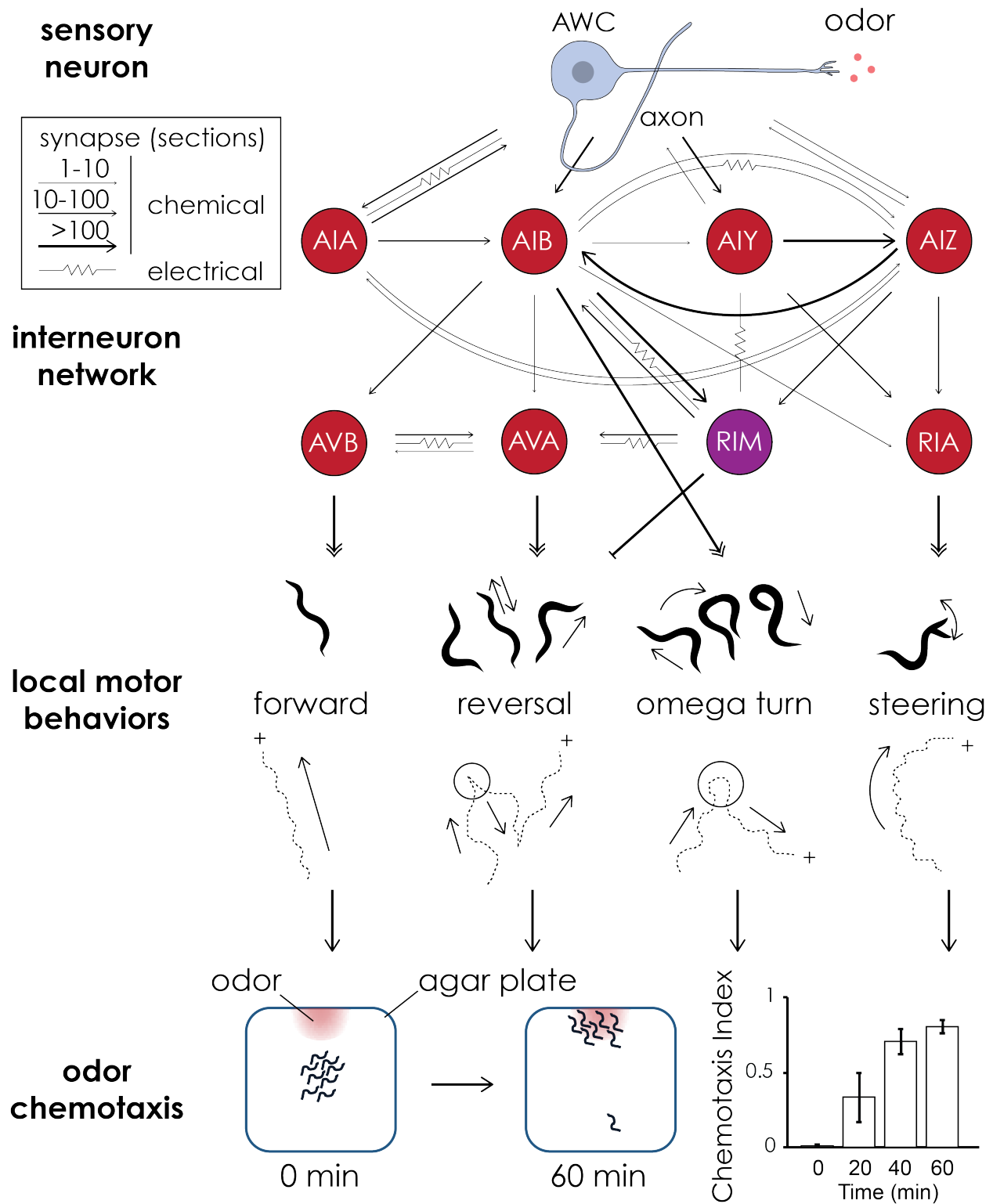
C. elegans is capable of moving towards and away from a variety of environmental stimuli including volatile odors, carbon dioxide, oxygen, and soluble chemicals such as sodium chloride (Ward S., 1973). This behavior is called chemotaxis. They can also respond to physical stimuli such as temperature (Hedgecock & Russell, 1975), blue light (Ward, Liu, Feng, & Xu, 2008), and mechanical stimuli (Chalfie, et al., 1985). *C. elegans* uses at least two different strategies for chemotaxis: the biased random walk (klinokinesis) and steering (klinotaxis) (Berg & Brown, 1972; Berg H. C., 1993; Iino & Yoshida, 2009). In the biased random walk (klinokinesis) model, when *C. elegans* detects an increase in an attractive gradient, it continues to move forward (“runs”). When *C. elegans* detects a decrease in the gradient, animals switch to a period of reorientations characterized by common reversals and omega turns (“pirouettes”) (Pierce-Shimomura, Morse, & Lockery, 1999). This trial-and-error method allows *C. elegans* to shorten the distance to the source of attractant. In the steering model, *C. elegans* gradually curves towards the high gradient side during a forward run, a finer navigation strategy that may be useful when moving at an angle to the odor source (Iino & Yoshida, 2009). In a simplified neuron network, the AWC^{ON} neuron connects to first layer interneurons AIA, AIB and AIY. Another first layer interneuron, AIZ, indirectly connects to AWC^{ON} through AIB and AIY (Tsalik & Hobert, 2003). AIA and AIY neurons functionally inhibit turns while AIB and AIZ

promote turns (Gray, Hill, & Bargmann, 2004; Wakabayashia, Kitagawab, & Shingaia, 2004). In butanone chemotaxis, a decrease in butanone concentration leads to depolarization of the AWC^{ON} neuron, inhibition of AIA and AIY neurons, and activation of AIB neurons (Chalasani, et al., 2007; Chalasani, et al., 2010). AIB neurons drive activation of a backward command neuron, AVA, which initiates reversals associated with the biased random walk and pirouettes (Figure 1.1). *C. elegans* can also use another mode of local motion called klinotaxis, or the weathervane mechanism, during sinusoidal dorsal-ventral head movement (Iino & Yoshida, 2009). Worms can sense the concentration fluctuation of isoamyl alcohol caused by the small displacement during the head movement with their sensory neuron (Kato, Xu, Cho, Abbott, & Bargmann, 2014). This information is relayed to the AIY and RIA inter-neuron which are implicated in klinotaxis. Signals from AIY neurons, sensing input, and the state of motor neurons are integrated by RIA neurons, allowing the dorsal and ventral axonal compartments of RIA to responded in different degrees when the head of the worm swings dorsally versus ventrally. This in turn generates a bias allows a worm to curve its sinusoidal path towards the odor gradually (Liu, et al., 2018). In salt chemotaxis, the AIZ neuron is to also important for the integration of head swings to RIA to control the weathervane response (Iino & Yoshida, 2009). Finally, odors can elicit other behaviors such as pauses that may also contribute to attraction (Albrecht & Bargmann, 2011).

Figure 1.1 Simplified neural circuit diagram and graphic illustration for *C. elegans* chemotaxis behavior

Simplified *C. elegans* neural circuit diagram relevant to butanone odor chemotaxis. Arrows are weighted on numbers of synaptic connections between neurons observed in electron micrographs. Data from www.wormwiring.org and (White, Southgate, Thomson, & Brenner, 1986; Gordus, Pokala, Levy, Flavell, & Bargmann, 2015). The AWC^{ON} neuron senses butanone odor using G protein-coupled chemoreceptors on the tip of its dendrite. The AWC^{ON} neuron forms synapses with a network of interneurons that integrate the output of AWC^{ON} with other signals, and with the state of the worm, before sending commands to motor neurons (not shown). The motor neurons and muscle then execute movement combinations. These movement combinations generate local motor behaviors such as forward, reverse, omega-turn and steering. The sequence of movements over time produces the chemotaxis behavior where worms move towards the odor source. Bottom left panel, schematic of experimental setup before and after chemotaxis, showing accumulation of worms at the odor (red spot). Bottom right panel, accumulation of animals at the odor source over time represented by quantification as chemotaxis index.

$$(\text{Chemotaxis Index} = \frac{\text{Animals at odor side} - \text{Animals at the opposite side}}{\text{Animals at odor side} + \text{Animals at control side} + \text{Animals in the middle}})$$



1.3 Molecular and neuronal mechanism of learning in *C. elegans*

Butanone exposure causes instantaneous, short-term and long-term changes in the signaling cascade in AWC^{ON} and interneurons. On an instantaneous scale, butanone activates a G protein –coupled pathway in sensory cilia. The AWC^{ON} neuron is active at rest, and inhibited by odor, analogous to the inhibition of vertebrate rod and cone photoreceptors by light (Palczewski, 2006). Each AWC neuron expresses multiple genes encoding G-Protein Coupled Receptors (GPCRs) derived from the many *sra*, *sraB*, *srb*, *srd*, *sre*, *srg*, *str*, *srt*, and *srx* families of potential chemoreceptors (Chen, et al., 2005; Troemel, Chou, Dwyer, Colbert, & Bargmann, 1995). During butanone exposure, the odor-sensing GPCR modulates levels of cGMP, leading to the closure of the cGMP-gated TAX-2/TAX-4 channel (Coburn & Bargmann, 1996). This in turn decreases intracellular calcium levels (Chalasani, et al., 2007) and glutamate release (Ventimiglia & Bargmann, 2017) from AWC. Upon odor removal, this process is reversed, and AWC^{ON} neurons increase their calcium level and release glutamate onto AIB and AIY neurons through synaptic vesicles (Chen, et al., 2013). AIB is excited by glutamate signals through its AMPA/kainate-like receptor GLR-1, which result in increased turning (Chalasani, et al., 2007). The AIY neuron is inhibited by glutamate signaling through its glutamate-gated chloride channel GLC-3 (Horoszok, Raymond, Sattelle, & Wolstenholme, 2001), and as AIY suppresses turns, its response to glutamate also results in increased turning due to dis-inhibition.

Pairing odors with appetitive or aversive stimuli, such as food or pathogens, can modify *C. elegans*'s chemotaxis preference (Colbert & Bargmann, 1995; Torayama, Ishihara, & Katsura, 2007; Zhang, Lu, & Bargmann, 2005; Melo & Ruvkun, 2013). For example, naïve *C. elegans* are attracted to low concentrations of butanone (1:1000). Pairing butanone with food deprivation can decrease this attraction to butanone (Colbert & Bargmann, 1995)(Figure 2.1), a process originally

referred as olfactory adaptation. The aversive learning to the other odors such as isoamyl alcohol and butanone is independent from butanone although they are all sensed by the AWC^{ON} neuron (Colbert & Bargmann, 1995). Although there are many different definitions to adaptation, it generally refers to a prolonged odor exposure, not to the short-term change while animals respond to an odor gradient (Bargmann C. I., 2006). Translocation of a cGMP-dependent protein kinase EGL-4 into the nucleus is necessary and may be sufficient for odor aversive learning (Lee, et al., 2010; L'Etoile, et al., 2002). This translocation of EGL-4 is independent of calcium level, but dependent on Gα protein activity (O'Halloran, Altshuler-Keylin, Lee, & L'Etoile, 2009).

Previous results suggested that there might be at least two components to odor adaptation, the desensitization of AWC from the odor exposure itself, and associative learning from pairing odor with food deprivation (Cho, Brueggemann, L'Etoile, & Bargmann, 2016). For the purpose of this thesis, I will categorize desensitization as reduced attraction induced by long-term exposure of odor, and aversive learning as reduced attraction induced by pairing odor with food deprivation. During desensitization, the sensory neuron temporarily suppresses its response to odor, as reflected in a decreased response of cell body calcium to odor input. One hypothesis suggested for this inhibition is binding of the beta-arrestin ARR-1 to the activated odor receptor GPCR and subsequent receptor internalization (Palmitessa, et al., 2005). Desensitization may require acute Ca²⁺ signaling in the sensory neuron, although the details of this activity in AWC are unknown (Colbert, Smith, & Bargmann, 1997) (Leinders-Zufall, Greer, Shepherd, & Zufall, 1998).

In appetitive learning, exposing *C. elegans* to butanone in the presence of food results in increased attraction to high concentrations of butanone (Torayama, Ishihara, & Katsura, 2007). A previous study showed that appetitive training (food + odor) and aversive training (starvation + odor) both decrease the calcium response of AWC^{ON} neurons to low concentration of butanone

(Cho, Brueggemann, L'Etoile, & Bargmann, 2016). Therefore, this change cannot explain the contrasting behaviors. At the molecular level, aversive learning requires insulin signals from the AIA interneuron to AWC that drive nuclear localization of a cGMP-dependent kinase, EGL-4; this pathway is not required for appetitive learning (Cho, Brueggemann, L'Etoile, & Bargmann, 2016). The mechanisms of memory storage for both aversive and appetitive learning are not totally understood, but the nuclear translocation of EGL-4 suggests that aversive learning may be associated with transcriptional changes in AWC^{ON} , and in appetitive learning, the activity-regulated CREB transcription factor is essential in AIM interneurons (Arey, Stein, Kaletsky, Kauffman, & Murphy, 2018).

1.4 Insulin pathway and learning in worm and mammals

Another pathway that has been frequently implicated in learning in *C. elegans* is the insulin pathway. A previous study showed that the insulin-like neuropeptide INS-1, secreted from the AIA neuron, is important for aversive olfactory learning (Cho, Brueggemann, L'Etoile, & Bargmann, 2016). Although there was no direct evidence of the receptor that recognized INS-1, it was shown that the insulin pathway effector AGE-1, a Phosphoinositide 3-kinase (PI3K) is required in the AWC^{ON} neuron for aversive learning. Insulin signaling in *C. elegans* also serves in a variety of other functions such as development, longevity, metabolism, and stress resistance. The single gene encoding a *C. elegans* insulin/IGF receptor, *daf-2*, is expressed in neurons, XXX neuroendocrine cells, hypodermis, intestine, and other tissues (Hunt-Newbury, et al., 2007; Kimura, Riddle, & Ruvkun, 2011). In the context of its widespread physiological functions, it is fascinating how insulin signaling also participates in the aversive learning of a specific odor in a specific neuron.

The answer to what enables insulin pathway to be multifunctional in different places might stem from its complexity. *C. elegans* has at least 40 genes that encode insulin-like peptides. These are generally expressed in different subsets of neurons (Li & Kim, 2008). This insulin-like neuropeptide signaling system harbors diverse functions including activation, suppression and pass-through signaling. Furthermore, insulins can work in parallel and in sequence to regulate complicated behaviors. The first insulin-like peptide to be characterized, DAF-28, is an agonist of DAF-2 that regulates development of the alternative dauer larva stage. In this context, INS-4 and INS-6 can also activate DAF-2, while INS-1 and INS-18 inhibit it. Others, like INS-9, INS-31, and INS-19, may signal through DAF-2 to affect other aspects of development, or modulate other insulins (Li & Kim, 2008). Different insulin-like neuropeptides

can also work in parallel in an antagonistic manner to facilitate the balance of a behavior. In pathogen avoidance, INS-16 is secreted by pheromone-sensing neuron ADL and INS-4 is secreted by bacteria sensing neuron AWA. Normally the worms will tend to avoid the pathogens. However, when worms grow in population, creating an overcrowding situation, pheromone is secreted by the worms to signal crowding. This increase in pheromone activates ADL and INS-16 secretion, while inhibiting AWA and INS-4 secretion. As a result, the worms increase their immune response and show more interest in eating the pathogenic bacteria as a group (Wu, et al., 2019). As they are saying: guys, we got too much people (worms), probably not enough food, let's toughen up and eat these pathogenic bacteria together. Furthermore, different insulin-like neuropeptides can also work in sequence by one regulating the secretion of another. In pathogen avoidance learning, INS-7 from the URX sensory neuron antagonizes the insulin/IGF receptor DAF-2 in RIA interneurons, to prevent learning. INS-6 secreted from the ASI sensory neurons suppresses INS-7 production from URX neurons, therefore dis-inhibiting RIA and allowing learning (Chen, et al., 2013).

As a complement to insulin diversity, there are seven alternative splice isoforms of insulin receptor DAF-2 that could be potentially be driven by different promotor elements with distinct features (Tomioka, Naito, Kuroyanagi, & Iino, 2016). For example, the DAF-2c isoform differs from DAF-2a isoform by having an additional 82 amino acids encoded by an alternative exon 11.5. While DAF-2a is expressed in the soma of ASE neuron and signals through the transcription factor DAF-16, DAF-2c is localized to the axon of ASE neuron and controls salt learning independent of DAF-16 (Ohno, et al., 2014). Another isoform of insulin/IGF receptor DAF-2b is not even a membrane bound receptor, and does not participate directly in insulin/IGF signaling. Instead, it is likely to be a secreted protein and functions to sequester circulating

insulin molecules (Martinez, et al., 2020). Therefore, studying insulin/IGF pathway in aversive learning can potentially uncover new mechanisms by which neuronal cells can dramatically expand their functionality using different forms of the same molecular pathway in confined spaces with limited connections.

In human and other mammals, Insulin and Insulin-like Growth Factor (IGF) pathways are well-known for their function regulating sugar transport, caloric intake, and cell proliferation. Depending on the cell type, insulin receptor signaling can utilize a variety of intracellular pathways. Particularly, the mitogen-activated protein kinase (MAPK) pathway and mammalian target of rapamycin complex 1 (mTORC1) pathway regulate cell growth and survival (Saltiel & Kahn, 2001). However, the regulation of glucose transport does not require the MAPK and mTORC1 pathways, but requires the phosphoinositide 3-kinase (PI3K) pathway. In skeletal muscle and fat cells, 95% of the glucose transporter GLUT4 lies dormant in endosomes and the trans-Golgi network. Upon activation of the insulin pathway, the effector AKT of the PI3K pathway facilitates the rapid translocation, targeting and fusion of vesicles containing the glucose transporter GLUT4 to the cell membrane (Leto & Saltiel, 2012).

It was long thought that insulin had no function in the brain until injection of insulin into the brain was shown to decrease food intake and body weight in baboons (Woods, Lotter, McKay, & Jr., 1979). Since then, many studies have shown that insulin and IGF signaling have crucial functions in mammalian CNS development, maintenance, and plasticity (Reviewed in (Ferrario & Reagan, 2018; Dyera, Vahdatpoura, Sanfeliub, & Tropeab, 2016)). Both insulin receptor and IGF receptor are widely expressed in the CNS during development and in the adult brain (Kar, Chabot, & Quirion, 1993; Marks, Jr., Stahl, & Baskin, 1990). Two areas of particularly high expression of insulin and IGF receptor expression are the hippocampus and

hypothalamus. In hippocampus, insulin is important for learning and memory. It has been shown that administering insulin enhances spatial learning in a dose-dependent manner (Moosavi, Naghdi, & Choopani, 2007). Furthermore, aging related insulin decrease and insulin resistance in type II diabetes have been implicated in memory impairment and cognitive loss (Ferrario & Reagan, 2018; Deak & Sonntag, 2012). Remarkably, appetitive learning in *C. elegans* also decreases during aging in a *daf-2* insulin receptor-dependent manner (Kauffman, Ashraf, Corces-Zimmerman, Landis, & Murphy, 2010).

Insulin appears to regulate synaptic transmission by regulating glutamate and GABA receptors in the hippocampus, an important memory-formation center. This has been shown by exogenous administration of insulin into the hippocampus. Insulin regulates the internalization of the AMPA-type glutamate receptor (Beattie, et al., 2000). This internalization is dependent on the phosphorylation of a tyrosine residue on the AMPA receptor, likely by the insulin receptor, which functions as a tyrosine kinase (Ahmadian, et al., 2004). AMPA receptor endo- and exocytosis is regulated by neuronal activity to mediate synaptic plasticity (Huganir & Nicoll, 2013). Downregulation of AMPA receptor by insulin functionally decreases spontaneous firing rate of hippocampal pyramidal neurons and drives the induction of Long-Term Depression in the CA1 region of hippocampus (Lin, et al., 2000). Similar effects of AMPA down-regulation and long-term depression can also be seen with exogenous administration of Insulin-like Growth Factor (IGF) (Wang & Linden, 2000). At the same time, other studies have observed that insulin drives the induction of Long-Term Potentiation by rapid delivery of NMDA-type glutamate receptors to the synapse (Chen & Leonard, 1996; Skeberdis, J. Lan, Zukin, & Bennett, 2001). In addition to glutamatergic signaling, insulin regulates GABAergic signaling by driving the trafficking of GABA receptors at the CA1 region of hippocampus (Jin, et al., 2011). These

discoveries suggest that glutamatergic and GABAergic signaling at synapses in the hippocampus are dynamically regulated by insulin signaling.

In hypothalamus, the most apparent effect of insulin signaling is to regulate metabolism and body weight (Reviewed in (Schwartz, Woods, Jr., Seeley, & Baskin, 2000)). Insulin signaling also regulates the nucleus accumbens (NAc), which controls behavior that is associated with reward and aversion, such as addiction, and depression. The nucleus accumbens (NAc) is part of the system called the mesolimbic pathway. The mesolimbic pathway is a reward-based pathway where a collection of dopaminergic neurons from the ventral tegmental area (VTA) project to the nucleus accumbens (NAc) and olfactory tubercle, which are collectively called the ventral striatum. The mesolimbic pathway is the gateway connecting primary rewards like food to emotional and motivational states (Castro, Cole, & Berridge, 2015). In other words, it directly controls food-derived learning like Pavlovian conditioning and further indirectly controls decision making, or even assignment of values (Ferrario & Reagan, 2018). Both Insulin Receptor (IR) and Insulin-like Growth Factor Receptor IGFR are expressed in the VTA neurons and NAc neurons (Figlewicz, Evans, Murphy, Hoen, & Baskin, 2003), and the VTA and NAc also produce Insulin-like Growth Factor (IGF). In the VTA, application of insulin reduces pre-synaptic glutamate release onto the VTA dopamine neurons. This leads to a long-lasting depression of the excitatory transmission of the VTA dopamine neurons, therefore potentially reducing the urge of food seeking behavior (Liu, Labouebe, Karunakaran, Clee, & Borgland, 2013). In NAc, it's even more fascinating that activation of Insulin Receptor (IR) increases pre-synaptic glutamate release, while the activation of Insulin-like Growth Factor Receptor (IGFR) decreases pre-synaptic glutamate release (Fetterly, et al., 2021). In addition to insulin/IGF regulation of NAc and VTA neurons through control of glutamate release, dopamine neuron-

derived IGF-1, which is induced by neuronal activity, modulates dopamine neuron firing, dopamine synthesis and ultimately dopamine-dependent behaviors (Pristerà, et al., 2019).

We have the unique advantage of using advanced genetic and imaging technology in *C. elegans* to dissect the mechanism of aversive learning, and function of insulin signaling pathways in learning behaviors at the synapse. This could contribute to further understanding of how memory is formed and stored in our brain, and therefore to further understand our brain in general.

CHAPTER 2.

**Behavior screening and discovery of *ist-1*
as a gene required for aversive olfactory learning**

Chapter 2 INTRODUCTION

C. elegans is the first multicellular organism that had its complete genome sequenced in 1998. Since then its 100 Mb genome has become one of the most well studied and well annotated genomes compared to other eukaryotic organisms. This knowledge base combined with powerful genetic methods makes *C. elegans* very attractive for exploring new molecular mechanisms that can be translated to higher organisms for understanding biological processes and eventual therapeutic development. One of its advantages is the ease of generating and maintaining mutant *C. elegans* animals to be used for genetic screening. Mutants can be generated by chemical mutagens, ionic radiation, or recently by CRISPR-Cas9 induced mutations. Once the worm strain has been established by homozygosing the mutation, it usually requires no special maintenance as long as it's viable, since the self-fertilizing hermaphrodite can propagate even as very sick strains. Worm strains carrying mutations can also be frozen in liquid nitrogen for long-term storage. As a result, there is a large deposit of mutant animal strains in the Caenorhabditis Genetics Center (CGC), and in the Bargmann Lab, and others labs as well. Therefore, it was possible for me to propose using a targeted forward genetic screen to uncover new genes, or existing genes with unknown functions in aversive learning.

Although many studies have been published about butanone aversive learning, the conditions of training and boundary between mixed behaviors are not well defined. Aversive learning is usually referred as the combination of Unconditional Stimulus (US), in this case food deprivation, plus the Conditional Stimulus (CS), in this case butanone exposure. However, there is an embedded component here that can be called desensitization, in which exposure to a strong CS (odor exposure) alone without US (food deprivation) often leads to subject become less sensitive to the CS. Much like when someone get too close to the flower for a prolonged time,

the scent tends to become fainter. I modified a number of features of the training and testing conditions to allow separation of desensitization behavior from the aversive learning behavior.

Chapter 2 RESULTS

2.1 Conditions of chemotaxis

The basic assay conditions used for aversive learning are shown in Figure 2.1. Unlike desensitization, which requires only the presence of odor, associative aversive learning requires the pairing of odor with food deprivation. However, these forms of behavioral plasticity have been difficult to disentangle systematically.

I set off to refine the training and chemotaxis conditions to more consistently test animals' odor preference state in all chemotaxis conditions. Previous studies showed that after food deprivation for about 15 minutes, *C. elegans* started to be motivated to venture further to look for food (López-Cruz, et al., 2019). Therefore, I asked whether the time of food deprivation affects chemotaxis as well. I discovered that animals do not chemotax well to butanone unless they have been food-deprived for at least 15 minutes, and therefore standardized the washing conditions to include a 15-minute food deprivation step before they were tested on the chemotaxis plate (Figure 2.2). I also noted that the chemotaxis plate has a different ionic composition from the training plate and the wash buffer, a historical remnant of the fact that the conditions were first developed to test salt chemotaxis. To avoid conflicting sensory signals, I switched the training plate, wash buffer and chemotaxis plate to the same salt composition to the NGM plates that the worms were raised on (NGM buffer and NGM chemotaxis plate). This adjustment in the protocol increased the difference in results between control and experimental groups and improved the consistency of the experiments.

In addition to desensitization and aversive learning, a different type of olfactory plasticity is called appetitive olfactory learning, or enhancement. *C. elegans* is innately attracted to low

concentrations of butanone (1:1000 dilution), but less attracted to high concentrations of butanone (1:10).

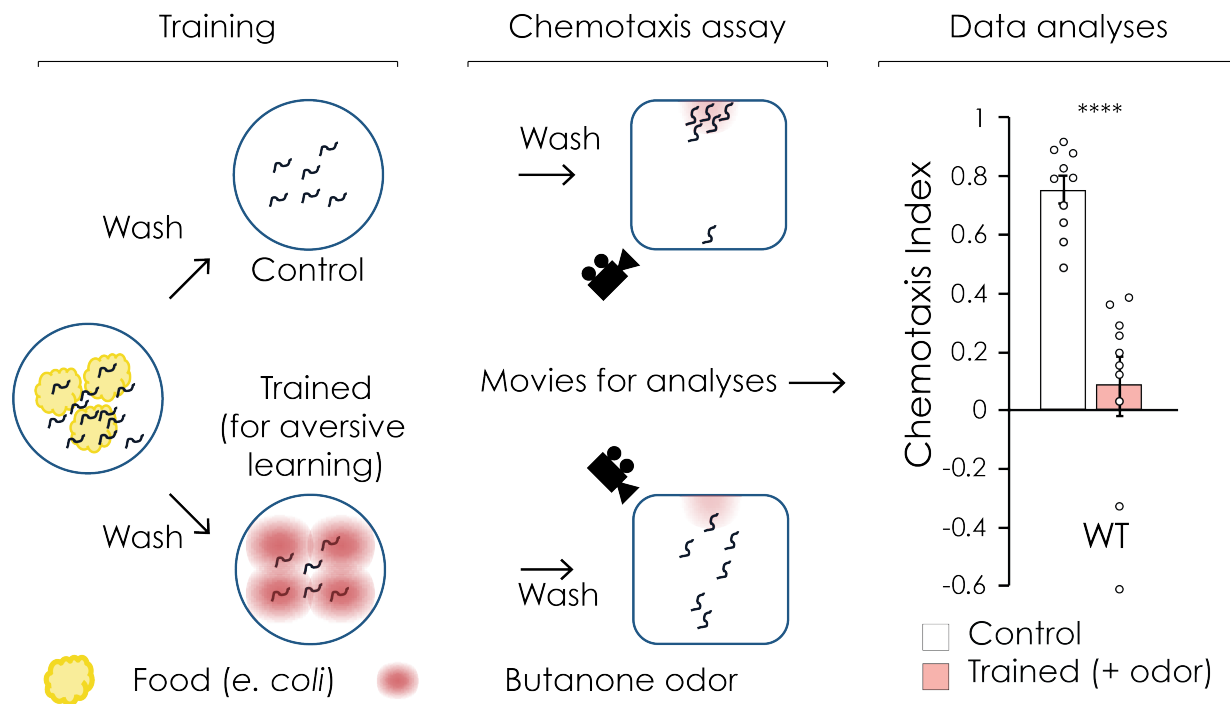


Figure 2.1 Schematic of experimental procedure used to study aversive learning behavior.

Schematic of experimental procedure used to study aversive learning behaviors, the analyses method used and example results. To study aversive learning behavior, *C. elegans* worms were first grown and maintained on NGM agar plates seeded with *E. coli* bacteria as their food. Young adult worms were then washed off food with buffer and moved onto training plates with different conditions. In aversive learning, worms were subjected to food deprivation with odor exposure, and the controls were subjected to food deprivation without odor, for 90 minutes before they were washed again and placed in the middle of a square chemotaxis plate. A small spot of diluted odor was placed at one side of the plate and a spot of solvent was placed on the opposite side. The lid of the plate was closed for 60 minutes, while worm behavior was tracked by video cameras. The videos from the camera were analyzed by custom MATLAB software to track the position of each worm over time. Parameters calculated included distance to odor over time, head angles, and whether they were moving forward, reversing, or doing an omega turn at any given time. Animals were either only deprived from food (control, white bars), or subjected to food deprivation with butanone odor (20 μ l) for 90 mins (Trained, pink bars). Animals were allowed to chemotax for 60 min to 2 μ l of 1:1000 butanone diluted in EtOH with control odor spot of 2 μ l EtOH only.

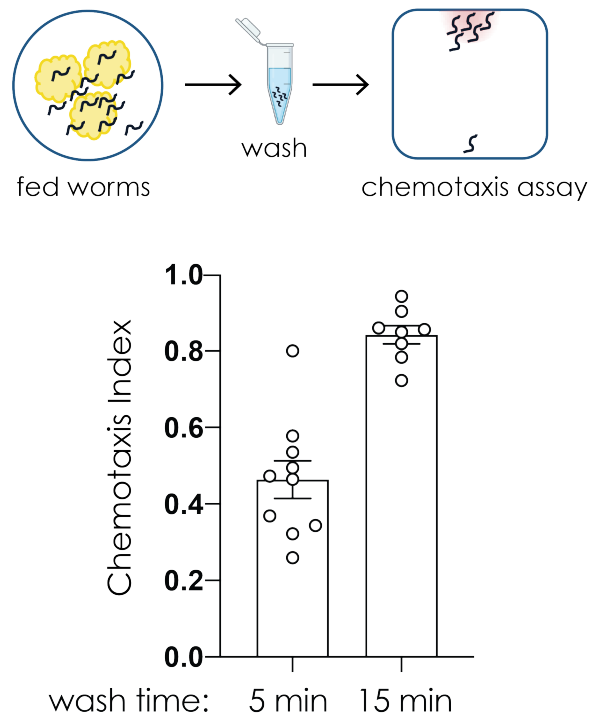


Figure 2.2 Schematic and chemotaxis index of fed vs food deprived worms.

Fed *C. elegans* do not chemotax well to butanone when washed in buffer for only five minutes, but chemotax efficiently when washed in buffer for 15 minutes. This 15 min wash time is used to test animals that were desensitized but not food deprived during the 90 min training.

2.2 Conditions of different types of olfactory learning

To better understand the conditions required for aversive learning, desensitization, and appetitive learning, I systematically varied the butanone concentration used for training (Figure 2.3A), and the butanone concentration in the test chemotaxis assay (Figure 2.3B). In the past, 20 ul of butanone was used for aversive conditioning and 2 ul for appetitive conditioning. I discovered that chemotaxis to 1:1000 butanone was suppressed by training with 20 ul of butanone regardless of whether the animals were fed or food deprived (Figure 2.3C). I define the food-independent response to training with >20 ul butanone as desensitization.

Next, I lowered the training concentrations of butanone, while continuing to test at 1:1000 butanone. I found that as little as 0.2 ul of butanone paired with food deprivation suppressed chemotaxis to 1:1000 butanone, but the presence of food eliminated this effect. I define the suppression of chemotaxis by 2 ul of butanone under food deprivation as aversive learning.

Finally, I tested chemotaxis to 1:10 butanone. I observed an enhanced response after pairing a wide range of butanone concentrations with food (Figure 2.3). I define appetitive learning as the food-dependent enhancement of chemotaxis to 1:10 butanone.

Combining a focused screen of candidate mutants with serendipity, as described below, I identified *ist-1* (insulin receptor substrate-1) as a new gene required for aversive learning. I tested *ist-1* mutants in each of these learning assays, and in basal chemotaxis, and found that *ist-1* was normal in chemotaxis to high and low butanone concentrations, appetitive learning, and desensitization. However, *ist-1* was almost completely defective in aversive learning after training with 0.2, 2, or 20 ul butanone. It was also defective in learning after training in food with 20 ul butanone, a concentration at which both desensitization and aversive learning are observed.

Together, this work suggests that desensitization (odor exposure) and aversive learning (odor exposure with starvation) are genetically distinct processes: the newly identified function of *ist-1* is essential for aversive learning, but only partly required for odor desensitization. The *C. elegans ist-1* is a homolog to the human Insulin Receptor Substrate (IRS). In the following chapters I decode the molecular mechanism of *ist-1* action in aversive learning.

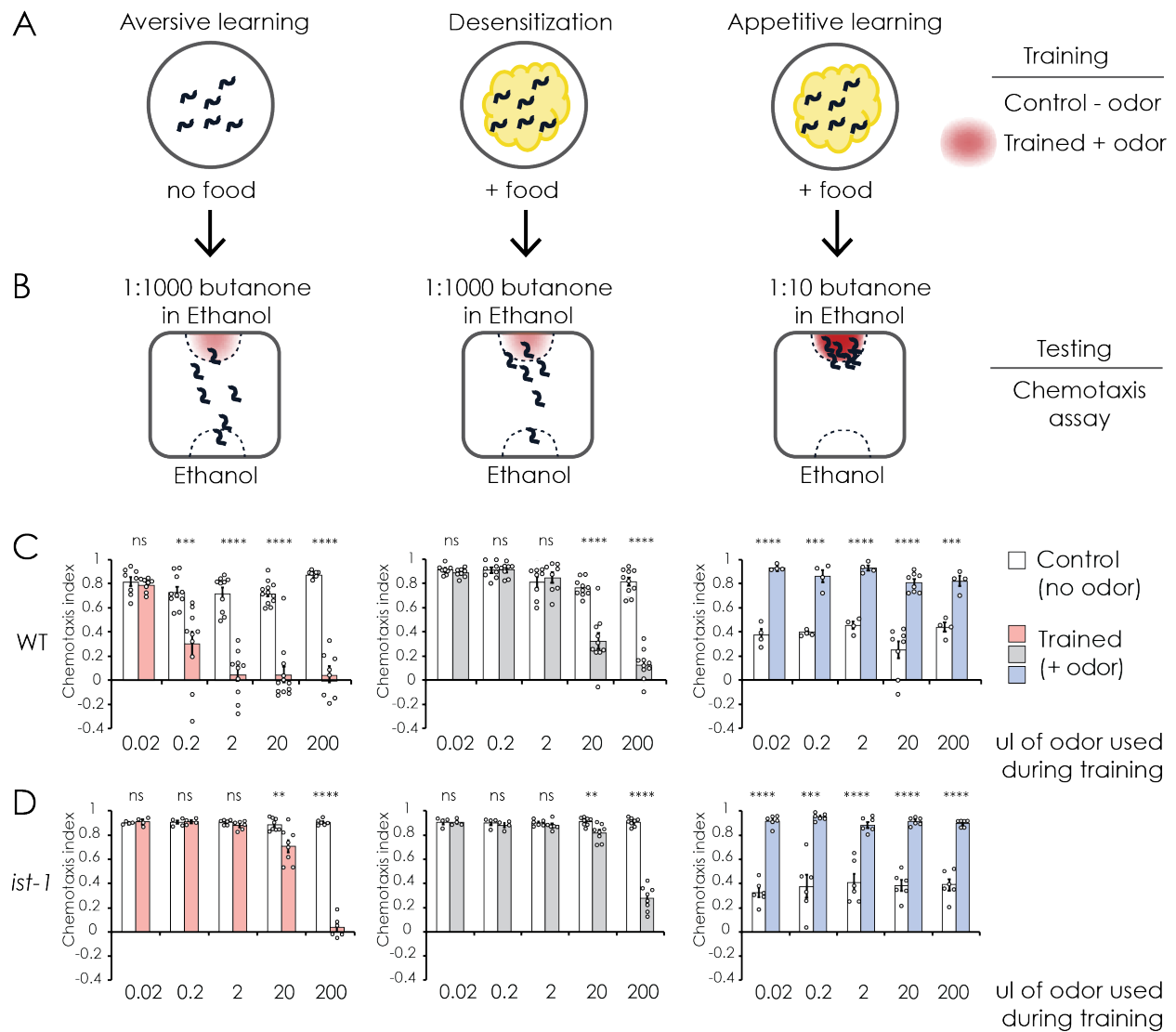
Figure 2.3 Amount of butanone required for different types of behavioral plasticity in wild-type and in learning deficient *ist-1* mutant animals.

Associative learning to butanone has previously been divided into aversive learning and appetitive learning, distinguished by whether butanone was paired with food versus food deprivation, and also by the concentration of odor used for the final chemotaxis assay. I have developed training conditions that reliably distinguish desensitization by butanone exposure, which occurs regardless of the presence of food, from true aversive learning. The key difference is the concentration of butanone required. Desensitization requires high concentrations of butanone during training (>2 ul), whereas both aversive learning and appetitive learning are induced by lower butanone concentrations (≤ 2 ul). (A,B) show training (A) and testing (B) conditions for each type of behavior scheme. (C,D) Chemotaxis index of wild-type (C) and *ist-1* mutant (D) animals resulting from different types of training shown above, in panels (A) and (B).

In aversive learning experiments, animals were either only deprived of food (Control, white bars), or subjected to food deprivation with 0.02-200 ul butanone odor for 90 mins (Trained, pink bars). Animals were allowed to chemotax for 60 min to 2 ul of 1:1000 butanone diluted in EtOH with control odor spot of 2 ul EtOH.

In desensitization experiments, animals were either fed (Control, white bars), or exposed to 0.02-200 ul butanone odor for 90 mins while on food (Trained, grey bars). Animals were allowed to chemotax for 60 min to 2 ul of 1:1000 butanone diluted in EtOH with control odor spot of 2 ul EtOH.

In appetitive learning experiments, animals were either fed (Control, white bars), or exposed to 0.02-200 ul butanone odor for 90 mins while on food (Trained, blue bars). Animals were allowed to chemotax for 60 min to 2 ul of 1:10 butanone diluted in EtOH with control odor spot of 2 ul EtOH only.



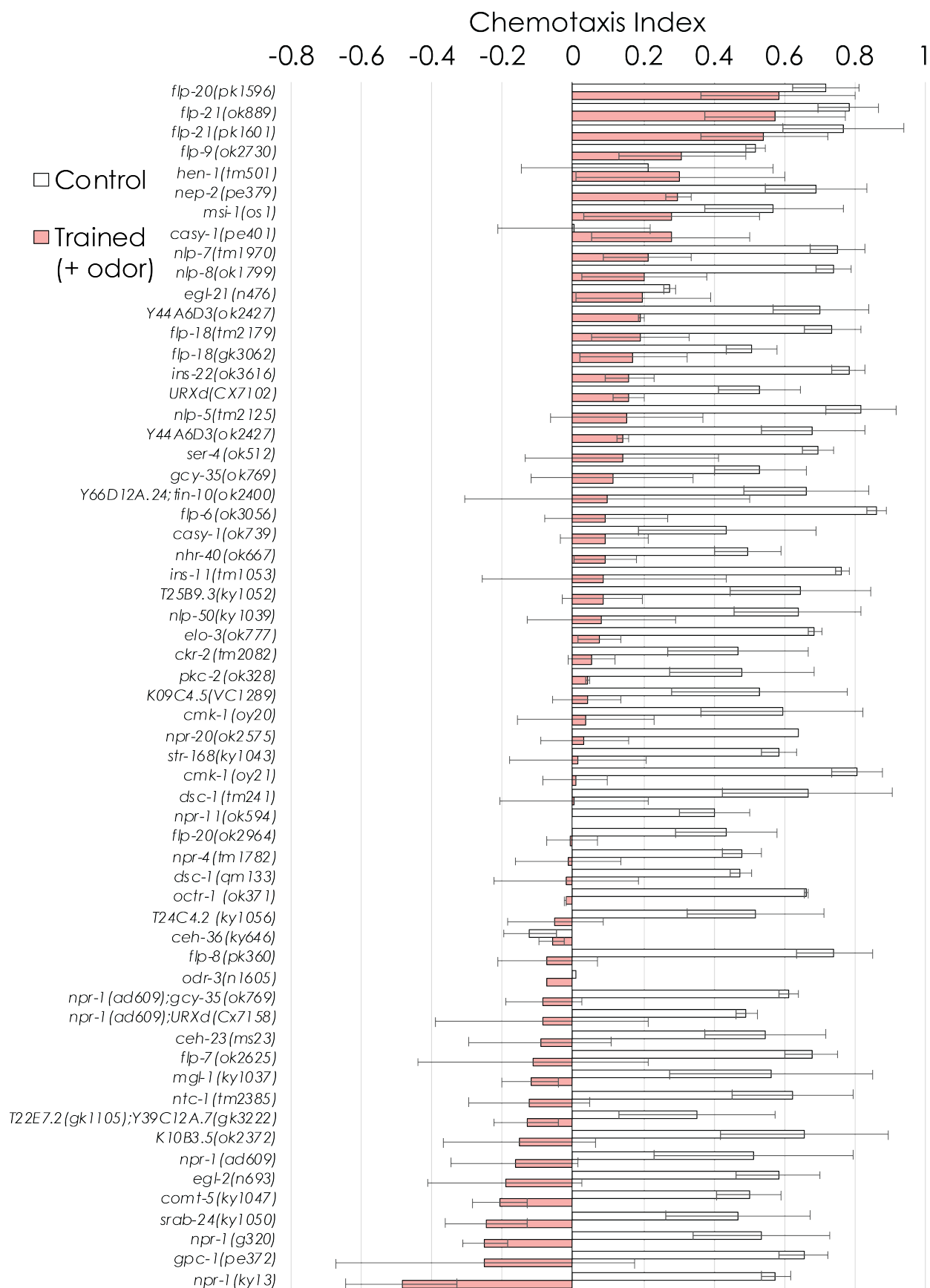
2.3 Identifying mutants with aversive learning defects

With a better understanding of the behavioral paradigm, I conducted a candidate gene screen to uncover new mechanisms of aversive learning. The genes I chose for analysis were guided by RNA-seq analysis of genes enriched in AWC, based on a published dataset (Cao, et al., 2017) and on an unpublished experiment conducted by Christine Cho in the lab and analyzed by me, in which genes expressed in AWC and a few other cell types were labeled in food and food deprived animals (see Appendix). In addition to genes directly selected from the RNA-seq analyses, I also examined gene candidates in neuropeptide genes including insulin-like peptides (ins), FMRFamide-related peptides (flp), and other neuropeptides (nlp), neuropeptide receptors, genes indicated in caloric regulation, and genes previously implicated in learning in other type of habituation or associative learning paradigms in *C. elegans*. Strains were obtained from the *Caenorhabditis* Genetics Center, the Bargmann lab strain collection, or other labs, and in some cases I generated new alleles with CRISPR/cas-9.

Each test strain was subjected to aversive learning (20 ul butanone paired with food deprivation) using food deprived animals as controls for the ability to chemotaxis (Figure 2.4). The most striking phenotypes in this screen were observed in *flp-20(pk1596)*, *flp-21(pk1601)* and *flp-21(ok889)* animals, which were highly defective in aversive learning but had normal baseline chemotaxis. I found an unanticipated opposite phenotype in *npr-1(ky13)*, *npr-1(g320)*, and *npr-1(ad609)* animals: they showed exaggerated aversive learning, with strong butanone repulsion after training. While these results are shown so that they can be pursued by others in the future, and I describe some preliminary analysis here, readers should be cautioned that none of these genes that showed interesting results in this screen ended up as the gene I pursued for study.

Figure 2.4 Candidate gene screen for mutants with defects in aversive learning.

Chemotaxis index results of mutants screened for defects in aversive learning. Candidate gene mutant animals were subjected to aversive learning to butanone. Animals were either only deprived from food (control, white bars), or subjected to food deprivation with 20 ul butanone for 90 mins (trained, pink bars). This amount of butanone elicits full aversive learning and partial desensitization, and therefore might detect defects in either process. The order of genes was ranked from low to high by the chemotaxis index of the animals subjected to aversive learning.



I first focused on the *npr-1* gene. Three different *npr-1* mutants were not only less attracted to butanone after training, but were repelled by the butanone odor and accumulated on the opposite side of the chemotaxis plate. NPR-1 is a G protein-coupled neuropeptide receptor that has sustained a gain-of-function mutation in the wild-type Bristol N2 strain during cultivation in laboratory conditions. In fact, one of the three mutations that showed an increase in aversive learning was *npr-1(g320)*, the ancestral *npr-1* allele found in wild strains. Several peptide ligands for NPR-1 have been identified, including FLP-21, but as none of these appear to have the same defects as loss of function mutations, it is possible that the Bristol N2 NPR-1 allele has ligand-independent constitutive activity.

Wild isolates of *C. elegans*, as well as *npr-1* mutant N2 Bristol animals, display strong avoidance of environmental oxygen. They tend to aggregate on the thickest part of the bacterial lawn to avoid oxygen; if they cannot find low oxygen levels, they are hyperactive (de Bono & Bargmann, 1998) (Cheung, Cohen, Rogers, Albayram, & de Bono, 2005) (Gray, Hill, & Bargmann, 2004). These *npr-1* behaviors are suppressed by mutations that inactivate the soluble guanylate cyclases required for oxygen sensation (*gcy-35,36*), and by mutations that inactivate the oxygen-sensing URX, AQR, and PQR neurons. To ask whether *npr-1*'s effect on aversive learning is related to its oxygen avoidance, I tested an *npr-1(ad609); gcy-35(ok769)* strain and an *npr-1(ad609); URXd* strain in which URX, AQR, and PQR neurons were killed by caspase expression. In both cases, the strains had wild-type N2-like behaviors, with normal butanone chemotaxis and normal (rather than exaggerated) aversive learning after pairing butanone with food deprivation (Figure 2.5). I conclude that the exaggerated aversive learning in *npr-1* results from a signal from the oxygen-sensing neurons, and speculate that high oxygen might act as a second aversive unconditioned stimulus (in addition to food deprivation) in the training

paradigm. Notably, training is conducted on open plates, which have higher oxygen concentrations than the bacterial lawns that are used to grow animals. The FMRFamide-related neuropeptide FLP-21 is a known ligand of NPR-1, but *flp-21* mutants did not share the exaggerated learning of *npr-1* mutants. Instead, two different *flp-21* alleles were highly deficient in aversive learning. This gene is an interesting candidate for further study, but was not pursued further.

A strain bearing a mutation in a second FMRFamide-related peptide, *flp-20(pk1596)*, was highly deficient in aversive learning. However, a second *flp-20* mutant strain, *flp-20(ok2964)*, had normal aversive learning although it was also predicted to be a null allele. I then asked if the learning defect in the *flp-20(pk1596)* strain could be rescued by a genomic fragment that contained the *flp-20* gene. *flp-20* genomic fragments failed to rescue the behavior of *flp-20(pk1596)*. A parsimonious explanation for these results is that the aversive learning defect was not caused by *flp-20*, but rather due to a mutation in a different gene in the same worm strain. I tested this possibility by backcrossing *flp-20(pk1596)* with wild-type animals for eight generations, genotypically selecting *flp-20(pk1596)* animals by PCR every two backcrosses. After 2, 4, 6, and 8 backcrosses, the progeny of four mutant animals were tested for aversive learning behavior. All strains were defective in aversive learning after 2, 4, and 6 backcrosses. After 8 backcrosses, 3 of 4 tested strains showed no defect in aversive learning. Genomic DNA of the aversive-learning deficient backcrossed strain was sequenced on an Illumina Hi-seq at the Genomics Resource Center of the Rockefeller University, and the sequence was analyzed by Patrick McGrath, a former lab member. One of the background mutations was a T->G change at the splicing acceptor site at the end of the 2nd exon of the *ist-1* (insulin receptor substrate-1) gene (Figure 2.6). As described in the following section, this mutation is the cause of the aversive

learning defect. Ironically, *ist-1* was not indicated in the RNA-seq data set, nor was it on any list of candidates that we chose for screening based on other hypotheses or criteria. Instead, *ist-1* arose as a background mutation in a heavily mutagenized strain that also had a mutation in the candidate gene *flp-20*. This is not uncommon for *C. elegans* mutant strains generated by radiation or chemical mutagens, as *flp-20(pk1596)* was, and in fact two other genes studied in the lab were identified in similar ways (Larsch, et al., 2015; López-Cruz, et al., 2019). This serendipity shows that there is still much to discover from hypothesis-free forward genetics.

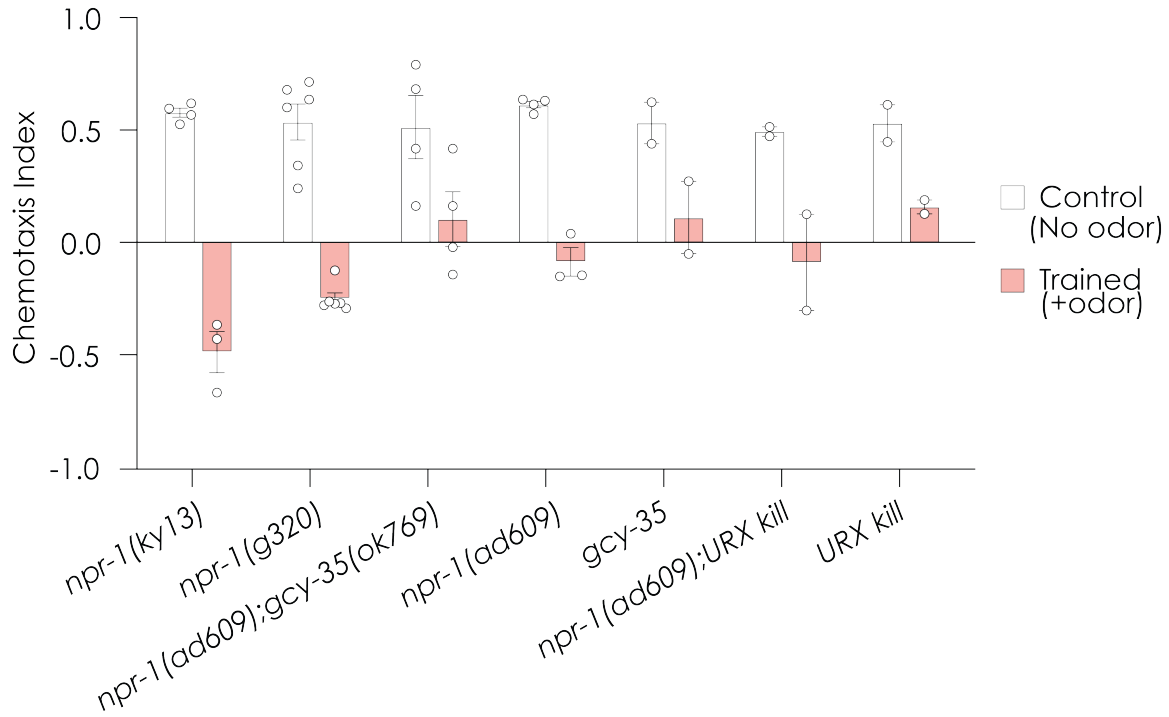


Figure 2.5 Chemotaxis index of *npr-1* mutants and *npr-1* mutants with oxygen sensing defects.

Chemotaxis index of *npr-1* mutant animals and *npr-1* mutant animals in which oxygen sensation (*gcy-35*) or oxygen sensing neurons (*URX kill*) were knocked out. Animals were either only deprived from food (control, white bars), or subjected to food deprivation with butanone odor (20 ul) for 90 mins (Trained, pink bars).

2.4 Genetic characterization of *ist-1*

To evaluate the possibility that *ist-1* might be the gene responsible for the aversive learning phenotype, a strain bearing a deletion in the *ist-1* coding region (*ist-1(ok2706)*) was obtained from the *Caenorhabditis* Genetics Center and tested for aversive learning. *ist-1(ok2706)* had normal butanone chemotaxis but was defective for aversive learning to butanone (Figure 2.6). The 1873 base pair deletion of *ok2706* spans exons 10-15, which encode a conserved domain predicted to bind to phosphatidylinositol-3-kinase (PI3K), an essential substrate of the insulin receptor (Figure 2.6). Unlike *ist-1(ky1071)*, the mutation identified serendipitously, *RB2621 ist-1(ok2706)* also had a phenotype of slow growth and low brood size. Backcrossing *ist-1(ok2706)* twice to the Bristol N2 wild-type strain resolved the slow growing phenotype, while the aversive learning phenotype was retained. The new strain was assigned the number CX17790 and was used in all subsequent experiments.

The *ist-1* gene is predicted to encode four mRNAs, which differ because of different initiation sites and 5' exons (*ist-1b/e* versus *ist-1c/d*) or because of different internal splicing that included or excluded two internal exons (*ist-1b/c* versus *ist-1d/e*). To ask whether specific isoforms were important for *ist-1* activity, I used CRISPR-cas9 mutagenesis to make small indels in the coding region specific to the *ist-1b/e* long isoforms. These two strains showed significant aversive learning defects, but were not as severe as *ky1071*, *ok2706*, or *ky1075*, another CRISPR-cas9-induced indel strains that I generated that inactivated all isoforms of *ist-1*. I conclude that the long isoforms are important for aversive learning, with some contribution from the short isoforms, although my experiments do not distinguish whether the importance of the long isoform derives from its coding sequence or its site of expression.

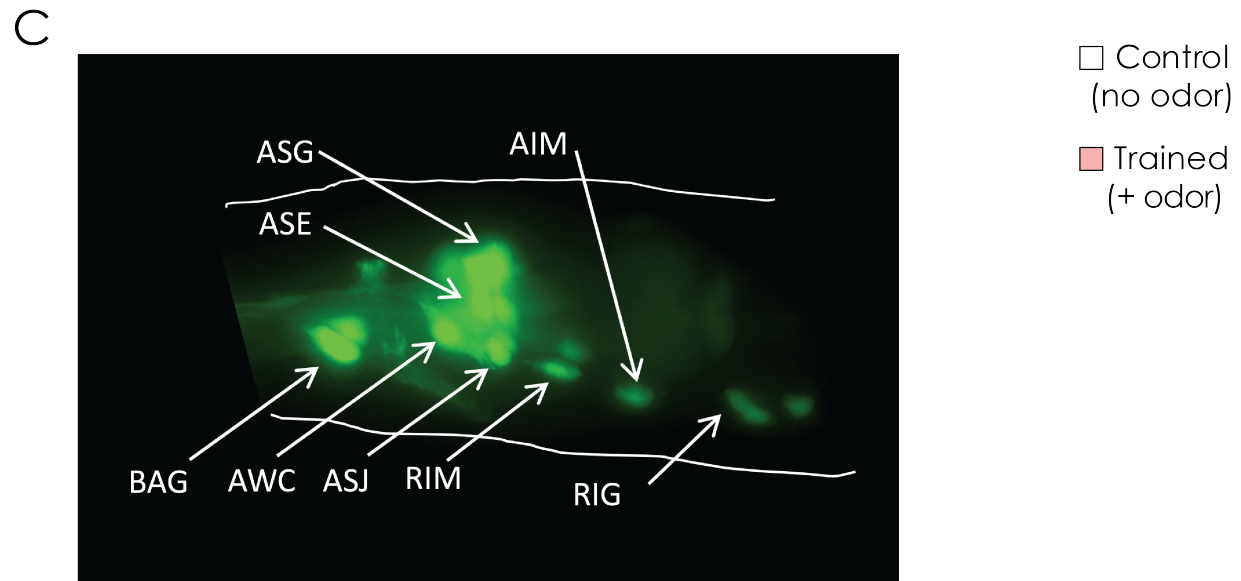
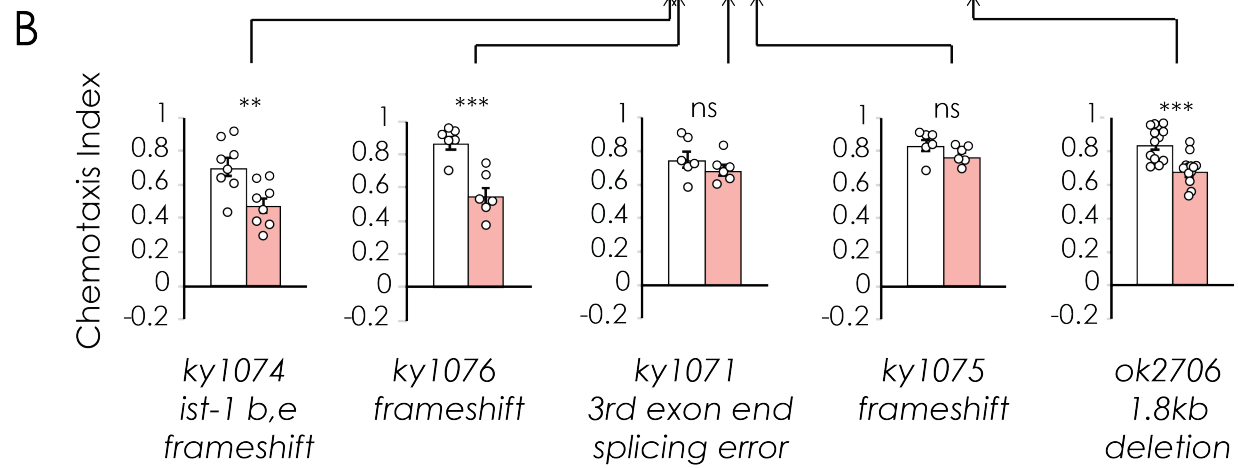
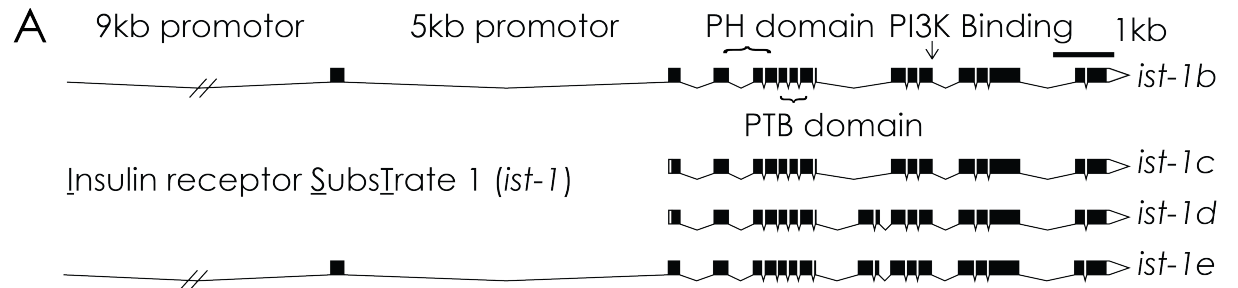
I next examined the expression pattern of *ist-1* by making GFP fusion genes. The *ist-1*

Figure 2.6 Genetic structure, mutant alleles and expression pattern of *ist-1* gene.

A) Genomic structure of the *C. elegans* insulin receptor substrate-1 gene. There are four known isoforms of *ist-1* derived from alternative promoters and alternative splicing. Solid blocks correspond to exons while lines connecting them correspond to introns. The location of mutation in the mutant alleles are indicated by a red line or bar. *ky1071* was a background mutation discovered in the *flp-20(pk1596)* strain. *ok2706* was obtained from CGC. *ky1074*, *ky1076* and *ky1075* were generated by targeted CRISPR/cas-9 mutagenesis. Although the trained animals from some groups are significantly different from control, they all have significant aversive learning defects compared to wild type.

B) Chemotaxis index of different alleles of *ist-1* mutant animals. Animals were either only deprived from food (control, white bars), or subjected to food deprivation with butanone odor (20 ul) for 90 mins (Trained, pink bars).

C) Expression pattern of *ist-1*, based on a GFP fusion to a 14 kb fragment encompassing 9 kb upstream of the first exon, which is the site of initiation of two isoforms *ist-1b* and *ist-1e*, and 5 kb upstream of the second exon, the site of initiation of two additional isoforms. Translation of the shorter isoforms *ist-1c* and *ist-1d* is initiated near the site mutated in *ky1071*.



gene is separated from the next gene 5' to the coding region by a 9 kb interval, which might contain promoter and enhancer elements. In addition, a long (~5kb) first intron separates the initiation site of the long *ist-1* isoforms from that of the shorter isoforms. In *C. elegans*, it is common that long introns in the beginning of the gene with multiple isoforms encode regulatory sequences. Taking these issues into account, I used both the 9 kb genomic region only (referred as the 9 kb promotor) and the 9 kb genomic region plus first exon and intron (referred as the 14 kb promotor) to drive the expression of eGFP in worms using pSM expression plasmid. While the 9 kb promotor did not give any visible fluorescent expression, the 14 kb promotor gave strong and reliable eGFP expression in 8 pairs of head neurons including AWC, ASJ, ASE, ASG, BAG, RIM, AIM, and RIG, but not in other parts of the body. These neuronal assignments were performed in L2 larval stage animals by a combination of DIC imaging and comparison to other known neuronal promoters. These neurons include chemosensory neurons (AWC, ASJ, ASE, ASG, BAG) and interneurons (RIM, AIM, and RIG). (Figure 2.6). An expression pattern exclusively in neurons suggest that *ist-1* might function to regulate behavior. Subsequent to this work, the expression of *ist-1* has been characterized in unbiased single-cell RNA sequencing experiments, and shown *ist-1* is expressed in ASE, BAG, PVT, AWC, RIR, ASG, ASK, AWB, RIG, AVG, ASH, AIM, AFD, ASI, RIC, AIB and HSN using the #4 (most stringent) data filtering method (Cao, et al., 2017; Hammarlund, Hobert, III, & Sestan, 2018; Taylor, et al., 2020).

To further narrow down the site of *ist-1* action, I conducted additional rescue experiments including cell specific rescues. I first injected the fosmid WRM062cC02 that contained the genomic fragment flanking the entire *ist-1* gene into the *ist-1(ky1071)* strain. Successful rescue of the aversive learning behavior by the fosmid confirmed that *ist-1* was indeed required for

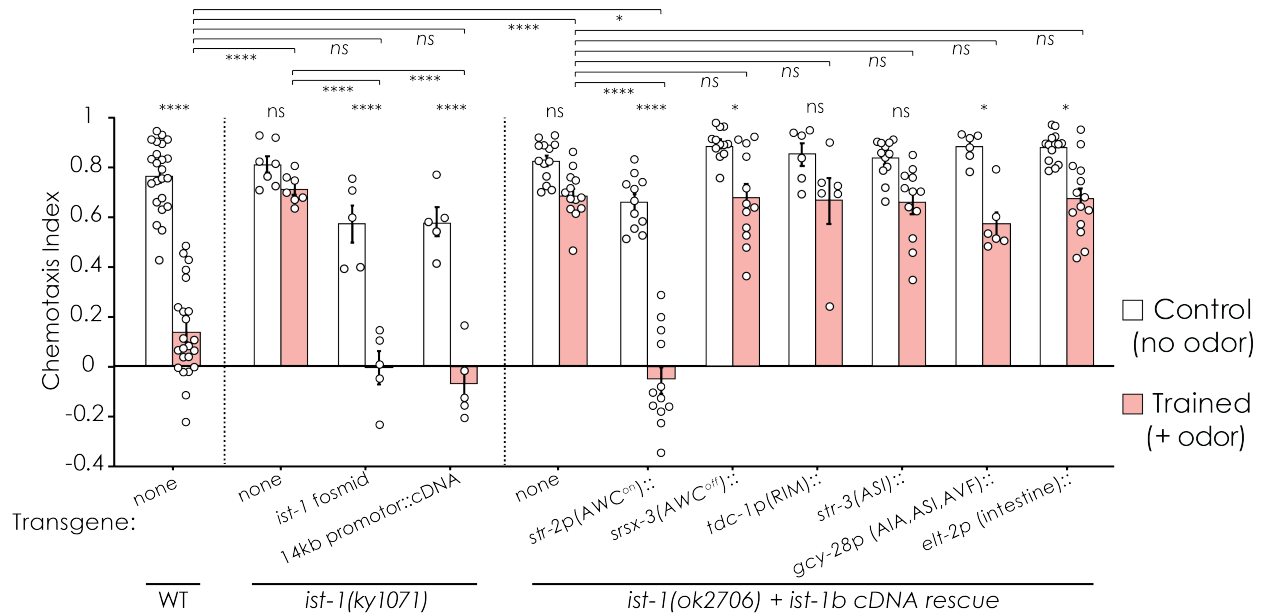


Figure 2.7 Genomic and cell-specific rescue of *ist-1*.

Chemotaxis index of different alleles of *ist-1* mutant animals and rescue of *ist-1* mutations with genomic fragments and cDNAs under different promoters. Animals were either only deprived from food (control, white bars), or subjected to food deprivation with butanone odor (20 μ l) for 90 mins (Trained, pink bars). Left, full rescue of *ky1071* mutants with a fosmid covering the entire genomic sequence of *ist-1* or a 14 kb promoter fragment driving an *ist-1b* cDNA. This strain included the original *flp-20* mutation, but was fully rescued by *ist-1* clones. Right, rescue of *ist-1(ok2706)* mutants with the *ist-1b* cDNA under different cell-specific promoters. Only the *str-2* promoter that expresses *ist-1* in AWC^{ON} rescued aversive olfactory learning.

aversive learning. I then cloned a full-length *ist-1b* cDNA from cDNA that was reverse-transcribed from worm RNA extract, created an expression construct with the 14 kb promoter region of *ist-1* driving the *ist-1b* cDNA, and injected it into the worms. This construct was sufficient to rescue aversive olfactory learning in the *ist-1(ky1071)* strain. I then subcloned the *ist-1b* cDNA under a cell-selective promoter for the AWC^{ON} neuron that senses butanone (*str-2* promoter, which is also weakly expressed in ASI neurons and intestine), and under promoters for other neurons and tissues functionally connected with the AWC^{ON} neuron. These neurons and tissues included the AWC^{OFF} neuron (*srsx-3* promoter), RIM neuron (*tdc-1* promoter), ASI neuron (*str-3* promoter), AIA, AFD, AVK neurons (*gcy-28* promoter), and the intestine (*elt-2* promoter). I established worm strains carrying each of these rescue constructs in the *ist-1(ok2706)* background and subjected them to behavior testing of aversive learning. Of these promoters, only the *str-2* promoter that drive *ist-1* cDNA in AWC^{ON} neuron was sufficient to fully rescue butanone aversive learning (Figure 2.7). All other promoters driving *ist-1* did not rescue aversive learning. Therefore, *ist-1* functions autonomously in the AWC^{ON} neuron to regulate aversive learning to butanone.

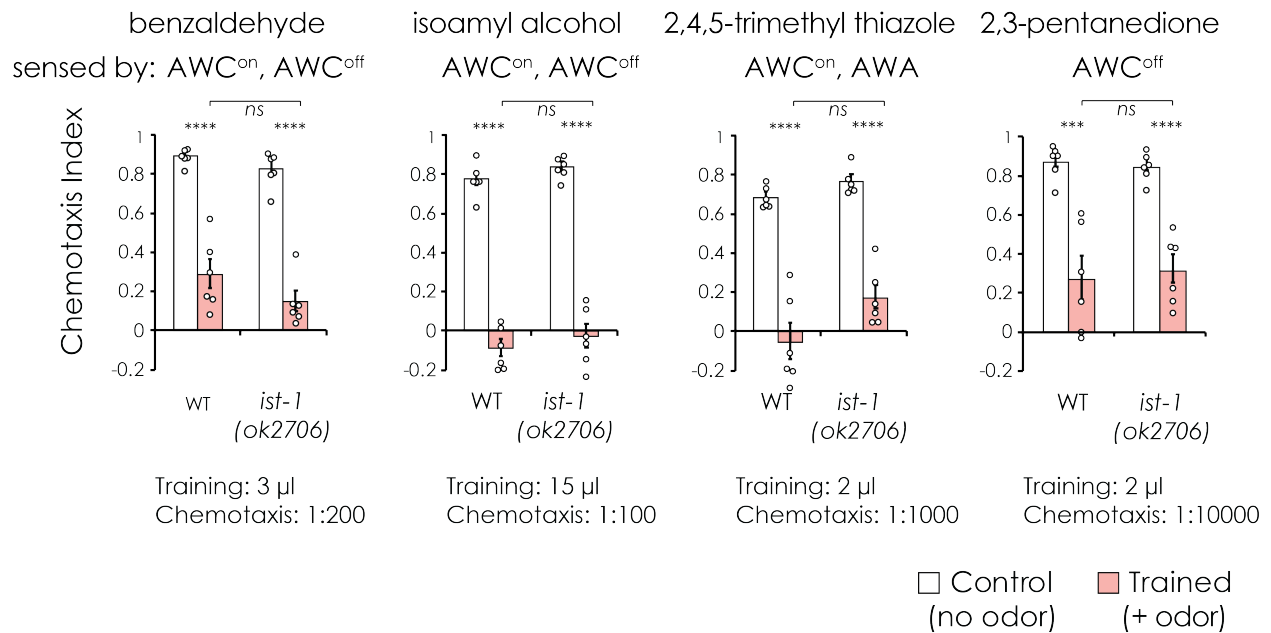


Figure 2.8 *ist-1* mutants have normal aversive learning to several other odors.

Chemotaxis index of wild-type and *ist-1(ok2706)* mutant animals tested for aversive learning to benzaldehyde, isoamyl alcohol, 2,4,5-trimethyl thiazole, and 2,3-pentanedione. Animals were either only deprived from food (Control, white bars), or subjected to food deprivation with different odors for 90 mins (Trained, pink bars). Animals were allowed to chemotax for 60 min to 2 μ l of different odors diluted in EtOH with control odor spot of 2 μ l EtOH. Concentration of odors used for training and chemotaxis assay are consistent with previously published studies (Colbert & Bargmann, 1995; Wes & Bargmann, 2001). When compared to wild-type animals, *ist-1(ok2706)* did not appear to have a defect in aversive learning to benzaldehyde, isoamyl alcohol, 2,3-pentanedione, and 2,4,5-trimethyl thiazole.

2.5 *ist-1* mutants and other odors sensed by AWC neurons

The AWC neurons sense multiple odors in addition to butanone, which is exclusively sensed by AWC^{ON}. Both AWC^{ON} and AWC^{OFF} detect benzaldehyde and isoamyl alcohol, AWC^{ON} and AWA detect 2,4,5-trimethylthiazole, and AWC^{OFF} detects 2,3-pentanedione. To my surprise, *ist-1* mutant did not show aversive learning defects odors other than butanone (Figure 2.8). One hypothesis is that butanone is the only odor that is sensed mainly by AWC^{ON} neuron, while other odors are sensed by at least one another neuron other than AWC^{ON} as well. In this possibility, *ist-1* could be uniquely important for sensory regulation of AWC^{ON}. Another hypothesis is that at high volume, odors can be toxic to *C. elegans*. The toxicity effect was seen in ~ 5 ul 100% benzaldehyde, ~20 ul 100% isoamyl alcohol or ~200 ul 100% butanone placed on the lid of the plate during training, which *C. elegans* appear to be temporarily immobilized after training (My result and mentioned in (Colbert & Bargmann, 1995; Bargmann, Hartwig, & Horvitz, 1993)). Also, 100% Benzaldehyde can repel *C. elegans* off the food lawn, a behavior that is dependent on the AWB neuron which governs avoidance (Harris, et al., 2019). It is also possible that chemical toxicity could cause aversive learning through a different unconditional stimulus (cellular stress) that is not present during butanone aversive learning (food deprivation) (Hajdú, Gecse, Taisz, Móra, & Söti, 2021). Among the odors tested, butanone has been shown to be produced by bacteria that can be used by *C. elegans* as a food source, therefore having biological relevance (Worthy, Rojas, Taylor, & Glater, 2018). It is also possible that *ist-1* is required only for aversive learning to odors sensed selectively by AWC^{ON}, and not required for other forms of sensory learning. However, since different odor chemicals have different vapor pressure and biological activity, a dose-response concentration of training and chemotaxis might uncover aversive learning defects to additional odors.

Chapter 2 DISCUSSION

C. elegans has state-dependent attraction to butanone. While animals starved for at least 15 minutes efficiently chemotax to low concentration butanone (a 2 ul spot of 1:1000 in plate), fed animals did not. Defining this minimum time of food deprivation was required to assess the effects of butanone training, much like in Pavlov's situation where if the dog is happy and fed, they might not care about the bell at all, and it would be impossible to test whether they get desensitized by the bell if you ring it all the time.

I demonstrated that prolonged exposure to odor with food leads to desensitization to low concentration butanone, while prolonged exposure to odor without food lead to aversive learning to low concentration butanone. The amount of odor chemical required for desensitization is 100-fold higher than the amount of odor chemical required for aversive learning.

Through forward genetics, I identified the *ist-1* gene that encodes the worm Insulin Receptor Substrate (IRS) protein as essential to aversive learning. I have demonstrated that IST-1 is expressed in 8 pairs of head neurons, but is only required in AWC^{ON} for butanone aversive learning. *ist-1* was not defective for the aversive learning of other odors that are partially sensed by AWC^{ON}.

Although there have been many studies in *C. elegans* chemotaxis and aversive learning, behavior experiments remain technically challenging. This is partly due to *C. elegans* being very sensitive to environmental stimuli that need to be well controlled. The first step I took to optimize the protocol for behavior testing was to gather different protocols, and unwritten experiences from researchers who had succeeded in this area. Experimenting with conditions that had been indicated by them established a strict protocol that gives the most consistent result possible. This allowed me to uncover subtle phenotypes that might not be uncovered previously.

ist-1, the gene encoding *C. elegans* Insulin Receptor Substrate (IRS), remained undiscovered from genetic screening for phenotypes until it was predicted by systematic sequence comparison to known protein kinase substrates (Plowman, Sudarsanam, Bingham, Whyte, & Hunter, 1999). The PH domain, PTB domain and the PI3K binding site were suggested by comparing to the *Drosophila* and human IRS. Epistatic study with dauer formation assay showed that although *ist-1* knock-down with RNAi alone does not produce a phenotype, it seems to work in parallel with *age-1* to inhibit *daf-16* (Wolkow, Muñoz, Riddle, & Ruvkun, 2002). Therefore *ist-1* signaling is considered somewhat non-canonical, with *age-1* signaling considered canonical. Since then, there has been no known report of any phenotype of *ist-1* till this study. The highly specific nature of expression of *ist-1* in the nervous system, especially in high levels in ASE and BAG neuron, suggests that it would be interesting to examine the function of *ist-1* in other behaviors, especially food-related learning behaviors.

Many questions remain on how exactly *ist-1* participates in the signaling in AWC neuron during aversive learning. Is it part of the *daf-2/age-1* pathway in the aversive learning process? Does the insulin/IGF pathway itself function in aversive learning? How do they all work together? How does the same pathway achieve the division of labor of aversive learning versus dauer formation? In the following chapter I will explore these questions.

CHAPTER 3.

Insulin signaling and aversive learning

Chapter 3 INTRODUCTION

3.1 Insulin pathway overview

ist-1 encodes the sole *C. elegans* homolog of mammalian IRS, the insulin receptor substrate that facilitates the interaction of the Insulin Receptor (IR) and its downstream target, Phosphoinositide 3-kinase (PI3K). The classical *C. elegans* Insulin/IGF-1 signaling (IIS) pathway is largely homologous to the mammalian Insulin-like Growth Factor (IGF) pathway (Figure 3.1). The mammalian Insulin Receptor (IR) and the type 1 Insulin-like Growth Factor (IGF) receptor (IGF1R) evolved from a single ancestral receptor involved in the regulation of metabolism, organismal size, and longevity. In mammals, insulin signaling regulates metabolite distribution between organs through controlling blood sugar level, whereas the IGF pathway serves important functions in regulating long-term cell growth. I will describe the IGF receptor pathway briefly below. The IGF receptor is a tyrosine kinase receptor homodimer that is allosterically activated upon ligand binding. Technically, it is a tetramer, since each subunit consists of two proteins due to the cleavage of the primary protein. The activated IGF receptor kinase subunits cross-phosphorylate each other, presenting phosphotyrosines as the docking sites for IRS, to initiate the internal signaling cascade machinery. IRS then recruits PI3K (Phosphatidylinositol-4,5-bisphosphate 3-kinase) to the cell membrane, where it converts the lipid PIP2 (Phosphatidylinositol 4,5-bisphosphate) to PIP3 (Phosphatidylinositol (3,4,5)-trisphosphate). PIP3 activates two downstream kinases, PDK and AKT, which further activate multiple targets to regulate cellular survival and growth pathways. Among their targets is FoxO, a transcription factor that activates transcription of genes in the nucleus, but is phosphorylated and retained in the cytoplasm in an inactive form when IGF signaling occurs. The IGF pathway is negatively regulated by PTEN, which is a phosphatase that

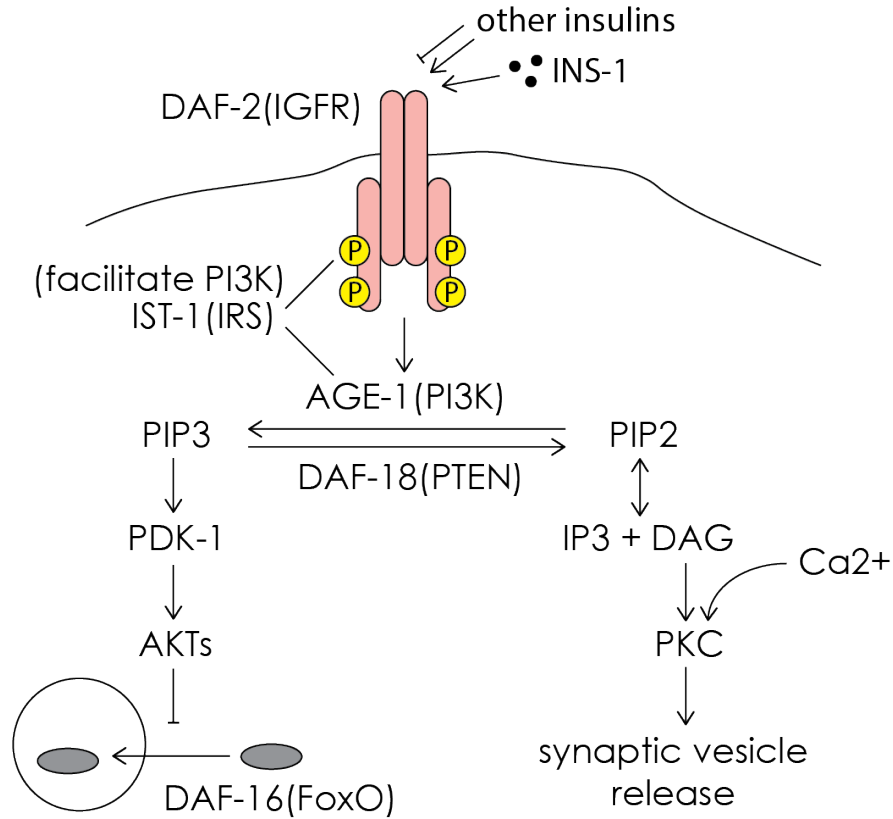


Figure 3.1 Simplified diagram of *C. elegans* insulin pathway relevant to chemosensation and aversive learning.

Schematic of simplified model of the insulin pathway in *C. elegans*. The insulin/IGF pathway of *C. elegans* is homologous to the human Insulin-like Growth Factor (IGF) pathway. The insulin/IGF receptor DAF-2 is a tyrosine kinase receptor. Insulin-like neuropeptides bind to DAF-2 and facilitate cross-phosphorylation of tyrosine residues. This allows the activation of AGE-1, the *C. elegans* phosphoinositide 3-kinase (PI3K). AGE-1 converts PIP2 to PIP3. PIP3 then activates the downstream PDK-1 and AKT-1/2 kinases, which inhibit the nuclear entry of the fork-head transcription factor (FoxO) DAF-16. In the canonical *C. elegans* insulin pathway, crowding and starvation decreases insulin signaling and lead to the nuclear entry of DAF-16, which in turn promotes dauer formation. Although the *C. elegans* IST-1 is predicted to have the PH domain that would bind to PIP2/PIP3 in the cell membrane, and the PTB domain that would bind to AGE-1, previous genetic studies showed that IST-1 had only a minor function in dauer formation assays. PIP2 is also an important signaling molecule. It is converted to diacylglycerol (DAG) when dephosphorylated by phospholipase C, downstream of G protein coupled receptors and Gq. DAG and Ca²⁺ together activate protein kinase C (PKC) signaling, which is required for multiple steps in synaptic vesicle packaging and release.

dephosphorylates PIP3 to form PIP2 and inorganic phosphate. PIP2 regulates synaptic function downstream of GPCRs and Gαq. PIP2 can be hydrolyzed by phospholipase C beta to form IP3 and diacylglycerol, or DAG, which can activate some isoforms of protein kinase C (PKC). PKC serves important function in neurotransmitter packaging and release (Ohno, Sakai, Adachi, & Iino, 2017).

In *C. elegans*, the insulin/IGF receptor is called DAF-2 (DAF for abnormal Dauer formation), PI3K is called AGE-1 (AGE for abnormal lifespan), and PTEN is called DAF-18. These genes have been extensively characterized for their role in regulating the formation of dauer larvae, which are developmentally arrested, non-feeding, non-reproductive forms that arise under unfavorable conditions. They have also been shown to regulate lifespan. In general, activation of DAF-2 insulin/IGF signaling in *C. elegans* eventually leads to the activation of AKTs, which inhibit the translocation of the fork-head transcription factor (FoxO) DAF-16 into the nucleus. Animals that are well fed have an active DAF-2 insulin pathway and inactive DAF-16. Upon starvation, crowding, and temperature stress, the insulin pathway is turned off and DAF-16 is disinhibited, which promote formation of dauers (Riddle, Swanson, & Albert, 1981; Vowels & Thomas, 1992).

Components of the insulin pathway have been shown to be important for associative learning in mammal and worms. The *C. elegans* insulin pathway consist of 40 insulin-like molecules (*ins-1* to *ins-39*). Among these insulins, the insulin ligand INS-1 is important for aversive learning of diacetyl (Kodama, et al., 2006), benzaldehyde (Lin, et al., 2010), and butanone (Cho, Brueggemann, L'Etoile, & Bargmann, 2016). The downstream effector of insulin pathway AGE-1/PI3K is important for the memory of cultivation temperature (Kodama, et al., 2006). In addition, INS-1 and AGE-1 are required for other kinds of associative learning such as

salt learning in the ASE neuron (Tomioka, et al., 2006) and thermotaxis learning (Murakami, Bessinger, Hellmann, & Murakami, 2005). In butanone learning, *ins-1* is secreted from the AIA interneuron to act on the AWC sensory neuron, and is important for conveying a food availability signal for aversive learning (Cho, Brueggemann, L'Etoile, & Bargmann, 2016).

A neuronal-specific isoform of the insulin receptor, DAF-2c, plays an important role in salt learning. During salt learning, expression of this isoform in the ASE salt-sensing neuron increases in the axon, where it responds to a local insulin signal (Ohno, et al., 2014; Tomioka, Naito, Kuroyanagi, & Iino, 2016). Another insulin receptor isoform, DAF-2a, is important for food signaling in salt chemotaxis (Tomioka, et al., 2006; Nagashima, Iino, & Tomioka, 2019). The DAF-2a isoform regulates DAF-16 signaling, following the classical insulin signaling pathway, but the DAF-2c isoform does not regulate DAF-16. While DAF-2a is mainly localized in the cell body, DAF-2c is localized to the axon of the ASE neuron. Compared to DAF-2a, DAF-2c includes an extra alternatively spliced exon 11.5 that encodes an extracellular 82 amino acid domain. This domain physically interacts with Calsyntenin CASY-1, which binds to the kinesin-1 light chain KLC-2. Kinesin is a molecular motor that is hypothesized to transport the DAF-2c-CASY-1 complex to the axon along microtubules.

Previous studies suggested that insulin signaling plays a role in learning in the AWC^{ON} neuron, but did not directly implicate DAF-2 in the process. Given the diverse forms and location of DAF-2, there could be many possibilities for it to interact with IST-1. In this chapter, I systematically explore the relationship of IST-1 and DAF-2, and their roles in learning.

Chapter 3 RESULTS

3.2 Cell specific insulin receptor function in aversive learning

To further dissect the role of *ist-1* in butanone aversive learning, I asked if *ist-1* functions in the *daf-2* insulin/IGF pathway in *C. elegans* for aversive learning. Previous studies of *daf-2* mutations had failed to show defects in aversive learning, but the many functions of *daf-2*, and the fact that all alleles are partial loss of function because null mutations are lethal and sterile, could have made that result misleading. To focus on the neuronal learning phenotypes, I obtained and tested alleles of *daf-2* that had previously been shown to affect salt chemotaxis learning from the Iino lab, but otherwise have no observable developmental defect (Ohno, et al., 2014).

I found that *daf-2(pe1230)*, a *daf-2* point mutant allele that disrupts salt learning phenotypes without affecting development and dauer formation, was defective for butanone aversive learning (Figure 3.2, Figure 3.3). *daf-2c(pe2722)*, which selectively disrupts the exon 11.5 exon in the *daf-2c* isoform, is also partly defective in aversive learning to butanone (Figure 3.2, Figure 3.3). These results suggest that *daf-2* has a role in aversive olfactory learning.

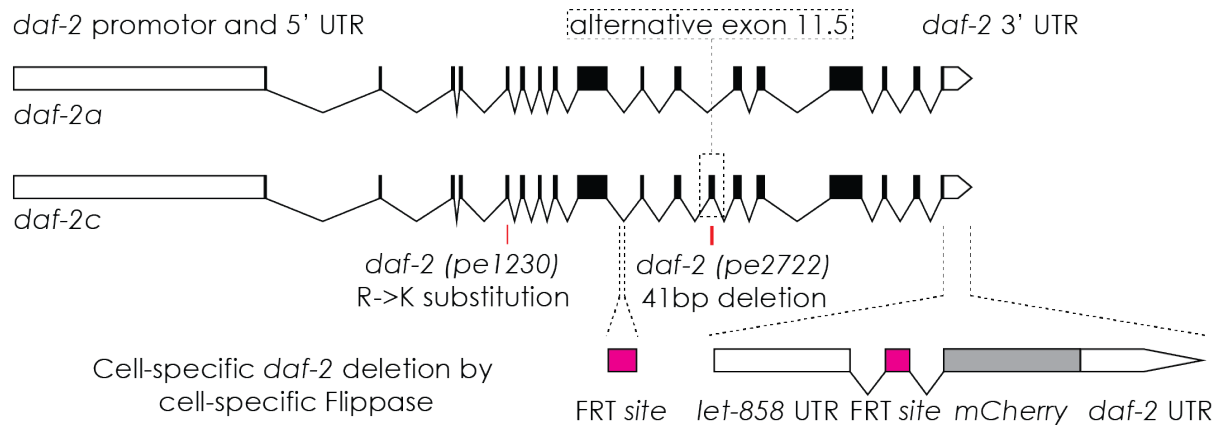


Figure 3.2 *daf-2* isoforms, and strategy for *daf-2* cell-specific knock-out

Top, genomic structure of *daf-2a* and *daf-2c*. Solid black boxes denotes exons while lines connecting them denote introns. The position of mutations in *daf-2(pe1230)* and *daf-2c(pe2722)* are indicated on the map. Both of these mutations fall within the extracellular domain of the predicted DAF-2 protein. To generate a cell-specific *daf-2* knockout locus, we inserted two FRT sites flanking half of the *daf-2* gene by CRISPR-Cas9 mutagenesis of the endogenous *daf-2* gene. Although the intention was for mCherry to be expressed under the *daf-2* promoter to verify Flippase recombination of *daf-2*, errors in design meant that the mCherry was not correctly expressed. Instead, Flippase activity was verified using a separate reporter strain where only cells that had flippase activity expressed GFP.

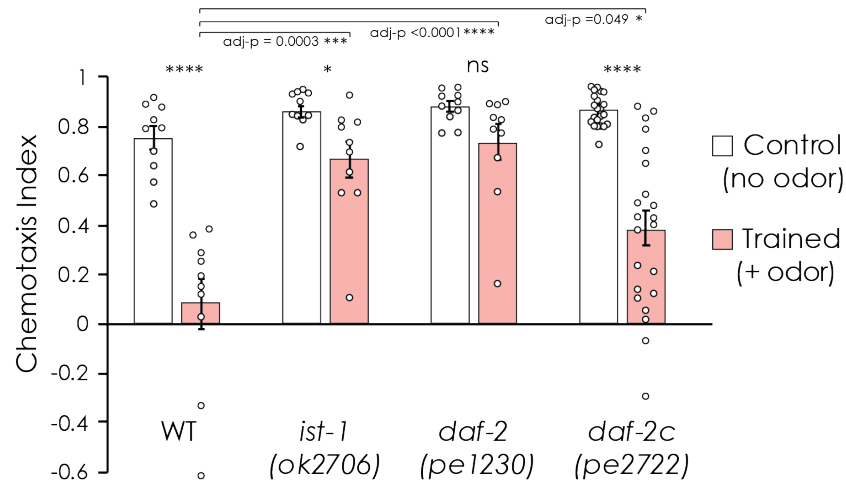


Figure 3.3 The function of insulin receptor isoform DAF-2c in aversive leaning.

Chemotaxis index of wild-type, *ist-1(ok2706)*, *daf-2(pe1230)* and *daf-2c(pe2722)* mutant animals tested for aversive learning to butanone. DAF-2 has multiple isoforms, including an alternatively spliced form called DAF-2c. Both *daf-2(pe1230)*, which affects all isoforms, and the *daf-2c*-specific *pe2722* allele showed defects in aversive learning to butanone. Animals were either only deprived from food (control, white bars), or subjected to food deprivation with butanone for 90 mins (trained, pink bars).

To ask in which cells *daf-2* insulin receptor acts to support aversive learning to butanone, I collaborated with a technician, Max Brown, to generate a cell-specific knockout for insulin receptor *daf-2*. We employed the flippase-FRT approach by knocking in two FRT sites flanking the second half of the *daf-2* gene, and then transgenically expressed flippase under cell-specific promoters. To test whether the knock-out construct works, I used the pan-neuronal H20 promotor to express flippase in the transgenic worms. *daf-2::ftr* animals bearing the H20::FLP transgene had severely impaired development. In two transgenes from separate injections of 20 ng/μL H20::FLP with *myo-3::mCherry* co-injection markers that were counted, 59/60 and 48/51 of the progeny carrying the co-injection markers arrested development at the L1 or L2 stage for 3-5 days before recovering and developing to adulthood with reduced size. Dauer larvae were not observed.

I expressed flippase under promoters that were active in the AWC^{ON} neuron, the 20 sensory neurons that use cGMP as a second messenger, and the ASI neurons, verifying the expression of flippase transgenes using a flippase activity reporter (Muñoz-Jiménez, et al., 2017). I quantified the activity of flippase with a reporter gene to calibrate the percentage of animals expected to have *daf-2* knockouts (Figure 3.4)

Knocking out *daf-2* in the AWC^{ON} neuron resulted in a partial learning defect consistent with the efficiency of flippase reporter expression in AWC^{ON}. The flippase reporter indicated that in addition to AWC^{ON} (10/13), the *str-2* promotor also expressed flippase in ASI neurons (8/26), so I also tested ASI-specific *str-3::flippase*, and did not observe an aversive learning defect. I also observe some expression of *str-2::flippase* in RIA interneurons (12/26), so as a separate confirmation that sensory neurons are required for learning, I tested *tax-4::flippase*, which is expressed in AWC and other sensory neurons but not in RIA. This transgene resulted in

a learning defect comparable to that of the AWC^{ON}-selective *str-2::flippase*. Together, these results support a role for *daf-2* in AWC^{ON}.

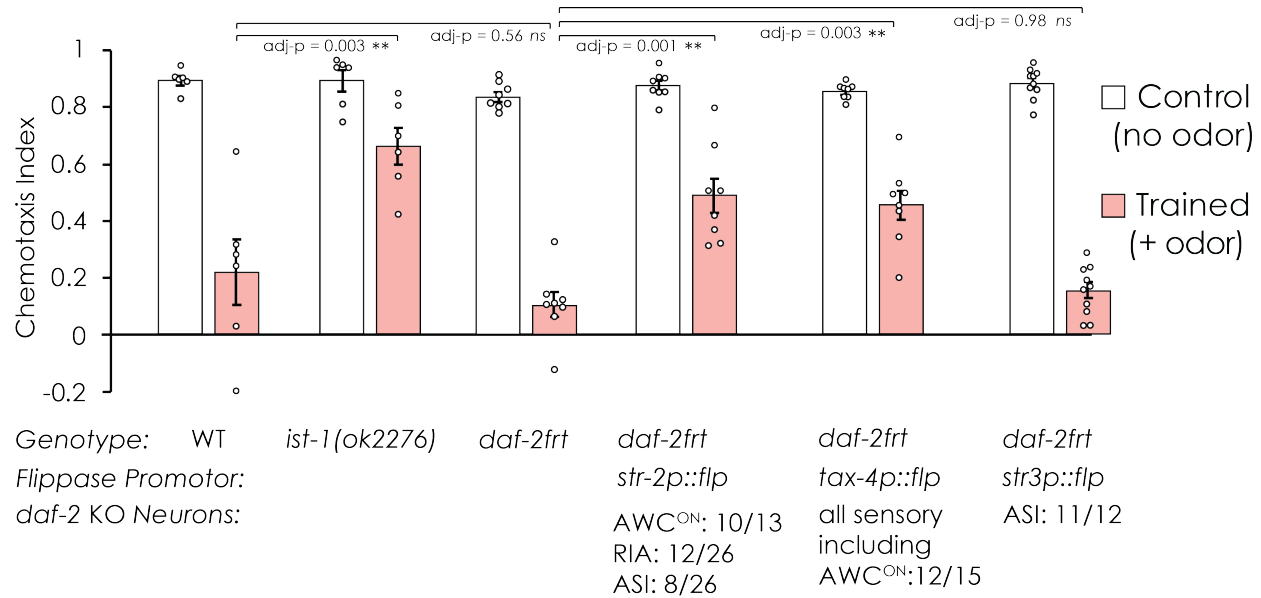


Figure 3.4 *daf-2* cell specific knockout.

Chemotaxis index of animals in which cell-selective flippase transgenes were injected into the *daf-2frt* strain, tested for aversive learning to butanone. Number of designated cells that express the flippase over total number of cells examined in each strain is also shown. The *daf-2frt* strain had normal chemotaxis and normal aversive learning in the absence of flippase expression. Flippase expression under the *str-2* promotor for AWC^{ON} neurons, or *tax-4* promotor for the 20 sensory neurons that use cGMP signal transduction, led to significant learning defects. To rule out the possibility that ASI is the neuron responsible for the *str-2::flippase* effect, I expressed flippase under the ASI-specific *str-3* promotor and did not observe an aversive learning defect. Together, these results support the hypothesis that *daf-2* signaling in AWC^{ON} is important for aversive learning. Animals were either only deprived from food (control, white bars), or subjected to food deprivation with different odors for 90 mins (trained, pink bars).

Next, I performed cell-specific rescue of *daf-2* with *daf-2* cDNAs. This experiment had two purposes: to confirm that *daf-2* can function in AWC^{ON} neurons, and to obtain more information about which of the alternatively spliced isoforms (Figure 3.3) are important for function. Dr. Masahiro Tomioka from Dr. Yuichi Iino's group in Japan generously provided *gcy-5::daf-2a* and *gcy-5::daf-2c* plasmids. The process of subcloning these plasmids under the *str-2* promoter proved immensely challenging, most likely due to toxicity of the tyrosine kinase to bacteria: in the first rounds of cloning, I found that all plasmids contained spontaneous stop codon mutations within the first 200 base pairs of the *daf-2* coding sequence. Dr. Masahiro stated this was a problem for him as well and provided a lot of good advice. After nine months of tweaking the cloning method, including different design and orientation of the plasmids, and different cloning conditions, I was finally able to successfully clone the *daf-2a* and *daf-2c* under the *str-2* promoter. These plasmids were then injected into *daf-2* mutant worm strains (Figure 3.2) to test *daf-2* cell-specific rescue. While *daf-2c* achieved significant rescue of aversive learning in both *daf-2(pe1230)* and *daf-2c(pe2722)*, *daf-2a* did not significantly rescue aversive learning in either mutant strain (Figure 3.5). Together, the results with an isoform-specific allele (Figure 3.2), cell-selective knockout (Figure 3.4), and cell-selective rescue (Figure 3.5) suggest that *daf-2c* in the AWC^{ON} neuron promotes aversive learning, although other neurons and isoforms might also have a role.

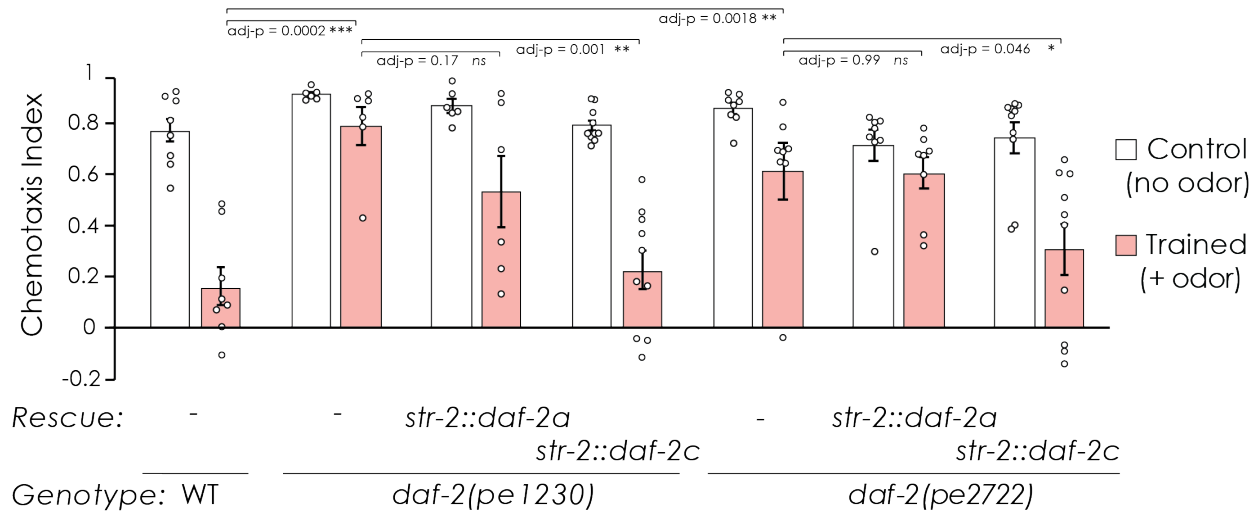


Figure 3.5 *daf-2* cell specific rescue.

Chemotaxis index of animals in which cell-selective isoform-specific *daf-2* rescue transgenes were injected into the *daf-2(pe1230)* and *daf-2c(pe2722)* mutant strains, and subjected to aversive learning to butanone. In both *daf-2(pe1230)* (point mutation in all *daf-2* isoforms) and *daf-2c(pe2722)* (*daf-2c*-specific mutation) strains, expressing the *daf-2a* cDNA under the *str-2* promoter in AWC^{ON} neuron did not achieve significant rescue of aversive learning. Expressing the *daf-2c* cDNA under the same promoter rescued aversive learning in both *daf-2(pe1230)* and *daf-2c(pe2722)* strains. I conclude that the DAF-2c isoform is important for aversive learning, while the DAF-2a isoform has a minor or non-significant role. Animals were either only deprived from food (control, white bars), or subjected to food deprivation with different odors for 90 mins (trained, pink bars).

3.3 Axonal localization of DAF-2c in AWC^{ON}

The predicted DAF-2c protein isoform differs from the DAF-2a isoform by the inclusion of 82 amino acids in the predicted extracellular domain of DAF-2 (Ohno, et al., 2014). In the ASE neurons that mediate salt chemotaxis learning, DAF-2c protein is only detectable in the cell body in naïve animals, but is also detectable in synaptic regions of the ASE axon after salt training (Ohno, et al., 2014). DAF-2a is only present in the ASE cell body, and is not regulated by training. To ask whether DAF-2c had similar properties in AWC^{ON}, I obtained the genetic construct of *gcy-5::daf-2a::mVenus* and *gcy-5::daf-2c::mVenus* from the Iino lab, exchanged the ASE-selective *gcy-5* promotor with the AWC^{ON}-selective *str-2* promotor, and injected the plasmids independently to make transgenic strains expressing either DAF-2a or DAF-2c in AWC^{ON} (Figure 3.6A,C).

DAF-2a::mVenus was easily detected in the dendrite and cell body of the AWC^{ON} neuron, with a somatic pattern suggesting nuclear exclusion (Figure 3.6B). However, DAF-2a was undetectable in the AWC^{ON} axon. By contrast, DAF-2c::mVenus was easily detected in the dendrite, cell body and axon of AWC^{ON}, although its overall expression was comparable to that of DAF-2a::mVenus (Figure 3.6D). This observation confirms the differential subcellular localization of DAF-2a and DAF-2c in a second neuronal cell type.

Next, I asked whether DAF-2 isoforms were regulated by food deprivation. Both DAF-2a::mVenus and DAF-2c::mVenus were significantly upregulated by food deprivation, but unchanged in their subcellular localization (Figure 3.7). A *str-2::GFP* control transgene was not upregulated by food deprivation, suggesting that the effect is independent of the *str-2* promoter and therefore that DAF-2 translation or stability in AWC^{ON} is regulated by food (Figure 3.7E-F).

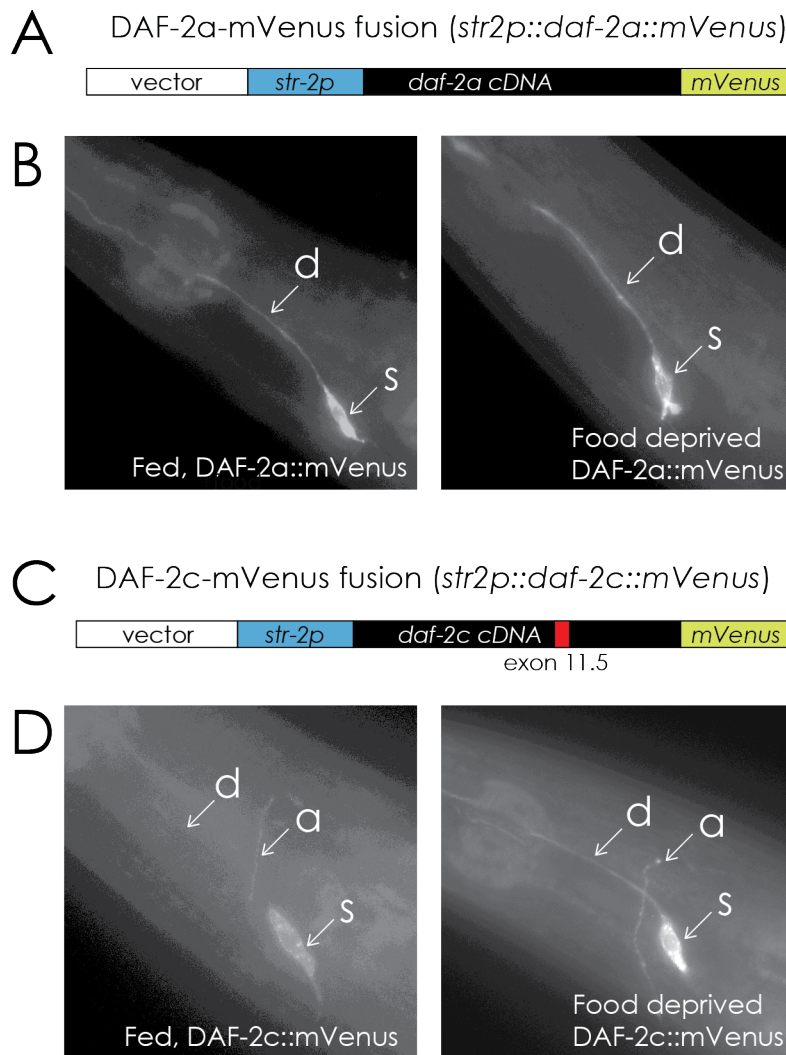


Figure 3.6 Subcellular localization of DAF-2 insulin receptor isoforms.

A) and C) Diagrams of expression constructs. B) and D) Example images of maximal intensity projection of Z-stack images acquired for each expression construct in wild-type animals; left, well-fed animals, and right, animals that were food-deprived for 90 minutes (d: dendrite, a: axon, s: soma). DAF-2a is detected in the dendrite and cell body, while DAF-2c is detected in dendrite, cell body, and the axon. Upon food deprivation, levels of DAF-2a and DAF-2c increased, without obvious changes in subcellular localization (see quantification in Figure 3.7).

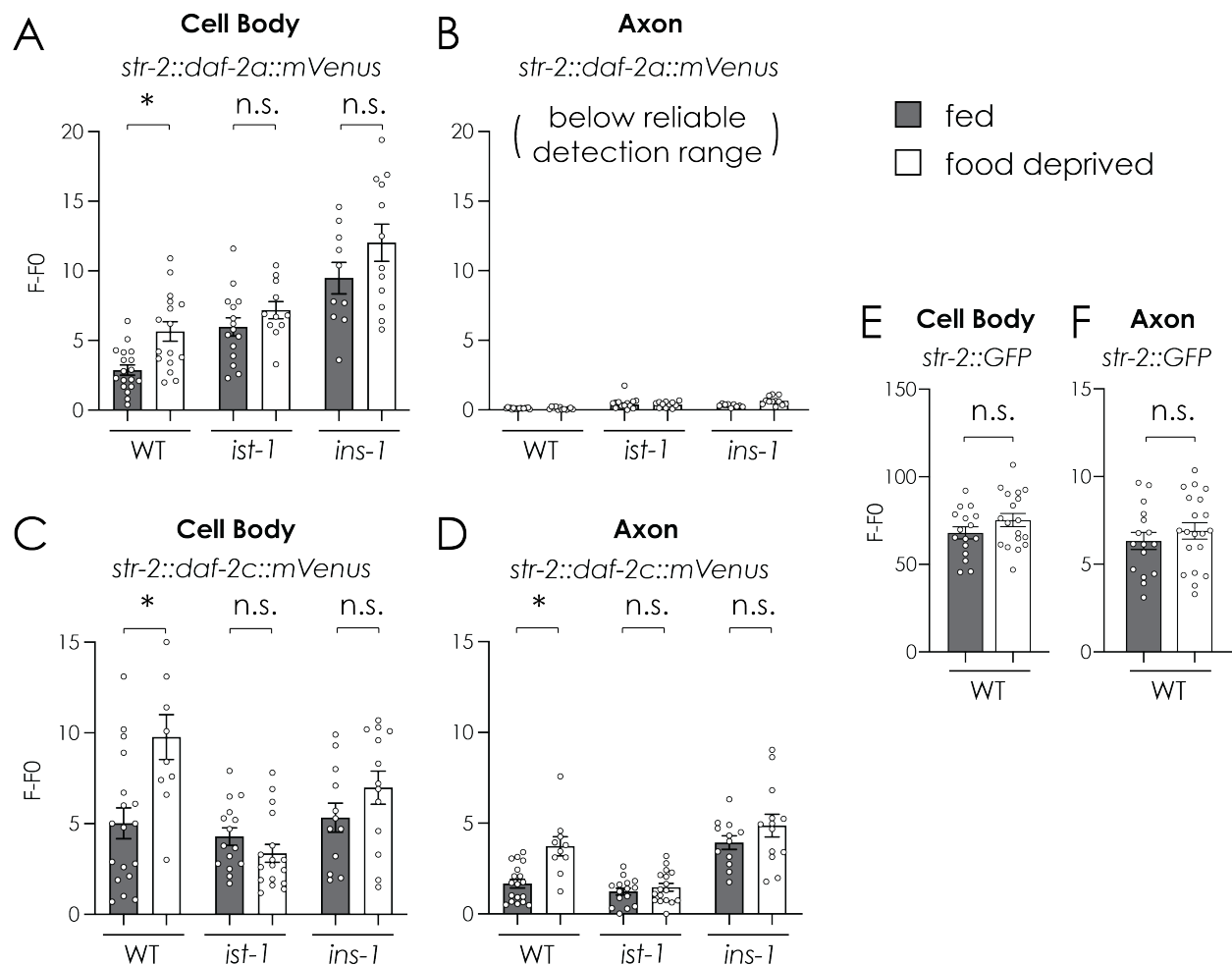


Figure 3.7 Quantification of Subcellular localization of DAF-2 insulin receptor isoforms

A)-D) DAF-2::mVenus signals quantified either immediately after removal from food or 90 minutes after food deprivation on NGM agar plates. E) and F) Quantification of *str-2::GFP* signals in wild-type animals either immediately after removal from food or 90 minutes after food deprivation on NGM agar plates. No change in GFP fluorescence was seen in the *str-2::GFP* strain, suggesting that changes in DAF-2::mVenus signal during food deprivation are due to the property of DAF-2, not the *str-2* promoter. F-F0 in the Y axis represent background subtracted fluorescent signals. Asterisks, values different between fed and food-deprived animals at $p < 0.05$. n.s., value between fed and food-deprived animals are not significantly different. Wild-type, *ist-1* and *ins-1* animals were injected separately thus carrying different transgenes, thus direct comparison of fluorescence between genotypes should not be made.

What role does the insulin signaling pathway itself have in DAF-2 regulation? DAF-2a and DAF-2c proteins were expressed at similar levels in wild-type and in *ist-1(ok2706)* or *ins-1(nr2091)* animals mutants, and in each case their subcellular localization was as in the wild-type, with axonal localization in DAF-2c but not DAF-2a. However, food deprivation did not alter the expression of DAF-2a and DAF-2c in AWC^{ON} of *ins-1* or *ist-1* mutants (Figure 3.7A, C, D). Together, these results suggest that the regulation of DAF-2 levels in AWC^{ON} is dependent on both *ist-1* and *ins-1*, with a stronger effect of *ist-1*.

To ask whether the IST-1 protein was similarly regulated, I fused GFP to the N-terminus of *ist-1* with a 5 amino acid linker and expressed it under the *str-2* promotor (Figure 3.8A). The resulting transgene rescued the *ist-1* aversive learning defect, indicating that it was functional. GFP::IST-1 was broadly distributed between the axon, dendrite and cell body (Figure 3.8B). The localization and levels of GFP::IST-1 appeared unchanged after odor training or food deprivation.

These results suggest that DAF-2 post-transcriptionally increase its level or stability during food deprivation in a process that depends both on receptor activation from the INS-1 ligand, and on binding and stabilizing by the insulin receptor substrate IST-1.

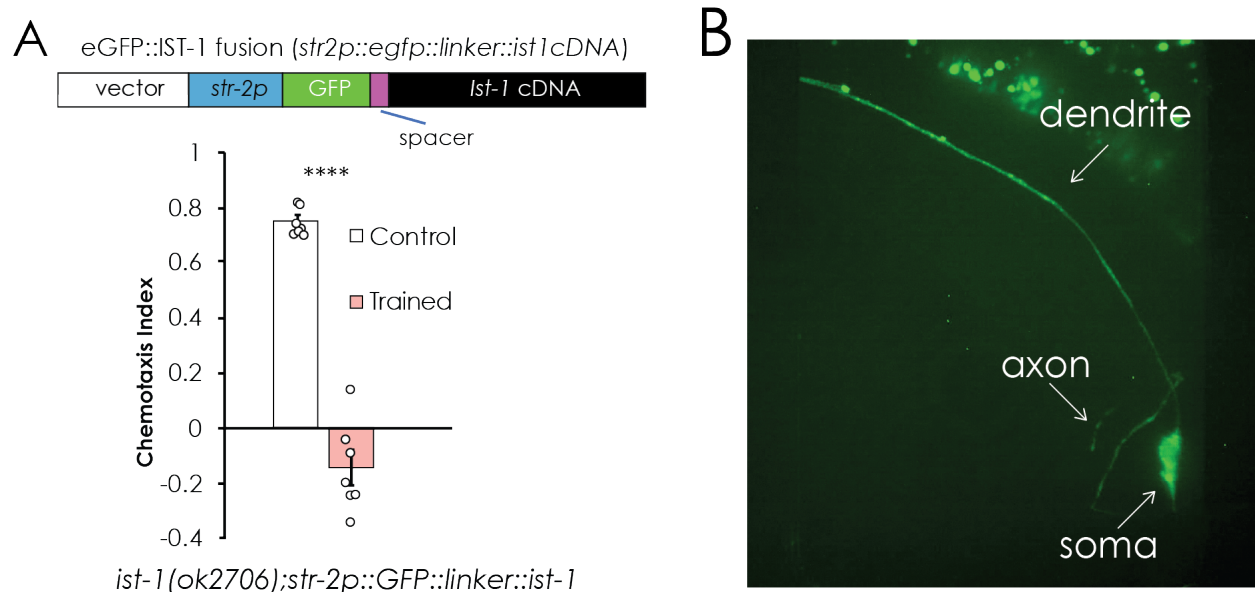


Figure 3.8 Subcellular localization of IST-1

I fused the coding sequence of IST-1 to eGFP and expressed it under the AWC^{ON}-selective *str-2* promoter to allow visualization of IST-1 localization. A) Chemotaxis index of animals in which AWC^{ON} specific *ist-1* transgenes were injected into the *ist-1(ok2706)* mutant strain. The fusion protein rescued aversive butanone learning to wild-type levels. Chemotaxis was tested in food-deprived animals (control, white bars), or in animals in which food deprivation was paired with butanone (trained, pink bars). B) Maximal intensity projection of Z-stack microscope images of IST-1::eGFP in AWC^{ON} neuron. The fluorescent signal appears evenly distributed in the dendrite, axon and cell body.

3.4 *ist-1* interacts with other insulin pathway genes in aversive learning.

To learn more about the relationship between *ist-1* and classical insulin signaling molecules, I examined the epistatic relationship of *ist-1* with other members of the insulin signaling pathway.

Aversive learning to butanone is regulated by *ins-1* expression in AIA and the *daf-2*-regulated PI3 kinase encoded by *age-1* in AWC^{ON} (Cho, Brueggemann, L'Etoile, & Bargmann, 2016). Double mutants of *ist-1* with *ins-1* resembled either single mutant in butanone chemotaxis and aversive learning, suggesting that the two genes have related functions (Figure 3.9). Notably, *ins-1* is a negative regulator of dauer formation (that antagonizes *age-1*), indicating different insulin ligand requirements for learning and dauer formation.

The PI3 kinase *age-1* is antagonized by the PTEN phosphatase encoded by *daf-18*. *daf-18* mutants were slightly repelled from butanone before training, and their behavior was not further altered by conditioning with butanone and food deprivation. Interestingly, *ist-1 daf-18* double mutants mutually suppressed each other: the double mutant was partially restored both for butanone chemotaxis, and for aversive learning (Figure 3.9). *age-1*, by contrast, is completely epistatic to *daf-18*; the double mutant resembles *age-1*, with robust chemotaxis and no aversive learning. These results are consistent with a model based on the mammalian insulin pathway: *daf-2* activates *age-1*, *ist-1* potentiates *daf-2* activation of *age-1*, and *daf-18* antagonizes *age-1*.

The downstream targets of *age-1* are the kinases *pdk-1*, *akt-1*, and *akt-2*. An *akt-1* null mutant was defective in aversive learning, suggesting that this kinase is essential (and not redundant with *akt-2*) in the learning pathway. An *akt-1* mutant that acts as a gain-of-function in the dauer pathway was normal for chemotaxis and learning (Figure 3.9). A strong *pdk-1* mutant was partly chemotaxis-deficient, but still showed aversive learning. These results suggest that the

genetic requirements for aversive learning are overlapping with, but partly distinct from, the genetic requirements for dauer formation.

The transcription factor encoded by *daf-16* is the final output of the *daf-2* pathway in dauer formation, and is epistatic to all other genes in the pathway. In agreement with a previous report, *daf-16* mutants do not chemotax to butanone (Figure 3.9). *ist-1* partly suppressed this defect, so that *ist-1 daf-16* double mutant animals had intermediate butanone chemotaxis. *ist-1 daf-16* double mutants did not show any learning after training with butanone. Since both *ist-1* and *daf-16* alleles were null alleles, the genetic interpretation of these mixed epistasis results is that each gene has at least some functions that are independent of the other, and support the model that the aversive learning pathway is related to, but not identical to, the classical *daf-2* pathway in *C. elegans*.

In a final double mutant experiment, I examined *pkc-1*, which is not a component of the dauer pathway but is regulated by the phosphatidyl inositol lipids that are substrates of *age-1* PI3K. *pkc-1* mutants are repelled by butanone (Ventimiglia & Bargmann, 2017), rather than attracted. Training with food deprivation and odor suppressed their aversion (Figure 3.9). *ist-1 pkc-1* double mutants were more strongly repelled by butanone than *pkc-1* alone, and this repulsion was retained after training with food deprivation and odor (Figure 3.9). Like the *daf-16* experiment, this mixed epistasis experiment indicates that *ist-1* and *pkc-1* function at least partly independently of one another.

In summary, *ist-1*, *ins-1* (an insulin), *daf-2* (insulin receptor), *age-1* (PI3K), and *akt-1* (AKT) are all required for aversive butanone learning, and *daf-18* antagonizes *ist-1* in a way that is consistent with action upstream of *age-1*. However, *ins-1* and *akt-1* have larger roles in

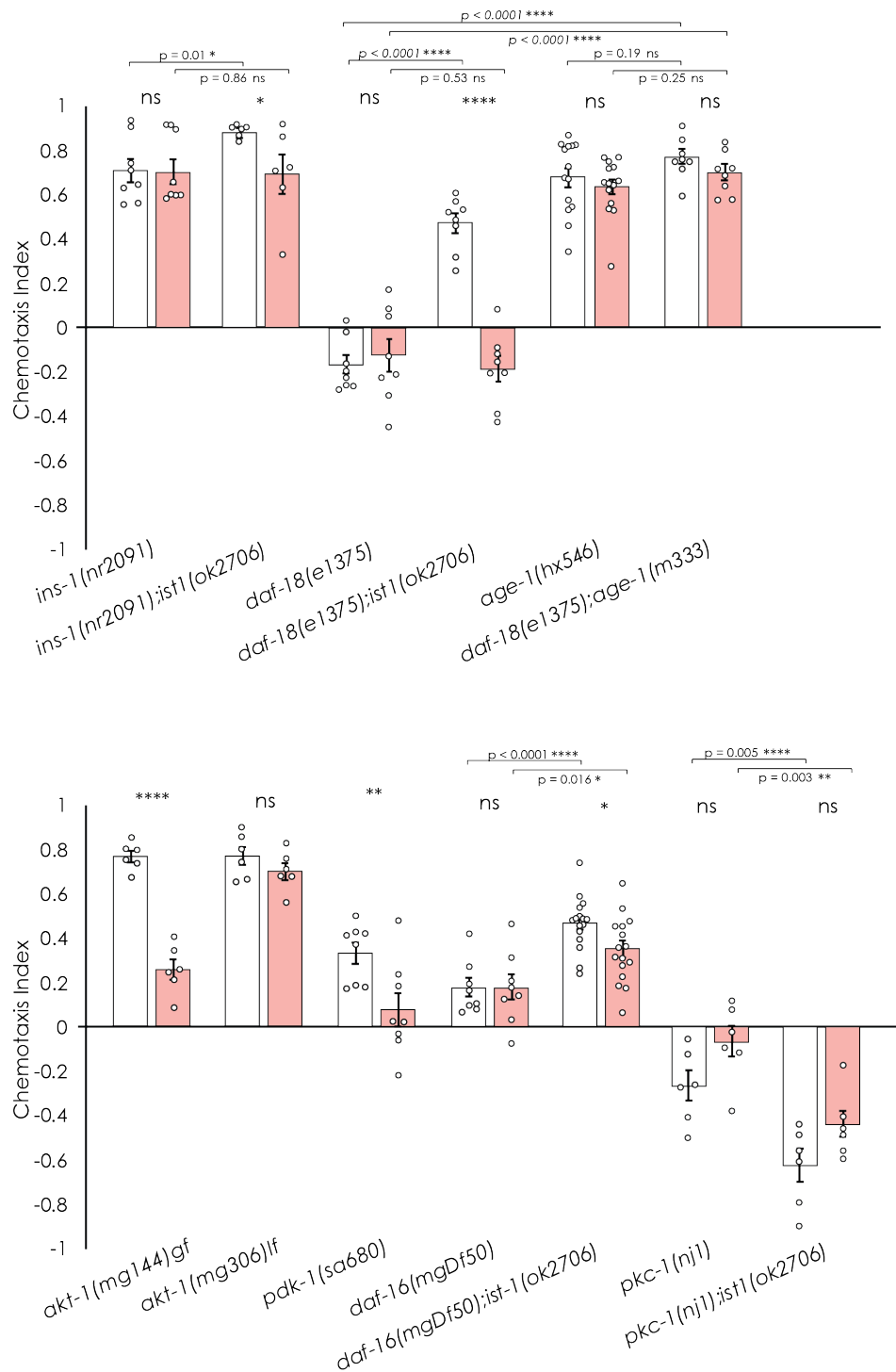


Figure 3.9 Epistatic study of insulin pathway members in aversive learning

Chemotaxis and aversive learning in animals bearing mutations in genes related to the insulin pathway, alone in and in double mutants with *ist-1*. Animals were either only deprived from food (control, white bars), or subjected to food deprivation with butanone for 90 mins (trained, pink bars).

aversive learning than they have in dauer formation, and *daf-16* may have a more subtle role in aversive learning than it has in the dauer pathway.

Chapter 3 DISCUSSION

These results demonstrate that the insulin/IGF receptor DAF-2 is necessary for aversive learning, and that the DAF-2c isoform is especially important in this case. When expressed in the AWC^{ON} neuron specifically, the DAF-2c isoform that is localized to the axon was sufficient to rescue learning in DAF-2 deficient mutants, while the DAF-2a isoform that is localized to the soma and dendrite was not. Moreover, food deprivation increased the amount of DAF-2c in the cell body and axon of AWC^{ON} neurons, and this increase depended on both IST-1 and INS-1. IST-1 is localized to the dendrite, soma and axon in AWC^{ON}. I demonstrated that among the effectors of the insulin pathway, AGE-1 (PI3K) and AKT-1 were required for aversive learning, while the downstream PDK-1 and DAF-16 (FOXO transcription factor) were required for chemotaxis.

DAF-2 is essential for the development, growth and survival of *C. elegans*. Homozygous *daf-2* null mutants cannot survive; therefore, most *daf-2* mutants exist as partial-loss of function alleles, temperature-sensitive alleles, or isoform-specific deletion alleles. We were fortunate to obtain the *daf-2(pe1230)* partial-loss of function allele and the *daf-2c(pe2722)* isoform-specific allele from the Iino Lab, and used these to confirm that DAF-2 is necessary for aversive learning. To identify the cell in which *daf-2* is required for aversive learning, we generated cell-specific knockouts in the endogenous *daf-2* gene with the Flippase-FRT based approach using CRISPR-cas9. Using this strategy, we showed that cell-specific knockout of *daf-2* in the AWC^{ON} neuron was able to cause a defect in aversive learning.

Using the *str-2* promotor for the cell-selective expression of DAF-2a or DAF-2c cDNA in the AWC^{ON} neuron, I showed that DAF-2c, not DAF-2a, is the primary isoform required in

the AWC^{ON} neuron for aversive learning. Similarly, single copy insertion of DAF-2c rescues salt learning, but single-copy insertion of DAF-2a does not (Ohno, et al., 2014).

What is the function of IST-1 in the insulin pathway? I observed that both DAF-2a and DAF-2c::mVenus fusion protein increased in fluorescent signal during food deprivation. This increase was not depended on promotor activation, since the *str-2* promotor does not increase the expression upon food deprivation. The increase in DAF-2 is, however, depended on IST-1 and INS-1. In parallel genetic epistasis studies, I obtained evidence that *daf-2* activates *age-1*, *ist-1* potentiates *daf-2* activation of *age-1*, and *daf-18* antagonizes *age-1*, in agreement with the classic insulin pathway. Protein levels in a cell are constantly regulated by the balance of synthesis and degradation, and my experiments do not distinguish whether DAF-2 is destabilized by food or upregulated upon food deprivation. In one model, I suggest that IST-1 may function to decrease the degradation of DAF-2 when the ligand-receptor-adaptor protein complex is formed by INS-1, DAF-2, and IST-1. In mammals, IRS (insulin receptor substrate) functions as a docking protein that connects insulin receptor to its downstream effector Phosphoinositide 3-kinases (PI3K) upon activation of DAF-2. The IGF-IR complex is turned over by internalization through binding of AP2 and formation of clathrin-coated pits. IRS blocks the AP2 binding sites on the IR, therefore allowing retention of the IGF-IR complex on the membrane (Yoneyama, et al., 2018). My results show that the food-deprivation induced increase of DAF-2 (insulin receptor) is dependent on IST-1, the worm IRS, and would suggest that IST-1 might also function to retain DAF-2 on the plasma membrane. This mechanism is different from the current model of salt learning in ASE neuron, where DAF-2c is transported from the soma to axon via CASY-1 and kinesin during starvation to enable learning.

There is a key difference between the ASE salt learning and butanone aversive learning, that is the definition of learned state. In salt learning, two salt concentrations are used, one paired with food and one with food deprivation. The learned state is defined as successful chemotaxis to the concentration animals previously associated with food, or did not associate with food deprivation. Axonal DAF-2c/PI3K signaling in ASE controls diacylglycerol (DAG) level, and the high or low DAG levels promote animals' migration toward high or low-salt concentration, respectively (Nagashima, Iino, & Tomioka, 2019). In other words, salt chemotaxis is a choice between two concentration, and the result of successful learning could rely on successful execution of chemotaxis to the more attractive concentration as well as the aversion to the less attractive one (Iino & Yoshida, 2009). In butanone aversive learning, animals are inherently attracted to the odor source, and successful learning relies on the suppression of the default chemotaxis infrastructure, not the attraction to an opposite stimulus. I found that CASY-1 animals have severe defects in butanone chemotaxis, suggesting that CASY-1 is part of the requirement for chemotaxis infrastructure in AWC^{ON} . Without the infrastructure itself, it's not possible to test its modification by learning. Taken together, the chemotaxis defect of CASY-1 mutant in butanone chemotaxis and the experience-dependent salt migration defect in CASY-1 suggest differences in basal function and learning mechanism, which are correctly being examined in the salt assay by the Iino lab. Future experiment should uncover the potential similarities of difference between the IST-1 dependent DAF-2 increase in soma and axon, and the CASY-1 dependent axonal transport of DAF-2c in AWC^{ON} and ASE.

CHAPTER 4.

Neuronal mechanism of aversive learning

Chapter 4 INTRODUCTOIN

Understanding how experience changes molecular activity in specific neurons, which subsequently lead to changes in the activity of a neuronal network, and then to differential outputs such as making a choice, is an example of complete mechanistic understand of a brain process. This level of understanding can assist in designing drugs that are targeted to the basic molecular level to treat complicated brain disease. For example, discovering the lack of dopamine in the substantia nigra as the pathology of Parkinson's disease led to the augmenting drug Levodopa, a drug for dopamine replacement therapy. However, understanding of the disease does not end at a non-cell-specific replacement therapy that has side effects. For example, we later learned that the destruction of substantia nigra can be caused by accumulation of misfolded alpha-synuclein. As science progress, we will eventually understand the root cause of the disease and hopefully develop a treatment targeting the cause.

In *C. elegans* we can examine all the steps of neuronal processing from molecules, to neuronal activity, to neural networks to behavior. I have shown that the *ist-1* gene that encodes the worm Insulin Receptor Substrate (IRS) protein IST-1 is essential to aversive learning. IST-1 functions in the insulin pathway by modulating a specific isoform of the insulin receptor DAF-2, which is also required for learning. What kind of neuronal circuit change does learning elicit? How does insulin regulate the circuit change that causes worms to abandon an attractive odor? In this chapter I will explore these questions with advanced microscopy and computational behavioral analyses.

There are two kinds of activity in the AWC^{ON} neuron that can be monitored using different molecular indicators. The neuron's direct response to odor input can be monitored by the flux of calcium through the genetically encoded calcium indicator GCaMP. The synaptic

output of the neuron can be observed by monitoring the release of vesicles containing neurotransmitters, using a reagent called pHluorin. In this chapter I use these two activity reporter to monitor AWC^{ON} neurons in control and trained worms receiving odor stimulus.

In most behavior experiments I conducted, the behavior of worms has been recorded as movies. This allowed me to utilize computer software to track the position and posture of each worm throughout the experiments. I can then analyze the worm's movements in detail, a first step to linking the change in specific behaviors to changes in the neuronal network. In this chapter, I describe how each of these steps of processing in the neuronal network contribute to change in behavior.

Chapter 4 RESULTS

4.1 Neuronal activity of AWC^{ON}

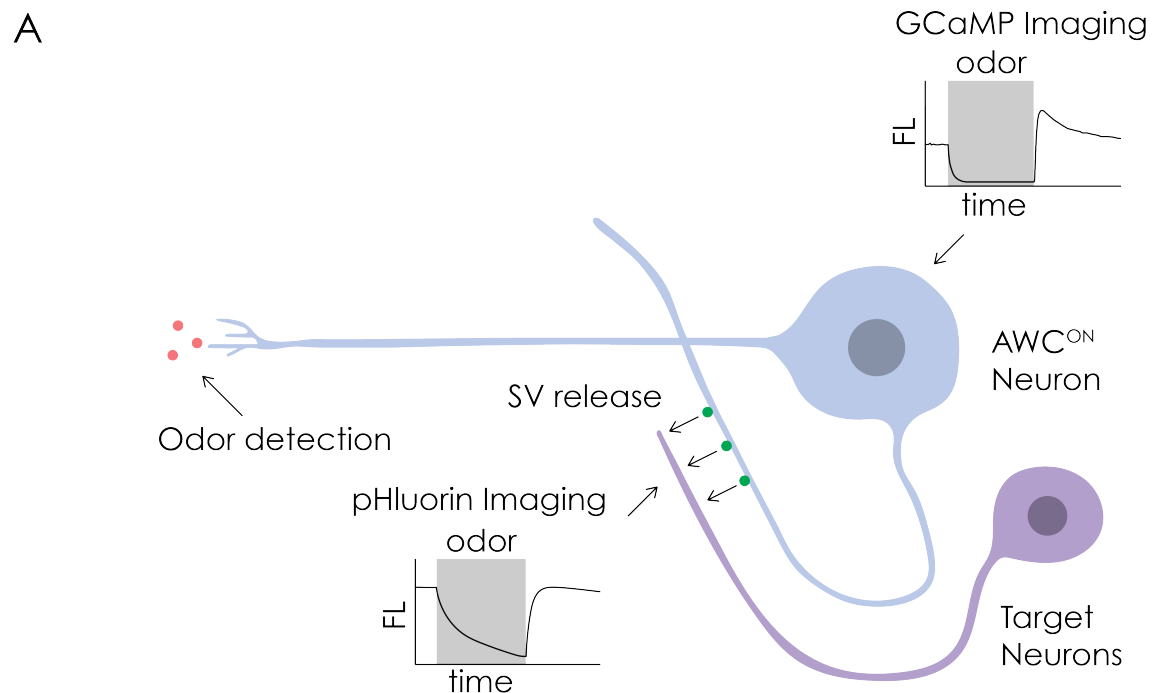
Desensitization and aversive learning have distinct effects on the odor sensitivity of the AWC^{ON} neuron. The high butanone conditions that elicit desensitization result in a 10-fold loss of butanone sensitivity in AWC^{ON} as reported by GCaMP calcium indicators (Cho, Brueggemann, L'Etoile, & Bargmann, 2016). Thus, naïve animals respond reliably to 10⁻⁸ M butanone, but the response is apparently saturated and recovers poorly when animals are exposed to 10⁻⁴ M butanone. Conversely, animals trained by exposing to 10⁻³ M butanone in the presence or absence of food require 10⁻⁷ M butanone for a reliable response, and continue to respond reliably to 10⁻⁴ M butanone addition and removal. This loss of sensitivity after odor exposure correspond to behavioral desensitization. Animals mutant for *age-1* or *ins-1* have normal desensitization by these imaging criteria (Cho, Brueggemann, L'Etoile, & Bargmann, 2016).

To understand the mechanisms by which *ist-1* affect behavior, I examined AWC^{ON} GCaMP signal in response to butanone addition and removal in control and trained animals (Figure 4.1). Training was conducted with 10⁻³ M butanone, which elicits both desensitization in calcium imaging and aversive learning. *ist-1* mutants had normal AWC^{ON} response to butanone across the full concentration range, resembling wild-type animals both before and after training (Figure 4.1). I conclude that the aversive learning defect reflects involvement of a process downstream of the calcium signal.

Figure 4.1 Calcium imaging of AWC^{ON} neuron showing desensitization in both wild-type and *ist-1* mutant animals.

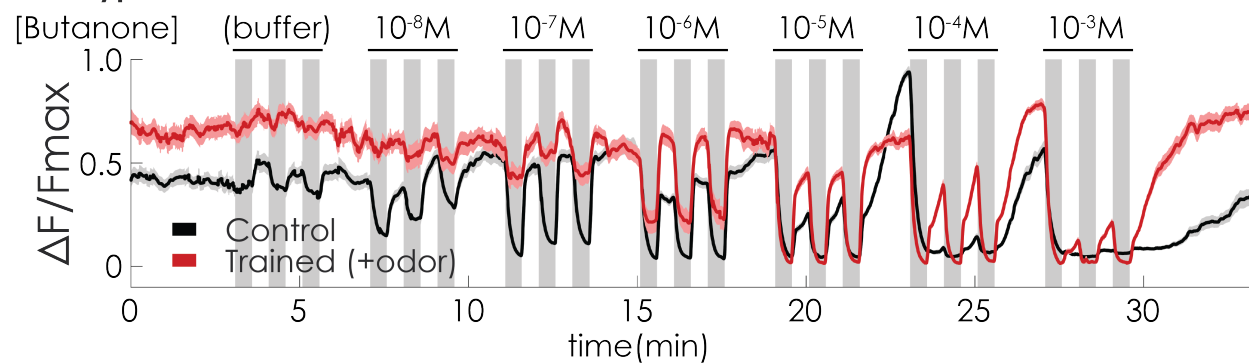
A) Diagram of AWC^{ON} neuron illustrating sites of odor detection in cilia, calcium imaging in the cell body, and pHluorin imaging in the axon.

B) Averaged GCaMP signals in AWC^{ON} to increasing doses of odor (three 30 seconds long odor pulses in buffer per concentration, with 30 seconds of buffer between pulses). Odor suppresses calcium levels in AWC^{ON} by driving closing of a cGMP-gated channel. After desensitization, the dose-response curve is shifted ~10-fold to the right (red) compared to naïve animals (black), across the full range of odor concentrations, resulting in a different dynamic range of odor sensed accurately by AWC^{ON}. *ist-1* mutants showed similar desensitization to wild-type animals. Grey shaded regions represent times when stimulus was present. Solid lines represent average data of multiple trials (WT control: n=64 worms from 7 independent experiments, WT trained: n=47 worms from 5 trials, *ist-1(ok2706)* control: n=65 worms from 7 independent experiments, *ist-1(ok2706)*: n=55 worms from 5 independent experiments). Shaded region tracking the solid data line represent S.E.M.

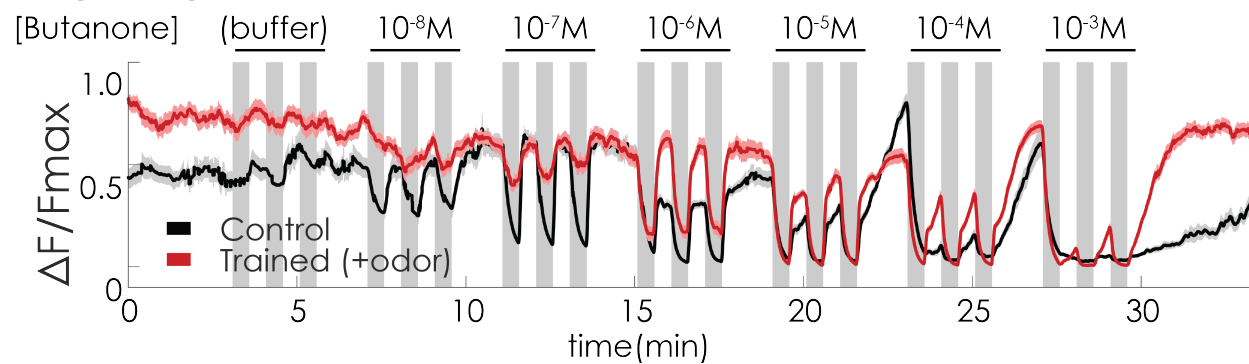


B

Wild-type



ist-1(ok2706)



4.2 Synaptic change in aversive learning

Signaling in the AWC^{ON} neuron begins with cGMP regulation in the sensory cilia, is propagated to the cell body as a change in calcium and membrane potential, and is then expressed at the synapse by the differential release of neurotransmitter (Figure 4.1A). The AWC^{ON} neuron releases the classical neurotransmitter glutamate as well as a number of neuropeptides. To confirm that glutamate from AWC is important for chemotaxis, I tested worms with AWC specific knockout of *eat-4*, the vesicular glutamate transporter, as well as *eat-4* null mutant. The AWC-specific knockout of the endogenous *eat-4* locus was generated using a flippase-FRT strategy (López-Cruz, et al., 2019). I found that AWC knockout of *eat-4* resulted in a butanone chemotaxis defect comparable to that of the *eat-4* null mutant (Figure 4.2). These animals did, however, still show a reduction in chemotaxis after pairing butanone and food deprivation, as did *eat-4* null mutants. I conclude that AWC glutamate release is important for butanone chemotaxis, but likely functions together with additional AWC neurotransmitters.

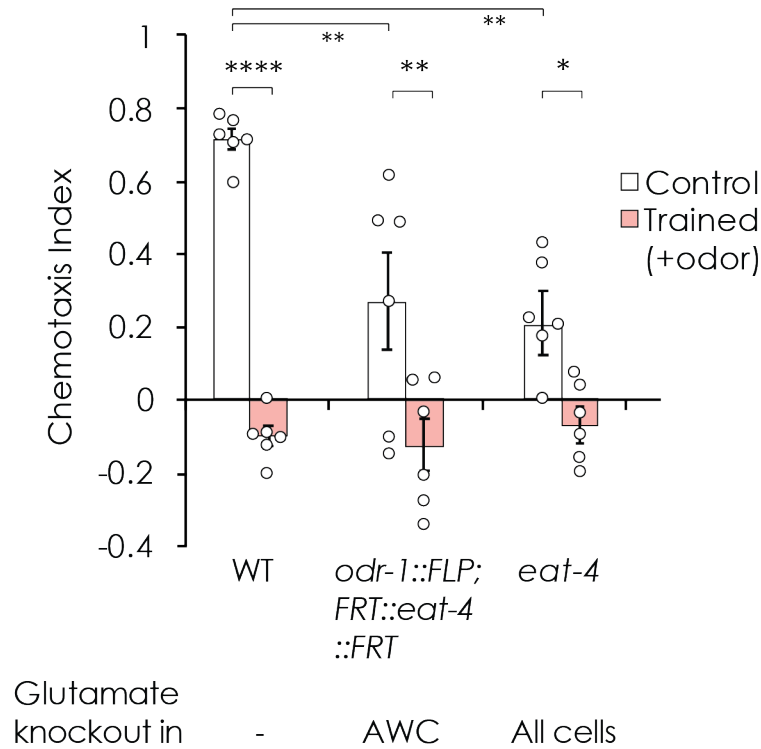


Figure 4.2 Role of glutamate release in butanone chemotaxis.

Chemotaxis index of wild-type and vesicular glutamate transporter knockout animals. Compared to wild-type, both control AWC cell-specific knockout of the vesicular glutamate transporter *eat-4* and *eat-4* null mutants had significant reduction of chemotaxis and in each case aversive learning was observed. Residual chemotaxis as well as reduced aversive learning in these strains indicate that glutamate and an additional transmitter released by AWC are required for normal butanone response.

To investigate the synaptic output of AWC neuron during chemotaxis, I utilized EAT-4-pH, a reporter of glutamate synaptic vesicle release based on pHluorin, a pH-sensitive version of GFP that becomes fluorescent when the acidic synaptic vesicle fuse with the plasma membrane. When the pHluorin reporter inserted into an internal domain of EAT-4 and expressed under the *str-2* promotor, it reports fusion of glutamatergic vesicles specifically in AWC^{ON} (Ventimiglia & Bargmann, 2017). An integrated *str-2::EAT-4-pH* transgene was crossed into the *ist-1(ok2706)* strain. Behavior tests confirmed that *str-2::EAT-4-pH* did not alter the behavior of WT or *ist-1(ok2706)* animals (data not shown). Both WT and *ist-1(ok2706)* were food-deprived in the presence or absence of butanone, then loaded into a single worm microfluidic chip for pHluorin imaging. I used a 10⁻⁵ M stimulus, an odor concentration at which reliable GCaMP responses were observed in AWC^{ON} in both control and trained animals (Figure 4.1). In controls that were food-deprived without butanone, wild-type animals responded similarly to the odor pulses by decreasing glutamate release as reported with *str-2::EAT-4::pH* (Figure 4.3). When odor was removed, glutamate release increased. By contrast, wild-type trained animals had a greatly diminished response to odor pulses, consisted with a dampened synaptic response to odor, as demonstrated by a smaller decrease in glutamate release upon odor addition and smaller increase in glutamate release when odor was removed. This result revealed that aversive learning reduces odor-regulated glutamate release from AWC^{ON}.

Next, I examined the *str-2::EAT-4::pH* reporter in an *ist-1* mutant. Control animals had a similar response to butanone as wild-type, with suppression of release by butanone addition and increased release upon odor removal. However, after training the *ist-1* mutant retained substantial odor-regulated glutamate release, providing a synaptic correlate of aversive learning.

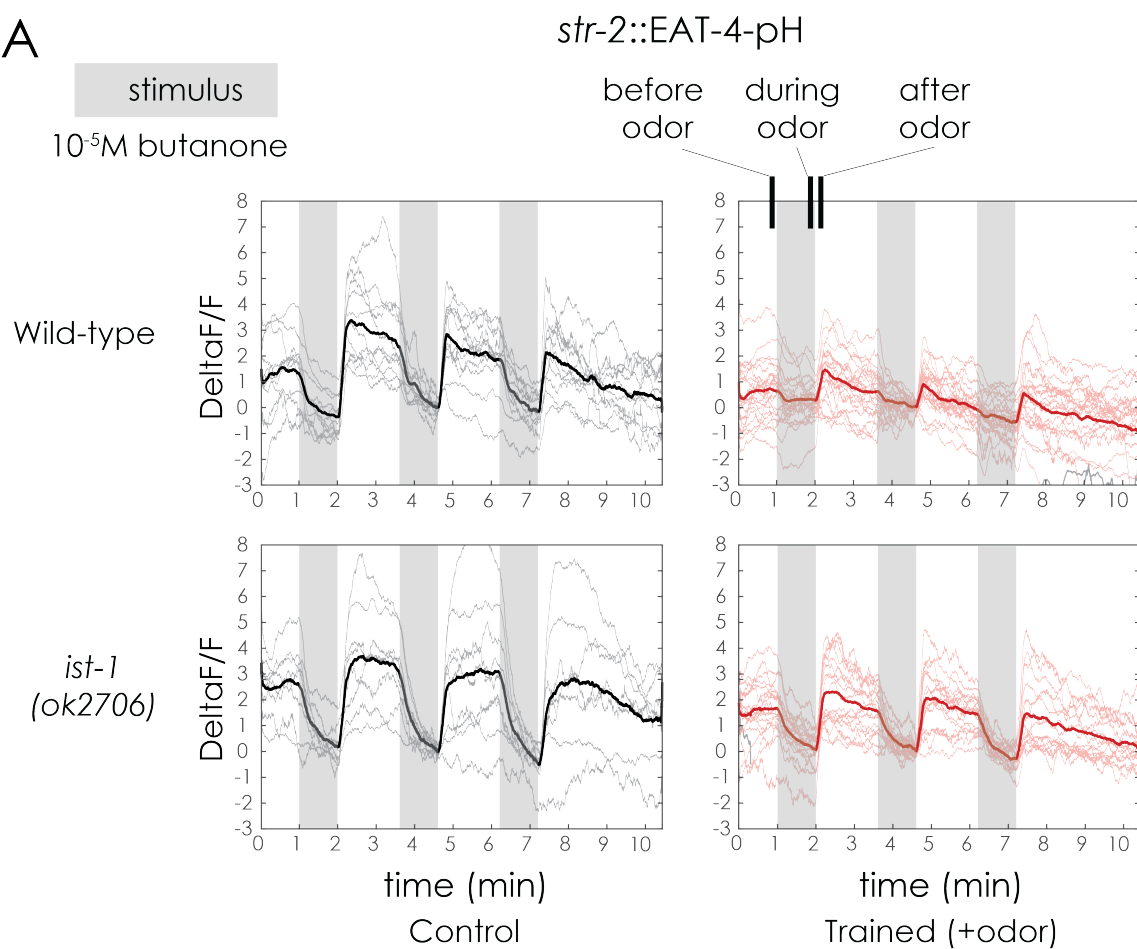
These results suggest that *ist-1*-associated insulin signaling induced by pairing odor with food deprivation decouples butanone sensation and glutamate release in the AWC^{ON} neuron.

Figure 4.3 pHluorin imaging reveals that changes in synaptic output during aversive learning are dependent on *ist-1*.

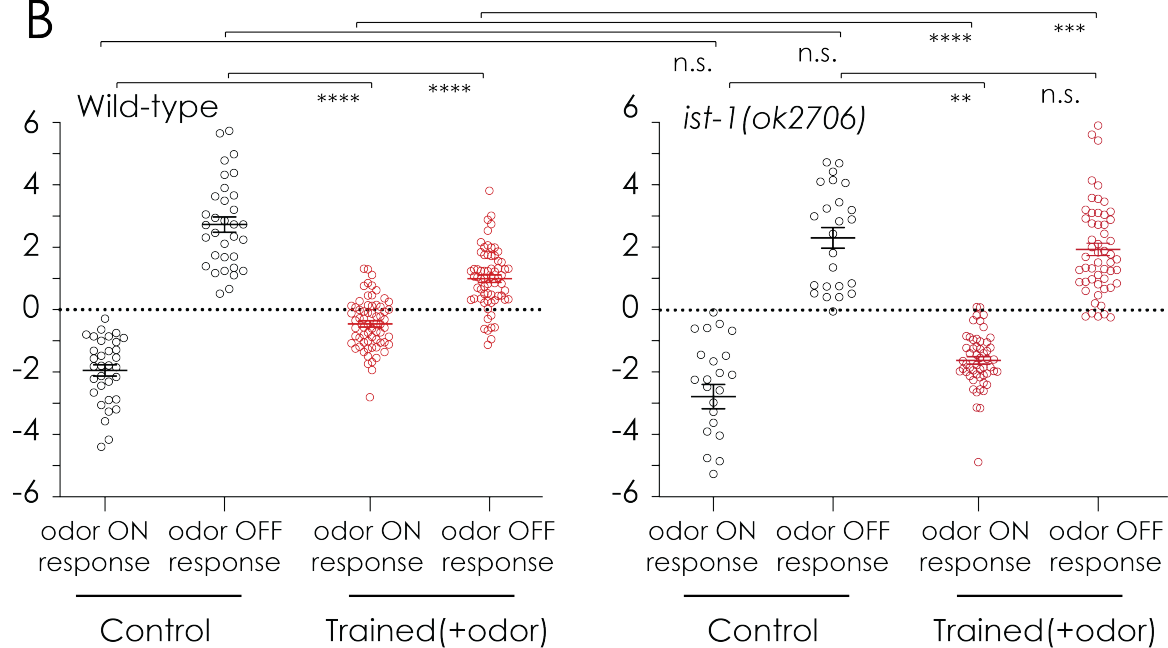
A) Average response of EAT-4-pH fluorescence in wild type (top) and *ist-1* mutant (bottom) animals in control (left) and trained (right) groups. Black line shows average across multiple trials; grey lines shows signal from each individual trial. Shaded region indicates times during the trial when the butanone stimulus was present. Control animals responded to the stimulus by decreasing synaptic output, and the signal quickly recovered when the stimulus was removed. Wild-type trained animals had less response when the odor was added and removed, compared to the control. Trained *ist-1* animals had higher responses than the trained wild-type animals.

B) Quantification of results. The average pHluorin signal 5 seconds before the butanone stimulus, 5 seconds before the end of the stimulus, and 5 seconds after the removal of the stimulus, was calculated and plotted in the panel on the right. (WT control: n=11 worms with 3 trials each, WT trained: n=22 worms with 3 trials each, *ist-1(ok2706)* control: n=10 worms with 3 trials each, *ist-1(ok2706)*: n=18 worms with 3 trials each).

A



B



4.3 Behavioral change in aversive learning

In a simplified neuron network, the AWC^{ON} neuron connects to first layer interneurons AIA, AIB and AIY. Another first layer interneuron, AIZ, indirectly connects to AWC^{ON} through AIB and AIY (Tsalik & Hobert, 2003). AIA and AIY neurons functionally inhibit turns while AIB and AIZ promote turns (Gray, Hill, & Bargmann, 2004; Wakabayashia, Kitagawab, & Shingaia, 2004) (Figure 1.1). In butanone chemotaxis, a decrease in butanone concentration leads to depolarization of the AWC^{ON} neuron, which inhibits AIA and promotes AIB activity (Chalasani, et al., 2007). AIB neurons in turn activate a backward command neuron, AVA, to induce reversals in a biased random walk (Figure 1.1). For the alternative steering mode the AIY and AIZ neurons appear to be most important. Finally, odors can elicit other behaviors such as pauses that may also contribute to attraction (Albrecht & Bargmann, 2011).

In contrast to other types of learning such as pathogen avoidance, where cellular and molecular memory signals are stored and integrated in the interneurons (Jin, Pokala, & Bargmann, 2016), we showed that olfactory memory can be formed at least in part in a single sensory neuron. Cho et al previously silenced interneurons during aversive training, and demonstrated that *ins-1* from AIA neurons is a likely source of insulin that activates the learning pathway in AWC. To further explore the possibility of involvement of interneurons during the execution of the memory formed in AWC, I used a histamine-gated chloride channel from *Drosophila* to silence individual neurons during chemotaxis. The histamine-gated chloride channel (hisCl) was expressed as transgenes driven by different cell-specific promoters. Histamine was added to the chemotaxis plate to activate the hisCl. As a result, the neuron expressing hisCl will be hyperpolarized and effectively silenced (Pokala, Liu, Gordus, & Bargmann, 2014).

Compared to the no histamine control, silencing AIB, RIA and RIM neurons individually during chemotaxis by adding histamine decreased animals' ability to chemotaxis to the butanone source, appearing as lowered chemotaxis index (Figure 4.4). The AIB, RIA double silencing also decreased the chemotaxis index of the control animals. AIZ silencing did not cause a defect. After pairing butanone with food deprivation, all interneuron silenced strains resembled wild-type strains in their behavior. I conclude that AIB, RIA and RIM promote chemotaxis, but did not find evidence that any specific interneuron is required for aversive learning or memory. These results are consistent with the imaging results, which indicate that butanone-evoked glutamate release from AWC^{ON} is reduced after training, and suggest that the same interneuron network could be used before and after training.

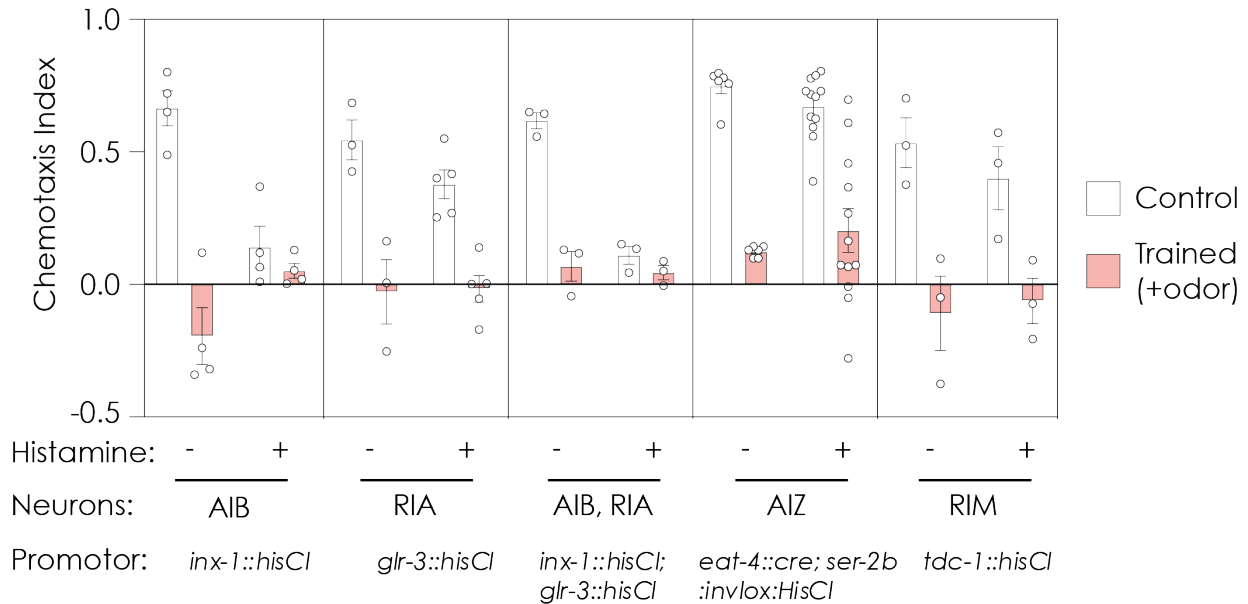


Figure 4.4 Selective interneuron silencing can disrupt chemotaxis but does not differentially affect aversive learning.

Chemotaxis index of interneuron silencing experiments using expression of the *Drosophila* histamine-gated chloride channel HisCl. Interneurons downstream of AWC^{ON} were silenced during chemotaxis after aversive training to see if any interneuron was the hub for storing the memory of aversive learning. Disrupting RIA and RIM decreases the chemotaxis index of control animals but did not affect aversive learning. Disrupting AIB caused a severe defect in chemotaxis that precluded analysis of learning. These results suggest that interneurons function as the infrastructure to allow chemotaxis, while learning is stored in the AWC neuron. Animals were either food deprived (control, white bars), or food deprived with butanone for 90 mins (trained, pink bars).

To test whether this decrease in interneuron response result in a change of interneuron-derived local motor behavior, I used data from computational tracking of worms (Figure 2.1) to calculate angle between headings of the worms and the direction of odor source (Figure 4.5). As expected in the biased random walk model, wild-type control animals conducted a higher frequency of long-reversal-omega turns when they moved away from the odor source, than when they moved towards the odor source. On the other hand, trained animals conducted similar frequency of long-reversal-omega turns, but these turns are regardless of the direction of the odor source (Figure 4.5), indicating they have lost the ability to conduct a biased random walk.

Next, I examined the biased random walk in *ist-1* mutant. Control animals had a similar response to butanone as wild-type, by conducting a higher frequency of long-reversal-omega turns when they moved away from the odor sources, than when they moved towards the odor source. However, after training the *ist-1* mutant retained substantial odor-oriented biased random walk (Figure 4.5), indicating they are behaviorally similar to animals that weren't trained.

These results suggest that biased random walk contributes to chemotaxis, and is suppressed by aversive learning in a process that requires *ist-1* (Figure 4.5).

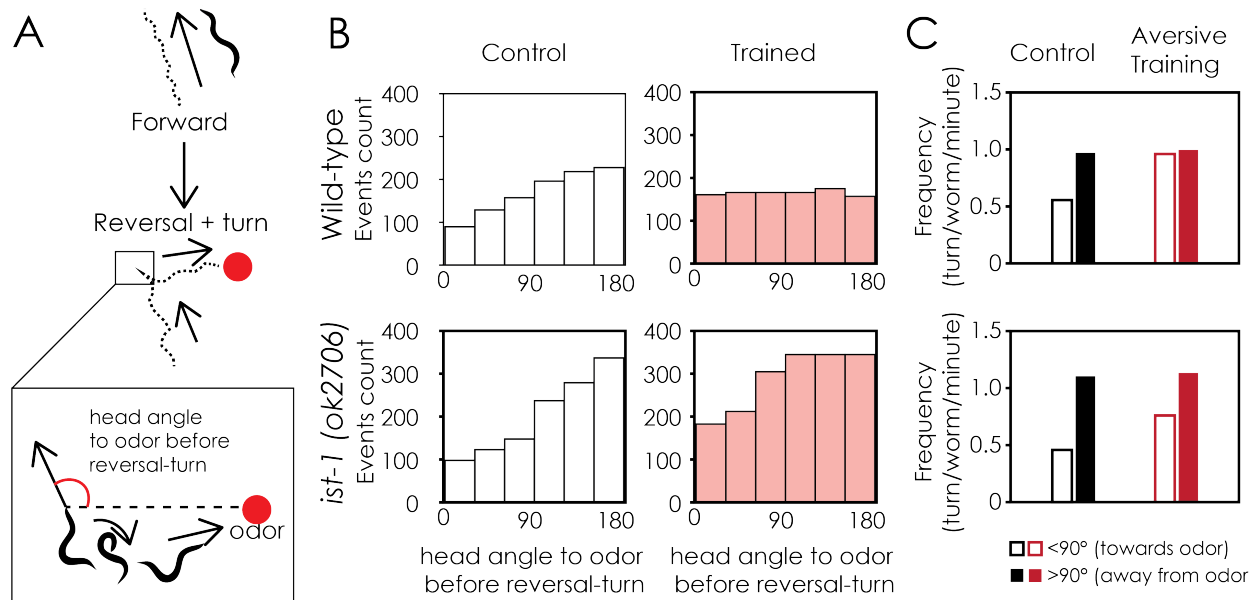


Figure 4.5 *ist-1* mutants maintain the ability to chemotaxis after aversive learning by maintaining the biased-random walk.

A) Diagram illustrating the angle between an animal's head and the odor source, which was measured each time animals start a long reversal-omega turn behavior.

B) Quantification of total local motion events of each chemotaxis assay (n=50 animals each). Wild-type and *ist-1* control animals showed a bias of initiating more long reversal-omega turns when headed away from the odors. This is consistent to the biased-random chemotaxis model. Wild-type trained animals no longer show the bias in initiating long reversal-omega turns. The *ist-1* animals retained the bias in initiating long reversal-omega turns, suggesting that *ist-1* is part of the pathway that suppressed the biased random walk after learning.

C) Frequency of initiating a long-reversal omega turn when head is pointed less than 90 degree from the odor (towards the odor) versus more than 90 degree from the odor (away from the odor).

Chapter 4 DISCUSSION

In this chapter, I examined the neuronal circuit mechanism of AWC^{ON} modification during odor chemotaxis and odor aversive learning. The AWC^{ON} neuron responds to odor addition and removal by a rapid change of calcium activity. AWC^{ON} then sends output signals to the interneuron network, in part through synaptic glutamate release from its axon. Butanone treatment at high concentrations desensitizes the calcium response to subsequent butanone pulses in AWC. This is consistent with a previous study (Cho, Brueggemann, L'Etoile, & Bargmann, 2016). Aversive learning, caused by lower concentration butanone treatment paired with food deprivation, does not modify the AWC^{ON} calcium response to odor, but instead dampens the glutamatergic output. IST-1 is not required for the change in calcium response during desensitization, but it is required for the change in synaptic glutamate output after aversive learning.

I also showed that the AWC^{ON} sensory neuron guides chemotaxis through glutamate neurotransmission to the downstream interneuron network. This is consistent with previous work on other behavior guided by AWC (Chalasani, et al., 2007; López-Cruz, et al., 2019). The interneurons integrate information to drive a variety of motor behaviors. I characterized a biased random walk strategy that *C. elegans* utilize during chemotaxis to butanone, showed that the biased random walk strategy is suppressed during learning, and found that this learning-induced suppression is dependent on IST-1.

In summary, IST-1 acts in a non-canonical insulin pathway by regulating the axonal insulin/IGF receptor DAF-2c, which in turn regulate synaptic glutamate release from the AWC^{ON} neuron to direct odor aversive learning (Figure 4.6).

4.4 Future Directions

Several studies have shown that learning in *C. elegans* is mediated by the change of communication between a few members of the interneuron network, usually with odor signal acting on one neuron, and aversive signals acting on another neuron (Wu, et al., 2019; Zhang, Lu, & Bargmann, 2005; Jin, Pokala, & Bargmann, 2016; Chen, et al., 2013). In the case of *Pseudomonas* pathogen avoidance learning, a form of imprinted memory formation in young animals requires AIB and RIM interneurons, while the memory retrieval requires the AIY and RIA interneurons (Jin, Pokala, & Bargmann, 2016). By contrast, in this study I showed that the AWC^{ON} neuron can integrate butanone and food signal to modify one sensory neuron, through an isoform-specific, compartmentalized insulin signaling mechanism.

IST-1 is expressed reliably in high levels in at least eight pairs of head neurons, mostly are sensory neurons and interneurons. We have started a collaboration with the Iino lab in Japan testing the function of IST-1 in salt learning. With BAG neurons being one of the neurons expressing IST-1, it is possible that IST-1 will participate in the process of regulating oxygen or carbon dioxide sensing. It will also be interesting to ask if IST-1 participate in the regulation of more complex food and pathogen related behaviors, not just limited to individual sensory cues.

Many questions remain, especially on the input on the insulin/IGF receptor DAF-2. As mentioned in Chapters 1 and 3, the diversity in number and function of insulin-like peptides is dauntingly large. A previous study showed that INS-1 secreted by AIA interneuron is required for aversive learning in AWC^{ON}, and I showed INS-1 is required for the increase of DAF-2 receptor level in AWC^{ON} during food deprivation (Cho, Brueggemann, L'Etoile, & Bargmann, 2016). However, we do not yet understand in this case if INS-1 directly binds to the DAF-2

receptor in AWC^{ON} neuron. In dauer formation, INS-1 inhibit DAF-2 (Kodama, et al., 2006), whereas in learning INS-1 and DAF-2 have similar effect. There are a few possible explanations.

In model A, one possibility is the involvement of an additional neuron between AIA and AWC^{ON} neuron. By analogy to other learning, insulins may antagonize one another using different neurons. In this scenario, INS-1 could be secreted by AIA, act on an unknown neuron, which secretes other insulins to regulate DAF-2 in AWC^{ON}. One way to test this hypothesis, is to screen additional insulin-like neuropeptide mutants.

In Model B, another possibility is that INS-1 may differentially act on DAF-2a and DAF-2c, in different neurons, or the same neuron. The relative activating and inactivating functions of a receptor/ligand complex are partially dependent on its intracellular adapter proteins and/or the availabilities of members of the different intracellular signaling cascade, as insulin/IGF receptor can regulate more than just the AGE-1 pathway (Murphy & Hu, 2013).

Another area of potential study can arise from understanding the role of *daf-16* in butanone chemotaxis and learning. In agreement with previous reports I found that *daf-16* mutant animals do not chemotax. Three different *daf-16* alleles all showed the similar result, although only one was shown. However, *daf-16* was able to chemotaxis to a higher butanone concentration in the appetitive learning assay. In salt learning, *daf-16* mutant animals also showed a defect in salt learning when pairing salt with food deprivation, but had no defect in salt learning when pairing salt with food (Nagashima, Iino, & Tomioka, 2019). I speculate that DAF-16, the fork-head transcription factor may regulate the worm's chemotaxis, either through regulation of the chemosensory receptors, or via the pathways that regulate desensitization. This question can be addressed by testing the calcium response of AWC^{ON} to butanone in *daf-16* mutant animals using GCaMP, and the synaptic glutamate output of AWC^{ON} by pHluorin.

Knowing the regulatory site of *daf-16* in the chemotaxis pathway can provide additional information on the role of canonical and non-canonical insulin pathways in odor sensation and learning.

EXPERIMENTAL PROCEDURES

Nematode maintenance and molecular biology

All strains were maintained in the 20°C incubator on Nematode Growth Medium (NGM) plates, seeded with *E. coli* OP50 bacteria as a food source (Brenner, 1974). Wild-type animals were genetically defined clonal strain PD1074 derived from the Bristol strain N2 (Yoshimura, et al., 2019).

Chemotaxis assays

Worms were grown at 20°C on 10 cm round NGM plates spotted with 900 μ l of *E. coli* OP50. Chemotaxis plates are square plates containing 12 mL of modified NGM agar (without peptone and cholesterol, 1.7% Agar-agar, 50 mM NaCl, 25 mM KH₂PO₄, 1 mM CaCl₂, 1 mM MgSO₄). The chemotaxis plates are allowed to air-dry without lids for 15 minutes before use, or are stored at 4°C for up to 2 weeks before use. Fifteen minutes before the start of the assay, one 1 μ l spot of NaN₃ is spotted at the midline of each end of the plate. Adult animals were washed three times with NGM buffer (50 mM NaCl, 25 mM KH₂PO₄, 1 mM CaCl₂, 1 mM MgSO₄) with strict timing of 15 min total wash time. After wash, 50-100 animals were placed at the center of the square plate. Plates were spotted with either one 2 μ l drop of butanone diluted at 1:10 or 1:1000 in ethanol, or an ethanol control. A piece of folded, absorbent paper (Kimwipe) was used to soak up the solutions from the droplet containing the worms in the middle of the plate before the lid was closed. Soaking up of the solution frees the worms from the droplet, marking the beginning of the assay.

Other odors were used for chemotaxis at the following concentrations: benzaldehyde at 1:200, isoamyl alcohol at 1:100, 2,4,5-trimethyl thiazole at 1:1000, and 2,3-pentanediol at 1:10000, diluted in ethanol. The assay was recorded in an imaging apparatus for 1 hour at 3

frames/second. The chemotaxis index was quantified at the last frame of the recording by counting animals that had left the origin, on the side closest to the odor (#Odor), the side closest to the control (#Control), and in the intermediate region (#Middle). Animals' positions were also tracked by algorithms and further analyzed of their behaviors. The formula used to calculate the chemotaxis index was: $\text{Chemotaxis index} = (\# \text{Odor} - \# \text{Control}) / (\# \text{Odor} + \# \text{Control} + \# \text{Middle})$

For histamine-dependent inhibition during the chemotaxis, histamine dihydrochloride (Sigma) was added to the modified NGM agar at a final concentration of 10 mM before the plates were poured.

Training for aversive learning

The training protocol for aversive learning is based on the assay developed by (Colbert & Bargmann, 1995) with some modifications. One-day old adults were washed three times with NGM buffer and placed on conditioning plates consisting of NGM agar without peptone and cholesterol (same as in chemotaxis plates). For the trained group, 20 ul of butanone were placed on four small pieces of agar on the inside of the lid of the plate, while the control group did not have butanone on the lid. The plates were then sealed with parafilm for 90 minutes before animals were washed off the training plate and further washed and then tested in chemotaxis assays according to the previous section.

Training for desensitization and appetitive learning

The training protocol for desensitization is identical to the appetitive learning (or enhancement) protocol. Training for appetitive learning is similar to those described in (Torayama, Ishihara, & Katsura, 2007). One-day old adults were washed three times with NGM

buffer and placed on conditioning plates consisting of NGM agar seeded with 900 ul of OP50. For the trained group, 20 ul of butanone were placed on four small pieces of agar on the inside of the lid of the plate, while the control did not have butanone on the lid. The plates were then sealed with parafilm and incubated for 90 minutes before animals were washed and tested in chemotaxis assays according to the section “**Chemotaxis assays**” with 1:1000 butanone for desensitization, and 1:10 butanone for appetitive learning.

Chemotaxis recordings and analyses

40-60 animals were placed on a square plate with modified NGM agar. A 1-hour movie was recorded at 3 frames per second with Streampix software and a 6.6 MP PL-B781F CMOS camera (Pixelink). Animals’ trajectories were extracted by a custom MatLab script. A long-reversal-omega turn (pirouette) event was defined as a reversal coupled with an omega turn, and identified as a sharp change in angular speed (≥ 75 degree/s), followed by a sharp reorientation (body-enclosing ellipse eccentricity ≤ 0.875 , filtered by an angular speed threshold ≥ 60 degree/s), as previously described (Pokala, Liu, Gordus, & Bargmann, 2014). Long-reversal-omega frequency was calculated by binning the events with respect to the angle between each worm’s heading and the direction of the odor source before the reorientation, at 30° intervals. The normalized long-reversal-omega frequency was calculated by binning the event/worm/minute with respect to angle between each worm’s heading and the direction of the odor source before the reorientation, at 90° intervals.

Calcium imaging in the arena chip

The chip design and stimulus delivery system is similar to that used in (Larsch, Ventimiglia, Bargmann, & Albrecht, 2013; Cho, Brueggemann, L'Etoile, & Bargmann, 2016) with slight modifications. PDMS chips with two arenas were made using a custom mold. The chips were flooded with NGM buffer containing 10 mM tetramisole hydrochloride, and 10-15 adult animals were loaded into each arena. Worms were trained for 90 minutes with butanone 10^{-2} M (or NGM buffer for control groups) followed by 15 minutes of NGM buffer to act as a wash step. Worms were then imaged on a Zeiss AxioObserver. An A1 microscope with a 2.5X objective and Metamorph software were used for synchronized image capture with pulsed illumination. A three-way valve was used to switch between buffer and odor flow into the chip, and a Hamilton valve was used to switch between different concentrations of odor. The stimulation protocol was three 30-second alternations between odor and buffer followed by 90 seconds of buffer, and then the sequence was repeated at 10-fold higher odor concentration for a total of six butanone concentrations, ranging from 10^{-8} M to 10^{-3} M, plus a buffer-to-buffer control. Fluorescence was measured using a custom imageJ script (Larsch et al., 2013).

Calcium imaging data analyses are identical to those used in (Cho, Brueggemann, L'Etoile, & Bargmann, 2016). Custom Matlab scripts were written to analyze calcium imaging data generated by ImageJ tracking programs.

pHluorin imaging in the single-animal trapped chip

The pHluorin imaging method is similar to that developed by (Ventimiglia & Bargmann, 2017). 1-day old adults containing the EAT-4-pHluorin transgene were picked off food and trained for aversive learning. After training, worms were washed 3 times for a total of 15 minutes with NGM buffer and loaded into the imaging chip. Polydimethylsiloxane (PDMS) imaging

chips were fabricated as described in (Chronis, Zimmer, & Bargmann, 2007) using a custom-design silicon mold. PDMS chips were cured and holes were punched in fluid inlets, and chips were then bonded to glass cover slips. Worms were immobilized in the chip by adding 1 mM tetramisole hydrochloride (Sigma) to the worm holding chamber. A time stack of images was captured using a CoolSnap HQ Photometrics camera and a Zeiss Axioscope upright microscope with a 40X objective.

Images were movement-corrected using the method developed by (Tseng, et al., 2011). To extract fluorescence measurements from the images, I used a custom, semi-automated tracking software in ImageJ script designed by (Ventimiglia & Bargmann, 2017) to track axon position and extract intensity measurement.

pHluorin imaging analysis was similar to that used in (Ventimiglia & Bargmann, 2017), with slight modifications. Data was smoothed with a moving average of 50 frames before it was used for analysis and plotting.

Quantitative analysis of DAF-2::mVenus subcellular localization

One-day old adult animals were either picked directly off plates (fed) or moved to an unseeded NGM plate for 90 minutes for food deprivation. Animals were then mounted and anaesthetized on a 3% agar pad containing 10 mM sodium azide. Images were taken within 5-30 minutes after mounting. Fluorescent images of live animals were acquired using a Zeiss Axio Imager Z1 apotome system with an AxioCamMR3 camera through an excitation filter of BP 500/20nm, with a beam splitter at 515 nm and an emission filter at BP 535/30 with a 20% attenuator setting on the light source. A Z-Stack of 30 images was taken at 1 μ m spacing with a 63X/1.40 NA objective with 500 ms exposure time per image. DAF-2a or DAF-2c::mVenus

fluorescence intensity was measured with ImageJ. An image containing the largest area of the AWC^{ON} cell body or axon based on mVenus expression was selected from z-series image for quantification. DAF-2::mVenus quantification was different from that described in (Ohno, et al., 2014), and more similar to described in (Nagashima, Iino, & Tomioka, 2019). This decision was based on the suggestion from the authors of the articles. A rectangular region of interest (ROI) was drawn manually inside the area of the cell body or a piece of axon before using ImageJ to calculate the average intensity of fluorescence in the ROI. Average fluorescence intensity from at least five ROIs was used to quantify axon fluorescence of a given image stack. Background fluorescence intensity was averaged from at least five ROIs right next to the cell body or axon. The background subtracted fluorescent level (F-F₀) was then calculated by subtracting the average fluorescence intensity of the background from the average fluorescence intensity of the cell body or axon.

Identification of *ist-1(ky1071)* allele from genomic sequencing of *flp-20(pk1596)*

Genomic DNA was prepared from wild-type and the four strains of *flp-20(pk1596)* backcrossed to wild-type. The strain CX17680, a 2X backcross of *flp-20(pk1596)*, and the strain CX17683, a 6X backcross of *flp-20(pk1596)*, are both defective to butanone aversive learning. The strain CX17681, a 6X backcross of *flp-20(pk1596)* and CX17685, an 8X backcross of *flp-20(pk1596)*, are both proficient in butanone aversive learning. Whole genome sequencing of these samples was performed by the Rockefeller Genomic Resource Center using an Illumina HiSeq 2500 System. Sequence reads were analyzed by Patrick McGrath (a collaborator) by comparing the sequence of the back-crossed strains to the wild-type strains using his custom

program (McGrath et al., 2011). A T->G mutation was found in the splicing motif for *ist-1* after the end of the 3rd exon and verified using Sanger sequencing.

The identified *ist-1(ky1071)* deletion is:

```
ggaatttcagTATCAATGGCAGCAAGAGAGGAGAGAATACGCGAAAGTAGACAACAAGGGCAAC
TGAAAGAAAAAAGGCTGAAAAATCCAGATTCAAAAGGTGATACAAGTCACGATAAGCCGACCAG
AGAAACATGGAAGCCGTTAGCCGTTGAAGACTTACCAAAGGATGAAGATCCGGATGAATTTGGA
ATTCCAGAAGTCTACAAATGTGGAAATTGTTTAGTAGGGTTTGCTCCAGTGgt[t->g]
atgtttatntagaaattatgtgcacaattcaatTTTTTgagcagttgtcgatcaaaaagaaaat
tctttcagattttatTTTTtaattatgcataaaatcttcattcc
```

(point mutation underlined, mutation in square bracket, 3rd exon in uppercase, introns in lowercase)

CRISPR/Cas9-generated mutant strains

To generate short frame-shift mutants for *ist-1* and other gene candidates used for screening, I used a co-CRISPR protocol (Arribere, et al., 2014). This approach uses a template-guided dominant mutation on the *rol-6* gene to induce a roller phenotype to aid selection of the mutant progeny. Young hermaphrodites with only a few eggs in the gonad were injected with a mix of plasmids encoding Cas9, a gRNA targeting *rol-6*, a gRNA targeting the gene of interest (such as *ist-1*), and a ssDNA repair template that induces the *rol-6(su1006)* mutation. F1 animals carrying roller phenotypes were isolated onto individual plates, allowed to lay eggs, and then screened for a target mutation by Sanger sequencing. Animals with frame-shift mutations were chosen to generate homozygous strains. The homozygous strains were then backcrossed twice to wildtype strains before being used to test behavior.

The generated *ist-1(ky1074)* mutation is:

AAAACAGTGAGCTTCAGCGCTTGCCAACAATAATAAACGGTGTCTGAGCTGATGTTGCCCCGCCGAGCC

(Deletion underlined)

The generated *ist-1(ky1075)* mutation is:

GCTAATGTTTGTGACACTCACGGAACGATGTTTAGAACTTCACGAGTCGGAGAAATCCTATCGTGCCG

(Deletion underlined)

The generated *ist-1(ky1076)* mutation is:

GCGCCAGGAAGAAACAGGAAGAAACTGTAAAGAAATgtaagtgtcgttctgttatggttggttaaatt

(Deletion underlined)

Generating the *daf-2* cell-specific knockout strain

We used a flippase-FRT system to generate the *daf-2* cell-specific knockout construct. The construct had one FRT site inserted in the beginning of the gene and one inserted at the end of the gene to achieve full excision of the gene upon flippase recombination. To generate a knock-out strain with a fluorescent reporter for successful deletion, we inserted a *let-858* 3'UTR-FRT-mCherry coding sequence between the stop codon and the 3' UTR of *daf-2*, with the intention that mCherry should be expressed after successful knockout of *daf-2* in cells of interest.

We used a protocol developed by the Mello lab to insert the FRT site sequence and the mCherry coding sequence after the 3' UTR of the *daf-2* gene (Dokshin, Ghanta, Piscopo, & Mello, 2018). Briefly, *S. pyogenes* Cas9 protein and synthesized tracrRNA and crRNA were used to generate the cut required for recombination. The *let-858* 3' UTR-FRT-mCherry insertion sequence was first assembled by standard cloning methods into a plasmid vector. Then oligos were used to generate the repair template by PCR: a pair of 55 nt 5' SP9 (TEG) modified oligos added 35 nt of homology to the insertion site in the genome, annealing 20 nt complimentary to the insertion sequence. The repair template was then heated and cooled with specific downsteps

in the thermal cycler (95°C-2:00 min; 85°C-10 sec, 75°C-10 sec, 65°C-10 sec, 55°C-1:00 min, 45°C-30 sec, 35°C-10 sec, 25°C- 10 sec, 4°C-forever. Ramp down at 1°C/sec). Although the mechanism is unknown, the Mello lab found these heating-cooling steps are critical to achieve high knock-in efficiencies. The repair template, tracrRNA, crRNA and *rol-6(su1006)* plasmid co-injection marker were then injected into young hermaphrodite gonads, and mutants were selected as described above. (See section “**CRISPR/Cas9-generated mutant strains**”).

The complexity of the *daf-2* gene complicated the design of this transgenic construct. Previous cell-specific knockout designs with fluorescent reporters entailed inserting the upstream FRT site before the first exon. However, there are many promotor-like enhancer regulatory elements embedded in the introns of *daf-2* isoforms, so full excision of the gene could cause inadequate expression of the fluorescent reporter that reports the excision. Therefore, we decided to insert the upstream FRT site in the middle of the *daf-2* gene to excise the second half of the gene that is common to all isoforms, hoping to get adequate expression of the reporter. The exons 10 through 17 should be excised by the FRT sites, which should delete all intracellular domains including the kinase domain, therefore adequately disable the *daf-2* pathway. However, we did not anticipate that our design would leave an unintended splicing signal in the intron right before the excision, which caused the fluorescent reporter to be fused to *daf-2* in an incorrect reading frame. Although this construct did not work perfectly as designed to report the deletion in the same cell, we were able to use a secondary strain BN294 to report the cell-specific flippase expression in the cells by the same transgene that was injected into the *daf-2* knock-out animals. The BN294 strain carries an integrated transgene that expresses mCherry in every cell, and a masked GFP. Upon flippase recombination, the mCherry is excised while unmasking GFP expression (Muñoz-Jiménez, et al., 2017). We were able to behaviorally verify the *daf-2* deletion

by observing a severe developmental delay in the *daf-2* knock-out construct strain (CX1095) injected with flippase transgene driven by a pan-neuronal promoter, the H20 promotor, while the *daf-2* knock-out construct without the flippase transgene was wild-type. A new study on the DAF-2b isoform consisting of exon 1-11 indicates that it generates a secreted form of insulin receptor that inhibits insulin-like neuropeptides (Martinez, et al., 2020). Our construct leaves the exon 1-9 intact, leaving a possibility that DAF-2b can be still partially functional. Margaret Ebert helped design the transgenic construct and CRISPR insertion methods. Max Brown helped perform reagent generation, worm injection and strain selections.

The sequence around the 5' insertion of the FRT site in *daf-2* (CX1095) cell specific knockout strain is:

ccgatttgccggaaattccaattccggcaattttccgatttgccggaaatttcaaattccgcca**GAAGTTCCTA**
TTCTCTAGAAAGTATAGGAACTTCacttgccgatttgccgtgaaatttcatttctctgcgattttccga
gttgcccggaaatttcaaaaaattttctgaaactctgaaactagaaaagtttcggaaagaagcgcctaaacaggcgct
tttaattgctgt

(Black letters: *daf-2* genomic sequence. Lower case: introns. Upper case: exons. **Bold letters:** **FRT site sequence.**)

The sequence around the 3' insertion of the *let-858* 3' UTR-FRT-mCherry in the *daf-2* (CX1095) cell specific knockout strain is:

CGAAACGGCAACAGCCGTGACATTTTCAACGGACGTTTCGGCTTTCGGTGAAAATGAGCATCTAA
TCGAGGATAATGAGCATCAT**CCACTT/GTCTGA**TAAATTTTCAAATTTTAAATACTGAATATTT
GTTTTTTTTCTATTATTTATTTATTCTCTTTGTGTTTTTTTTCTTGCTTTCTAAAAAATTAAT
TCAATCCAAATCTAAACATTTTTTTTTCTCTTTCCGTCTCCCAATTCGTATTCCGCTCCTCTCA
TCTGAACACAATGTGCAAGTTTATTTATCTTCTCGCTTTCATTTATTAGGACGTGGGGGGAAT
TGGTGGAAGGGGGAAACACACAAAAGGATGATGGAAATGAAATAAGGACACACAATATGCAACA

ACATTCAATTCAGAAATATGGAGGAAGGTTTAAAAGAAAACATAAAAAATATATAGAGGAGGAAG
GAAAACTAGTAAAAAATAAGCAAAGAAATTAGGCGAACGATGAGAATTGTCTCGCTTG**GAAGT**
TCCTATTCTCTAGAAAGTATAGGAACTTCA****ATGGTCTCAAAGGGTGAAGAAGATAACATGGCAA
TTATTAAAGAGTTTATGCGTTTCAAGGTGCATATGGAGGGATCTGTCAATGGGCATGAGTTTGA
AATTGAAGGTGAAGGAGAAGGCCGACCATATGAGGGAACACAAACCGCAAACTAAAGgtaagt
ttaaacatatatataactaactaaccctgattatttaaattttcagGTAACTAAAGCGGACCAT
TACCATTGCGCTGGGACATCCTCTCTCCACAGTTCATGTATGGAAGTAAAGCTTATGTTAAACA
TCCGGCAGATATAACCAGATTATTTGAAACTTTCATTCCCGGAGGGTTTTAAGTGGGAACGCGTA
ATGAATTTTGAAGACGGAGGAGTTGTTACAGTGACGCAAGACTCAAGgtaagtttaaacagttc
ggtactaactaaccatacatatttaaattttcagCCTCCAAGATGGAGAATTTATTTATAAAGT
CAAACTTCGAGGAACGAATTTCCCCTCGGATGGACCTGTTATGCAGAAGAAGACTATGGGATGG
GAAGCTTCAAGTGAAAGAATGTACCCTGAAGACGGTGCTCTTAAGGGAGAGATTAAACAACGTC
TTAAATTGAAAGATGGAGGACATTACGATGCTGAGGTGAAGACAACTTACAAAGCCAAAAACC
AGTTCAGCTGCCAGGAGCGTACAATGTTAATATTAACTGGATATCACCTCCCACAACGAGGAT
TACACTATCGTTGAGCAATATGAAAGAGCTGAAGGGCGGCACTCGACAGGTGGCATGGATGAAT
TGTATAAGTAGAACCCCCAAAAATCCCGCCTCTTAAATTATAAATTATCTCCACATTATCAT
 ATCTCTACACGAATATCGGATTTTTTTTTCAGATTTTTTCTG

(black letters: *daf-2* genomic sequence. Lower case: introns. Upper case: exons. **Yellow highlight**: CRISPR target sequence. Slash: / CRISPR cut sight. Blue letters: *let-858* 3' UTR. **Bold letters**: FRT site sequence. **Red letters**: mCherry sequence.)

Table 5.1 Strains generated for this study

Strain	Genotype	Description
CX17680	<i>ist-1(ky1071) flp-20(pk1596) X</i>	1x backcrossed from PT505
CX17681	<i>flp-20(pk1596) X</i>	3x backcrossed from PT505
CX17683	<i>ist-1(ky1071) flp-20(pk1596) X</i>	3x backcrossed from PT505
CX17685	<i>flp-20(pk1596) X</i>	8x backcrossed from PT505
CX17728	<i>ist-1(ky1071) flp-20(pk1596) X; kyEx6241[ist-1 fosmid, 10ng/μL; myo-3::mCherry, 10ng/μL]</i>	Fosmid WRM062cC02
CX17910	<i>ist-1(ky1071) flp-20(pk1596) X; kyEx6343[ist-1(14kb promotor)::ist-1b, 10ng/μL; myo-3::mCherry, 5ng/μL]</i>	cDNA rescue
CX1074	<i>ist-1(ky1074) X</i>	CRISPR generated allele
CX1075	<i>ist-1(ky1075) X</i>	CRISPR generated allele
CX1076	<i>ist-1(ky1076) X</i>	CRISPR generated allele
CX17790	<i>ist-1(ok2706) X</i>	2x backcrossed from RB2621
CX18202	<i>ist-1(ok2706) X; kyEx6343[ist-1(14kb promotor)::ist-1b, 50ng/μL; myo-3::mCherry, 5ng/μL]</i>	
CX17977	<i>ist-1(ok2706) X; kyEx6390[str-2::ist-1b, 50ng/μL; myo-3::mCherry, 5ng/μL]</i>	<i>ist-1</i> rescue in AWCON
CX17969	<i>ist-1(ok2706) X; kyEx6382[gcy-28::ist-1b, 50ng/μL; myo-3::mCherry, 5ng/μL]</i>	<i>ist-1</i> rescue in AIA, ASI, AVF
CX17971	<i>ist-1(ok2706) X; kyEx6384[tdc-1::ist-1b, 50ng/μL; myo-3::mCherry, 5ng/μL]</i>	<i>ist-1</i> rescue in RIM
CX18183	<i>ist-1(ok2706) X; kyEx6491[srsx-1::ist-1b, 50ng/μL; myo-3::mCherry, 10ng/μL]</i>	<i>ist-1</i> rescue in AWCOFF, AWB
CX18178	<i>ist-1(ok2706) X; kyEx6486[str-3::ist-1b, 50ng/μ ; myo-3::mCherry, 10ng/μL]</i>	<i>ist-1</i> rescue in ASI
CX18182	<i>ist-1(ok2706) X; kyEx6490[elt-2::ist-1b, 50ng/μL; myo-3::mCherry, 10ng/μL]</i>	<i>ist-1</i> rescue in the gut
CX18054	<i>ist-1(ok2706) X; kyEx6417[str-2::GFP::linker::ist-1b, 50ng/μL; myo-3::mCherry, 5ng/μL]</i>	GFP::IST-1 fusion
CX18112	<i>ist-1(ok2706) X; gcy-28(tm2411) I; kyEx6417[str-2::GFP::linker::ist-1b, 50ng/μL; myo-3::mCherry, 5ng/μL]</i>	GFP::IST-1 fusion
CX18114	<i>ist-1(ok2706) X; pkc-1(nj1) V; kyEx6417[str-2::GFP::linker::ist-1b, 50ng/μL; myo-3::mCherry, 5ng/μL]</i>	GFP::IST-1 fusion
CX18117	<i>ist-1(ok2706) X; daf-2(pe1230) III; kyEx6417[str-2::GFP::linker::ist-1b, 50ng/μL; myo-3::mCherry, 5ng/μL]</i>	GFP::IST-1 fusion
CX18044	<i>ins-1(nr2091) IV; ist-1(ok2706) X</i>	
CX18045	<i>daf-18(e1375) IV; ist-1(ok2706) X</i>	
CX18046	<i>daf-16(mgDf50) I; ist-1(ok2706) X;</i>	
CX18013	<i>pkc-1(nj1) V; ist-1(ok2706) X;</i>	
CX1095	<i>daf-2(ky1095) daf-2(ky1087) III; ky1087 = [let-858UTR::FRT::mCherry],III:2995919, ky1096=[FRT],III:3010987</i>	edited <i>daf-2</i> with 5' and 3' FRT
CX1087	<i>daf-2(ky1087) III, ky1087= [let-858UTR::FRT::mCherry],III:2995919</i>	edited <i>daf-2</i> with 3' FRT
CX18084	<i>daf-2(ky1095) daf-2(ky1087) III; kyEx6436[tax-4::nFLP, 20ng/μL; elt-2::nGFP, 2ng/μL]</i>	<i>daf-2</i> knockout in sensory neurons
CX18086	<i>daf-2(ky1095) daf-2(ky1087) III; kyEx6438[str-2::nFLP, 20ng/μL; elt-2::nGFP, 2ng/μL]</i>	<i>daf-2</i> knockout in AWCON, RIA, ASI
CX18184	<i>daf-2(ky1095) daf-2(ky1087) III; kyEx6492[str-3::nFLP, 20ng/μL; elt-2::nGFP, 2ng/μL]</i>	<i>daf-2</i> knockout in ASI
CX18084	<i>bqSi294[pBN154(unc-119(+)) Phsp16.41::FRT::mCh::his-58::FRT::gfp::his-58] II; daf-2(ky1095) daf-2(ky1087) III; kyEx6436;</i>	Flippase activity reporter in sensory neurons

Table 5.1 Strains generated for this study, continued

Strain	Genotype	Description
CX18086	<i>bqSi294[pBN154(unc-119(+)) Phsp16.41::FRT::mCh::his-58::FRT::gfp::his-58] I; 1daf-2(ky1095) daf-2(ky1087) III; kyEx6438;</i>	Flippase activity reporter in AWCON, RIA, ASI
CX18191	<i>bqSi294[pBN154(unc-119(+)) Phsp16.41::FRT::mCh::his-58::FRT::gfp::his-58] II; daf-2(ky1095) daf-2(ky1087) III; kyEx6439;</i>	Flippase activity reporter in ASI
CX18192	<i>ist-1(ok2706) X; kyls721[integrated str-2::GCaMP5 from 50ng/μL ; elt-2::mCherry 10ng/μL]</i>	<i>ist-1</i> GCaMP imaging strain
CX18125	<i>ist-1(ok2706) X; kyls623[integrated str-2::pHluorin from 30ng/μL ; Coel:dsRed 15ng/μL]</i>	<i>ist-1</i> pHluorin imaging strain
CX18187	<i>kyEx6495[str-2::daf-2a::mVenus, 50ng/μL; myo-3::mCherry, 5ng/μL]</i>	DAF-2a::mVenus
CX18190	<i>kyEx6498[str-2::daf-2c::mVenus, 50ng/μL; myo-3::mCherry, 5ng/μL]</i>	DAF-2c::mVenus
CX18203	<i>daf-2(pe1230) III; kyEx6505[str-2::daf-2a::mVenus, 50ng/μL; myo-3::mCherry, 5ng/μL]</i>	DAF-2a rescue
CX18205	<i>daf-2(pe1230) III; kyEx6507[str-2::daf-2c::mVenus, 50ng/μL; myo-3::mCherry, 5ng/μL]</i>	DAF-2c rescue
CX18206	<i>daf-2(pe2722) III; kyEx6508[str-2::daf-2a::mVenus, 50ng/μL; myo-3::mCherry, 5ng/μL]</i>	DAF-2a rescue
CX18207	<i>daf-2(pe2722) III; kyEx6509[str-2::daf-2c::mVenus, 50ng/μL; myo-3::mCherry, 5ng/μL]</i>	DAF-2c rescue
CX18216	<i>ist-1(ok2706) X; kyEx5616[str-2::daf-2a::mVenus, 50ng/μL; myo-3::mCherry, 5ng/μL]</i>	DAF-2a::mVenus
CX18217	<i>ist-1(ok2706) X; kyEx5614[str-2::daf-2c::mVenus, 50ng/μL; myo-3::mCherry, 5ng/μL]</i>	DAF-2c::mVenus
CX18262	<i>ins-1(nr2091) IV; kyEx5649[str-2::daf-2a::mVenus, 50ng/μL; myo-3::mCherry, 5ng/μL]</i>	DAF-2a::mVenus
CX18261	<i>ins-1(nr2091) IV; kyEx5648[str-2::daf-2c::mVenus, 50ng/μL; myo-3::mCherry, 5ng/μL]</i>	DAF-2c::mVenus

REFERENCES

- Ahmadian, G., Ju, W., Liu, L., Wyszynski, M., Lee, S., Dunah, A., . . . Wang, Y. (2004). Tyrosine phosphorylation of GluR2 is required for insulin-stimulated AMPA receptor endocytosis and LTD. *EMBO*, 23, 1040-1050.
- Albrecht, D. R., & Bargmann, C. I. (2011). High-content behavioral analysis of *Caenorhabditis elegans* in precise spatiotemporal chemical environments. *Nature Methods*, 8(7), 599-605.
- Arey, R. N., Stein, G. M., Kaletsky, R., Kauffman, A., & Murphy, C. T. (2018). Activation of Gαq Signaling Enhances Memory Consolidation and Slows Cognitive Decline. *Neuron*, 98(3), 562-574.
- Arribere, J. A., Bell, R. T., Fu, B. X., Artiles, K. L., Hartman, P. S., & Fire, A. Z. (2014). Efficient marker-free recovery of custom genetic modifications with CRISPR/Cas9 in *Caenorhabditis elegans*. *Genetics*, 198(3), 837-46.
- Bargmann CI. 2006. Chemosensation in *C. elegans*. WormBook, ed. The *C. elegans* Research Community, WormBook. doi: 10.1895/wormbook.1.123.1, <http://www.wormbook.org>.
- Bargmann, C. I., Hartwig, E., & Horvitz, H. R. (1993). Odorant-selective genes and neurons mediate olfaction in *C. elegans*. *Cell*, 515(27).
- Beattie, E., Carroll, R., Yu, X., Morishita, W., Yasuda, H., Zastrow, M. v., & Malenka, R. (2000). Regulation of AMPA receptor endocytosis by a signaling mechanism shared with LTD. *Nat. Neurosci.*, 3, 1291-1300.
- Berg, H. C. (1993). *Random walks in biology*. Princeton Univ. Press.

- Berg, H. C., & Brown, D. A. (1972). Chemotaxis in *Escherichia coli* analysed by three-dimensional tracking. *Nature*, 239(5374), 500-504.
- Brenner, S. (1974). The Genetics of *CAENORHABDITIS ELEGANS*. *Genetics*, 71-94.
- Cao, J., Packer, J. S., Ramani, V., Cusanovich, D. A., Huynh, C., Daza, R., . . . Shendure, a. J. (2017). Comprehensive single cell transcriptional profiling of a multicellular organism. 357(6352).
- Castro, D., Cole, S., & Berridge, K. (2015). Lateral hypothalamus, nucleus accumbens, and ventral pallidum roles in eating and hunger: interactions between homeostatic and reward circuitry. *Front. Syst. Neurosci.*, 9, 90.
- Chalasani, S. H., Chronis, N., Tsunozaki, M., Gray, J. M., Ramot, D., Goodman, M. B., & Bargmann, C. I. (2007). Dissecting a circuit for olfactory behaviour in *Caenorhabditis elegans*. *Nature*, 450, 63-70.
- Chalasani, S. H., Kato, S., Albrecht, D. R., Nakagawa, T., Abbott, L. F., & Bargmann, C. I. (2010). Neuropeptide feedback modifies odor-evoked dynamics in *Caenorhabditis elegans* olfactory neurons. *Nature Neuroscience*, 13(5).
- Chalfie, M., Sulston, J., White, J., Southgate, E., Thomson, J., & Brenner, S. (1985). The neural circuit for touch sensitivity in *Caenorhabditis elegans*. *Journal of Neuroscience*, 5(4), 956-964.
- Chang, A. J., Chronis, N., Karow, D. S., Marletta, M. A., & Bargmann, C. I. (2006). A Distributed Chemosensory Circuit for Oxygen Preference in *C. elegans*. *PLOS Biology*, 9, e274.
- Chen, C., & Leonard, J. (1996). Protein tyrosine kinase-mediated potentiation of currents from cloned NMDA receptors. *J. Neurochem*, 67(1), 194-200.

- Chen, N., Pai, S., Zhao, Z., Mah, A., Newbury, R., Johnsen, R. C., . . . Stein, L. D. (2005). Identification of a nematode chemosensory gene family. *Proceedings of the National Academy of Sciences*, 102(1), 146-151.
- Chen, Z., Hendricks, M., Cornils, A., Maier, W., Alcedo, J., & Zhang, Y. (2013). Two insulin-like peptides antagonistically regulate aversive olfactory learning in *C. elegans*. *Neuron*, 77(3), 578-85.
- Cheung, B. H., Cohen, M., Rogers, C., Albayram, O., & de Bono, M. (2005). Experience-dependent modulation of *C. elegans* behavior by ambient oxygen. *Current Biology*, 15(10).
- Cho, C. E., Brueggemann, C., L'Etoile, N. D., & Bargmann, C. I. (2016). Parallel encoding of sensory history and behavioral preference during *Caenorhabditis elegans* olfactory learning. *eLIFE*, 5, e14000.
- Chronis, N., Zimmer, M., & Bargmann, C. I. (2007). Microfluidics for in vivo imaging of neuronal and behavioral activity in *Caenorhabditis elegans*. *Nature Methods*, 4(9), 727-31.
- Coburn, C. M., & Bargmann, C. I. (1996). A putative cyclic nucleotide-gated channel is required for sensory development and function in *C. elegans*. *Neuron*, 17(4), 695-706.
- Colbert, H. A., & Bargmann, C. I. (1995). Odorant-Specific Adaptation Pathways Generate Olfactory Plasticity in *C. elegans*. *Neuron*, 14(4), 803-812.
- Colbert, H. A., Smith, T. L., & Bargmann, C. I. (1997). OSM-9, A Novel Protein with Structural Similarity to Channels, Is Required for Olfaction, Mechanosensation, and Olfactory Adaptation in *Caenorhabditis elegans*. *J Neurosci*, 17(21), 8259-69.

- Daniels, S. A., Ailion, M., Thomas, J. H., & Sengupta, P. (2000). *egl-4* acts Through a Transforming Growth Factor-beta/SMAD Pathway in *Caenorhabditis elegans* to Regulate Multiple Neuronal Circuits in Response to Sensory Cues. *Genetics*, 156(1), 123-41.
- de Bono, M., & Bargmann, C. I. (1998). Natural variation in a neuropeptide Y receptor homolog modifies social behavior and food response in *C. elegans*. *Cell*, 94(5), 679-89.
- Deak, F., & Sonntag, W. E. (2012). Aging, synaptic dysfunction, and insulin-like growth factor (IGF)-1. *J Gerontol A Biol Sci Med Sci*, 67(6), 611-25.
- Dokshin, G. A., Ghanta, K. S., Piscopo, K. M., & Mello, C. C. (2018). Robust Genome Editing with Short Single-Stranded and Long, Partially Single-Stranded DNA Donors in *Caenorhabditis elegans*. *Genetics*, 210(3), 781-787.
- Dyera, A. H., Vahdatpoura, C., Sanfeliub, A., & Tropeab, D. (2016). The role of Insulin-Like Growth Factor 1 (IGF-1) in brain development, maturation and neuroplasticity. *Neuroscience*, 325, 89-99.
- Ferrario, C. R., & Reagan, L. (2018). Insulin-mediated synaptic plasticity in the CNS: Anatomical, functional and temporal contexts. *Neuropharmacology*, 136, 182-191.
- Fetterly, T. L., Oginsky, M. F., Nieto, A. M., Alonso-Caraballo, Y., Santana-Rodriguez, Z., & Ferrario, C. R. (2021). Insulin Bidirectionally Alters NAc Glutamatergic Transmission: Interactions between Insulin Receptor Activation, Endogenous Opioids, and Glutamate Release. *J Neurosci.*, 41(11), 2360–2372.
- Figlewicz, D., Evans, S., Murphy, J., Hoen, M., & Baskin, D. (2003). Expression of receptors for insulin and leptin in the ventral tegmental area/substantia nigra (VTA/SN) of the rat. *Brain Res.*, 964, 107-115.

- Gordus, A., Pokala, N., Levy, S., Flavell, S. W., & Bargmann, C. I. (2015). Feedback from network states generates variability in a probabilistic olfactory circuit. *Cell*, 161(2), 215-227.
- Gray, J. M., Hill, J. J., & Bargmann, a. C. (2004). A circuit for navigation in *Caenorhabditis elegans*. *Proc Natl Acad Sci U S A*, 102(9), 3184-3191.
- Hajdú, G., Gecse, E., Taisz, I., Móra, I., & Sőti, C. (2021). Toxic stress-specific cytoprotective responses regulate learned behavioral decisions in *C. elegans*. *BMC Biol*, 19(1), 26.
- Hammarlund, M., Hobert, O., III, D. M., & Sestan, N. (2018). The CeNGEN Project: The Complete Gene Expression Map of an Entire Nervous System. *Neuron*, 99(3), 430-433.
- Harris, G., Wu, T., Linfield, G., Choi, M.-K., Liu, H., & Zhang, Y. (2019). Molecular and cellular modulators for multisensory integration in *C. elegans*. *PLOS GENETICS*, 15(3), e1007706.
- Hayao Ohno, N. S. (2017). Dynamics of Presynaptic Diacylglycerol in a Sensory Neuron Encode Differences between Past and Current Stimulus Intensity. *Cell Reports*, 20(10), 2294-2303.
- Hedgecock, E., & Russell, R. (1975). Normal and mutant thermotaxis in the nematode *Caenorhabditis elegans*. *Proc Natl Acad Sci U S A*, 72(10), 4061-5.
- Horoszok, L., Raymond, V., Sattelle, D. B., & Wolstenholme, A. J. (2001, March). GLC-3: a novel fipronil and BIDN-sensitive, but picrotoxinin-insensitive, L-glutamate-gated chloride channel subunit from *Caenorhabditis elegans*. *British Journal of Pharmacology*, 132(6), 1247-1254.
- Huganir, R., & Nicoll, R. (2013). AMPARs and synaptic plasticity: the last 25 years. *Neuron*, 80, 704-717.

- Hunt-Newbury, R., Viveiros, R., Johnsen, R., Mah, A., Anastas, D., Fang, L., . . . Alexeyenko, A. (2007). High-throughput in vivo analysis of gene expression in *Caenorhabditis elegans*. *Plos Biology*, 5(9), e237.
- Iino, Y., & Yoshida, K. (2009). Parallel use of two behavioral mechanisms for chemotaxis in *Caenorhabditis elegans*. *The Journal of Neuroscience*, 29(17), 5370-5380.
- Jin, X., Pokala, N., & Bargmann, C. I. (2016). Distinct Circuits for the Formation and Retrieval of an Imprinted Olfactory Memory. *Cell*, 164(4), 632-43.
- Jin, Z., Jin, Y., Kumar-Mendu, S., Degerman, E., Groop, L., & Birnir, B. (2011). Insulin reduces neuronal excitability by turning on GABA(A) channels that generate tonic current. *PLoS One*, 6, e16188.
- Kandel, E., Schwartz, J. H., & Jessell, T. (2012). *Principles of Neural Science*. New York: McGraw-Hill.
- Kaplan, J. M., & Horvitz, H. R. (1993). A dual mechanosensory and chemosensory neuron in *Caenorhabditis elegans*. *Proc Natl Acad Sci U S A*, 90(6), 2227–2231.
- Kar, S., Chabot, J.-G., & Quirion, R. (1993). Quantitative autoradiographic localization of [125I]Insulin-like growth factor I, [125I]Insulin-like growth factor II and [125I]Insulin binding sites in developing and adult rat brain. *J. Comp. Neurol*, 333, 375-397.
- Kato, S., Xu, Y., Cho, C. E., Abbott, L. F., & Bargmann, C. I. (2014). Temporal responses of *C. elegans* chemosensory neurons are preserved in behavioral dynamics. *Neuron*, 81(3), 616–628.
- Kauffman, A. L., Ashraf, J. M., Corces-Zimmerman, M. R., Landis, J. N., & Murphy, C. T. (2010). Insulin Signaling and Dietary Restriction Differentially Influence the Decline of Learning and Memory with Age. *PLOS Biology*, 8(5), e1000372.

- Kimura, K. D., Riddle, D. L., & Ruvkun, G. (2011). The *C. elegans* DAF-2 insulin-like receptor is abundantly expressed in the nervous system and regulated by nutritional status. *Cold Spring Harb Symp Quant Biol*, 76, 113-20.
- Kodama, E., Kuhara, A., Mohri-Shiomi, A., Kimura, K. D., Okumura, M., Tomioka, M., . . . Mori, I. (2006). Insulin-like signaling and the neural circuit for integrative behavior in *C. elegans*. *Genes Dev*, 20(21), 2955-2960.
- Larsch, J., Flavell, S. W., Liu, Q., Gordus, A., Albrecht, D. R., & Bargmann, C. I. (2015). A circuit for gradient climbing in *C. elegans* chemotaxis. *Cell Reports*, 12(11), 1748-60.
- Larsch, J., Ventimiglia, D., Bargmann, C. I., & Albrecht, D. R. (2013). High-throughput imaging of neuronal activity in *Caenorhabditis elegans*. *Proc Natl Acad Sci U S A*, 110(45), E4266-73.
- Lee, J., O'Halloran, D., Kaye, J., Juang, B., Goga, A., & L'Etoile, N. (2010). Nuclear accumulation of the cGMP-dependent kinase EGL-4 instructs olfactory adaptation in the AWC neurons of *C. elegans*. *Proc Natl Acad Sci U S A*, 6016-21.
- Leinders-Zufall, T., Greer, C. A., Shepherd, G. M., & Zufall, F. (1998). Imaging Odor-Induced Calcium Transients in Single Olfactory Cilia: Specificity of Activation and Role in Transduction. *Journal of Neuroscience*, 18(15), 5630-9.
- Leto, D., & Saltiel, A. R. (2012). Regulation of glucose transport by insulin: traffic control of GLUT4. *Nature Reviews Molecular Cell Biology*, 13, 383-396.
- L'Etoile, N., Coburn, C., Eastham, J., Kistler, A., Gallegos, G., & Bargmann, C. (2002). The cyclic GMP-dependent protein kinase EGL-4 regulates olfactory adaptation in *C. elegans*. *Neuron*, 36(6), 1079-1089.

- Li, C. and Kim, K. Neuropeptides (September 25, 2008), WormBook, ed. The *C. elegans* Research Community, WormBook, doi/10.1895/wormbook.1.142.1, <http://www.wormbook.org>.
- Lin, C. H., Tomioka, M., Pereira, S., Sellings, L., Iino, Y., & Kooy, D. v. (2010). Insulin Signaling Plays a Dual Role in *Caenorhabditis elegans* Memory Acquisition and Memory Retrieval. *Journal of Neuroscience*, 30(23), 8001-8011.
- Lin, J., Ju, W., Foster, K., Lee, S., Ahmadian, G., Wyszynski, M., . . . Sheng, M. (2000). Distinct molecular mechanisms and divergent endocytotic pathways of AMPA receptor internalization. *Nature Neuroscience*, 3(12), 1282-90.
- Liu, H., Yang, W., Wu, T., Duan, F., Soucy, E., Jin, X., & Zhang, Y. (2018). Cholinergic Sensorimotor Integration Regulates Olfactory Steering. *Neuron*, 97(2), 390-405.
- Liu, S., Labouebe, G., Karunakaran, S., Clee, S., & Borgland, S. (2013). Effect of insulin on excitatory synaptic transmission onto dopamine neurons of the ventral tegmental area in a mouse model of hyperinsulinemia. *Nutrition & Diabetes*, 3, e97.
- López-Cruz, A., Sordillo, A., Pokala, N., Liu, Q., McGrath, P. T., & Bargmann, C. I. (2019). Parallel Multimodal Circuits Control an Innate Foraging Behavior. *Neuron*, 102(2), 407-419.
- Marks, J., Jr., D. P., Stahl, W., & Baskin, D. (1990). Localization of insulin receptor mRNA in rat brain by in situ hybridization. *Endocrinology*, 127, 3234-3236.
- Martinez, B. A., Rodrigues, P. R., Medina, R. M., Mondal, P., Harrison, N. J., Lone, M. A., . . . Gill, M. S. (2020). An alternatively spliced, non-signaling insulin receptor modulates insulin sensitivity via insulin peptide sequestration in *C. elegans*. *Elife*, 9, e49917.

- McCance-Katz, E. F. (2020). *The National Survey on Drug Use and Health: 2019*. Washington, DC: Substance Abuse and Mental Health Services Administration.
- McCulloch, W. S., & Pitts, W. (1990). A logical calculus of the ideas immanent in nervous activity. *Bulletin of Mathematical Biology*, 52(1-2), 99-115.
- Melo, J. A., & Ruvkun, G. (2013). Inactivation of conserved genes induces microbial aversion, drug detoxification, and innate immunity in *C.elegans*. *Cell*, 149(2), 452-466.
- Moosavi, M., Naghdi, N., & Choopani, S. (2007). Intra CA1 insulin microinjection improves memory consolidation and retrieval. *Peptides*, 28, 1029-1034.
- Muñoz-Jiménez, C., Ayuso, C., Dobrzynska, A., Torres-Mendéz, A., Ruiz, P. d., & Askjaer, P. (2017). An Efficient FLP-Based Toolkit for Spatiotemporal Control of Gene Expression in *Caenorhabditis elegans*. *Genetics*, 206(4), 1763-1778.
- Murakami, H., Bessinger, K., Hellmann, J., & Murakami, S. (2005). Aging-dependent and -independent modulation of associative learning behavior by insulin/insulin-like growth factor-1 signal in *Caenorhabditis elegans*. *Journal of Neuroscience*, 25(47), 10894-904.
- Murphy C.T., Hu P.J. Insulin/insulin-like growth factor signaling in *C. elegans* (December 26, 2013), WormBook, ed. The *C. elegans* Research Community, WormBook, doi/10.1895/wormbook.1.164.1, <http://www.wormbook.org>.
- Nagashima, T., Iino, Y., & Tomioka, M. (2019). DAF-16/FOXO promotes taste avoidance learning independently of axonal insulin-like signaling. *PLoS Genetics*, 15(7), e1008297.
- O'Halloran, D. M., Altshuler-Keylin, S., Lee, J. I., & L'Etoile, N. D. (2009). Regulators of AWC-Mediated Olfactory Plasticity in *Caenorhabditis elegans*. *PLoS Genetics*, 5(12), e1000761.

- Ohno, H., Kato, S., Naito, Y., Kunitomo, H., Tomioka, M., & Iino, Y. (2014). Role of synaptic phosphatidylinositol 3-kinase in a behavioral learning response in *C. elegans*. *Science*, 345(6194), 313-7.
- Ohno, H., Sakai, N., Adachi, T., & Iino, Y. (2017). Dynamics of Presynaptic Diacylglycerol in a Sensory Neuron Encode Differences between Past and Current Stimulus Intensity. *Cell Reports*, 20, 2294–2303.
- Palczewski, K. (2006). G Protein–Coupled Receptor Rhodopsin. *Annual Review of Biochemistry*, 75, 743-767.
- Palmitessa, A., Hess, H. A., Bany, A., Kim, Y.-M., Koelle, M. R., & Benovic, J. L. (2005). *Caenorhabditis elegans* arrestin regulates neural G protein signaling and olfactory adaptation and recovery. *Journal of Biological Chemistry*, 280(26).
- Pierce-Shimomura, J. T., Morse, T. M., & Lockery, S. R. (1999). The Fundamental Role of Pirouettes in *Caenorhabditis elegans* Chemotaxis. *Journal of Neuroscience*, 19(21), 9557-9569.
- Plowman, G. D., Sudarsanam, S., Bingham, J., Whyte, D., & Hunter, T. (1999). The protein kinases of *Caenorhabditis elegans*: A model for signal transduction in multicellular organisms. *Proc Natl Acad Sci U S A*, 96(24), 13603-13610.
- Pokala, N., Liu, Q., Gordus, A., & Bargmann, C. I. (2014). Inducible and titratable silencing of *Caenorhabditis elegans* neurons in vivo with histamine-gated chloride channels. *Proc Natl Acad Sci U S A*, 111(7), 2770-2775.
- Pristerà, A., Blomeley, C., Lopes, E., Threlfell, S., Merlini, E., Burdakov, D., . . . Ang, S.-L. (2019). Dopamine neuron-derived IGF-1 controls dopamine neuron firing, skill learning, and exploration. *Proc Natl Acad Sci U S A*, 116(9), 3817-3826.

- Reber, P. (2010). Ask the Brains. *Scientific American Mind*, 21(2).
- Reinert, M., Nguyen, T., & Fritze, D. (2021). *The State Of Mental Health In America*.
Alexandria: Mental Health America, Inc.
- Riddle, D. L., Swanson, M. M., & Albert, P. S. (1981). Interacting genes in nematode dauer larva formation. *Nature*, 290(5808), 668-71.
- Saltiel, A. R., & Kahn, C. R. (2001). Insulin signalling and the regulation of glucose and lipid metabolism. *Nature*, 414(6865), 799–806.
- Schwartz, M., Woods, S., Jr., D. P., Seeley, R., & Baskin, D. (2000). Central nervous system control of food intake. *Nature*, 404(6778), 661-671.
- Skeberdis, V., J. Lan, X. Z., Zukin, R., & Bennett, M. (2001). Insulin promotes rapid delivery of N-methyl-D- aspartate receptors to the cell surface by exocytosis. *Proc Natl Acad Sci U S A*, 98(6), 3561-3566.
- Sylvia, D., Fuhrmann, J., Hartel, P., & Zuberer, D. (1998). *Principles and Applications of Soil Microbiology*. Upper Saddle River, New Jersey: Prentice Hall.
- Taylor, S. R., Santpere, G., Weinreb, A., Barrett, A., Reilly, M. B., Xu, C., . . . III, D. (2020). Molecular topography of an entire nervous system. *BioRxiv*.
- Theysohn, J. M., Kraff, O., Maderwald, S., Schlamann, M. U., Greiff, A. d., Forsting, M., . . . Gizewski, E. R. (2009). The human hippocampus at 7 T--in vivo MRI. *Hippocampus*, 19(1), 1-7.
- Tomioka, M., Adachi, T., Suzuki, H., Kunitomo, H., Schafer, W. R., & Iino, Y. (2006). The insulin/PI 3-kinase pathway regulates salt chemotaxis learning in *Caenorhabditis elegans*. *Neuron*, 51(5), 613-25.

- Tomioka, M., Naito, Y., Kuroyanagi, H., & Iino, Y. (2016). Splicing factors control *C. elegans* behavioural learning in a single neuron by producing DAF-2c receptor. *Nature Communication*, 7(11645), doi: 10.1038/ncomms11645.
- Torayama, I., Ishihara, T., & Katsura, I. (2007). *Caenorhabditis elegans* Integrates the Signals of Butanone and Food to Enhance Chemotaxis to Butanone. *The Journal of Neuroscience*, 27(4), 741-750.
- Troemel, E. R., Chou, J. H., Dwyer, N. D., Colbert, H. A., & Bargmann, C. I. (1995). Divergent seven transmembrane receptors are candidate chemosensory receptors in *C. elegans*. *Cell*, 83(2), 207-218.
- Troemel, E. R., Kimmel, B. E., & Bargmann, C. I. (1997). Reprogramming Chemotaxis Responses: Sensory Neurons Define Olfactory Preferences in *C. elegans*. *Cell*, 91(2), 161-169.
- Tsalik, E. L., & Hobert, O. (2003). Functional mapping of neurons that control locomotory behavior in *Caenorhabditis elegans*. *Developmental Neurobiology*, 56(2), 178-197.
- Tseng, Q., Wang, I., Duchemin-Pelletier, E., Azioune, A., Carpi, N., Gao, J., . . . Balland, M. (2011). A new micropatterning method of soft substrates reveals that different tumorigenic signals can promote or reduce cell contraction levels. *Lab Chip*, 11(13), 2231-40.
- Ulivì, A. F., Castello-Waldow, T. P., Weston, G., Yan, L., Yasuda, R., Chen, A., & Attardo, A. (2019). *Longitudinal Two-Photon Imaging of Dorsal Hippocampal CA1 in Live Mice*. JoVE.

- Ventimiglia, D., & Bargmann, C. I. (2017). Diverse modes of synaptic signaling, regulation, and plasticity distinguish two classes of *C. elegans* glutamatergic neurons. *Elife*, 6(e31234), doi: 10.7554/eLife.31234.
- Vowels, J. J., & Thomas, J. H. (1992). Genetic analysis of chemosensory control of dauer formation in *Caenorhabditis elegans*. *Genetics*, 130(1), 105-23.
- Wakabayashia, T., Kitagawab, I., & Shingaia, R. (2004). Neurons regulating the duration of forward locomotion in *Caenorhabditis elegans*. *Neuroscienc Research*, 50(1), 103-111.
- Wang, Y., & Linden, D. (2000). Expression of cerebellar long-term depression requires postsynaptic clathrin-mediated endocytosis. *Neuron*, 25(3), 635–647.
- Ward, A., Liu, J., Feng, Z., & Xu, X. Z. (2008). Light-sensitive neurons and channels mediate phototaxis in *C. elegans*. *Nature Neuroscience*, 11(8), 916-22.
- Ward, S. (1973). Chemotaxis by the Nematode *Caenorhabditis elegans*: Identification of Attractants and Analysis of the Response by Use of Mutants. *Proc Natl Acad Sci U S A*, 70(3), 817-821.
- Wes, P., & Bargmann, C. (2001). *C. elegans* odour discrimination requires asymmetric diversity in olfactory neurons. *Nature*, 401(6829), 698-701.
- White, J., Southgate, E., Thomson, J., & Brenner, S. (1986). The Structure of the Nervous System of the Nematode *Caenorhabditis elegans*. *Philosophical transactions of the royal society B*, 314(1165), 1-340.
- Wolkow, C. A., Muñoz, M. J., Riddle, D. L., & Ruvkun, G. (2002). Insulin receptor substrate and p55 orthologous adaptor proteins function in the *Caenorhabditis elegans* *daf-2*/insulin-like signaling pathway. *Journal of Biological Chemistry*, 277(51), 49591-7.

- Woods, S., Lotter, E., McKay, L., & Jr., D. P. (1979). Chronic intracerebroventricular infusion of insulin reduces food intake and body weight of baboons. *Nature*, 282(5738), 503-505.
- Worthy, S. E., Rojas, G. L., Taylor, C. J., & Glater, a. E. (2018). Identification of Odor Blend Used by *Caenorhabditis elegans* for Pathogen Recognition. *Chemical Senses*, 43(3), 169-180.
- Wu, T., Duan, F., Yang, W., Liu, H., Caballero, A., Abreu, D. A., . . . Zhang, Y. (2019). Pheromones Modulate Learning by Regulating the Balanced Signals of Two Insulin-like Peptides. *Neuron*, 104(6), 1095-1109.
- Yoneyama, Y., Lanzerstorfer, P., Niwa, H., Umehara, T., Shibano, T., Yokoyama, S., . . . Takahashi, S.-I. (2018). IRS-1 acts as an endocytic regulator of IGF-I receptor to facilitate sustained IGF signaling. *Elife*, 7(e32893), doi: 10.7554/eLife.32893.
- Yoshimura, J., Ichikawa, K., Shoura, M. J., Artiles, K. L., Gabdank, I., Wahba, L., . . . Schwarz, E. M. (2019). Recompleting the *Caenorhabditis elegans* genome. *Genome Research*, 29(6), 1009-1022.
- Zhang, Y., Lu, H., & Bargmann, C. I. (2005). Pathogenic bacteria induce aversive olfactory learning in *Caenorhabditis elegans*. *Nature*, 438(7065), 179-184.